The expression and function of the mucin-like glycoprotein podoplanin in glioblastoma

Dissertation

Faculty of Biosciences
Ruperto-Carola University of Heidelberg

Tanja Eisemann

2017

Dissertation

submitted to the

Combined Faculties for the Natural Sciences and for Mathematics

of the Ruperto-Carola University of Heidelberg, Germany

for the degree of

Doctor of Natural Sciences

presented by

Tanja Eisemann, M.Sc.

Born in Heilbronn

Oral examination: 02.03.2018

The expression and function of the mucin-like glycoprotein podoplanin in glioblastoma

Referees: Prof. Dr. Peter Angel

Prof. Dr. Michel Mittelbronn

Science is simply the word we use to describe a method of organizing our curiosity.

Tim Minchin

SUMMARY

The mucin-like sialoglycoprotein podoplanin (PDPN) is widely expressed throughout the human and rodent body. Although numerous studies have revealed its essential function in development, especially of the lymphatic system, the lungs and heart, the overall picture of its physiologic function is still incomplete. Emerging evidence of the past decade has associated PDPN *de novo* or overexpression with numerous cancer entities including glioblastoma, and in particular with the invasive behavior of tumor cells. As the infiltrative growth of tumor cells is one major challenge in glioblastoma therapy, the identification of novel candidates in tumor cell migration remains an essential pre-requisite for the development of new and effective therapeutic means. However, the postulated pro-tumorigenic and pro-invasive function of PDPN in glioblastoma has never been validated *in vivo*. Moreover, the underlying mechanism of a potential malignant effect of PDPN has not been addressed. Thus, the aim of this study was to close this gap of knowledge by the combination of correlative and functional assays. Descriptive *in vivo* approaches involving patient-derived xenografts were primarily taken to confirm the previous correlations of PDPN expression and malignant progression and to establish a model that enables the investigation of underlying mechanisms. For the functional validation of the hypothesis that PDPN is a major driver of glioblastoma progression and especially invasion, the gene was deleted by the novel CRISPR/Cas9 technology. Xenotransplantations of control and knockout cells indicated the dispensability of PDPN for glioblastoma growth and progression. The reliable analysis of the postulated pro-invasive function of PDPN required the optimization of a three-dimensional invasion assay based on organotypic brain slice cultures. The usage of adult murine brain slices and a red emitting fluorescent membrane dye significantly improved the assay quality. The application of this advanced technique identified PDPN as a non-rate limiting component in glioblastoma cell invasion. These data and the detailed analysis of further malignant features including proliferation, apoptosis and angiogenesis have rebutted the previous assumption of a tumor promoting effect of PDPN. Despite the dispensability of PDPN for tumor development and tumor cell invasion, the obtained results suggest PDPN as a marker for malignant glioblastoma cells. In conclusion, this study represents an important contribution in the process of preclinical drug development, as the results object the frequently suggested development of a PDPN blocking therapeutic agent. Instead, this work suggests PDPN as a marker for prognosis or targeted delivery of cytotoxic compounds into glioblastoma tumor cells.

ZUSAMMENFASSUNG

Das transmembrane Glykoprotein Podoplanin (PDPN) wird in zahlreichen Organen und Zelltypen des menschlichen und murinen Organismus exprimiert. Obwohl man PDPN eine essentielle Rolle in der Entwicklung, insbesondere des lymphatischen Gefäßsystems, Herz und Lunge, zuschreiben konnte, ist seine physiologische Funktion noch nicht vollständig entschlüsselt. PDPN ist auch Gegenstand pathologischer Untersuchungen, da vielfach eine *de novo*- bzw. Überexpression im Glioblastom und zahlreichen weiteren Krebsentitäten beobachtet werden konnte. Es gibt zudem zunehmende Hinweise auf eine migrationsfördernde Rolle des Oberflächenproteins. Aktuelle Glioblastomtherapien scheitern meist an Therapieresistenzen in Kombination mit stark invasivem Wachstumsverhalten der Zellen, die in umliegendes gesundes Gehirngewebe streuen und so eine chirurgische Entfernung verhindern. Im Fokus der Glioblastomforschung steht daher u.a. die Tumorzellinvasion, da ein Unterbinden der Infiltration die Heilungschancen drastisch erhöhen würde. Ob PDPN die pro-invasive Eigenschaft der Glioblastomzellen *in vivo* vermittelt und daher ein geeigneter Kandidat in der Therapieentwicklung darstellen würde, wurde bislang nicht bewiesen. Zudem ist unbekannt, wie PDPN die Glioblastomzellinvasion und –proliferation mechanistisch begünstigen könnte. Um potentiell tumorförderderne Eigenschaften von PDPN zu belegen und mechanistisch zu erläutern, wurden im Rahmen dieser Studie verschiedene deskriptive und funktionale Experimente durchgeführt. Ein deskriptives Modell der Xenotransplantation von primären humanen Glioblastomzellen diente zur Validierung der bereits publizierten negativen Korrelation von starker PDPN Expression und Überleben, was die Wahl des Modells für weitere mechanistische Untersuchungen bestätigte. Um zu zeigen, dass das maligne Verhalten der Tumorzellen auf der Expression von PDPN beruht, wurde PDPN mittels neuester Gentechnologie (CRISPR/Cas9) in Glioblastom-Primärkulturen und etablierten Glioblastomzelllinien deletiert. Die darauf folgende orthotope Injektion der PDPN Knockout- und Kontrollzellen ergab keinen Unterschied im Tumorwachstum oder Überleben der Rezipienten, was einer malignen Funktion von PDPN im Glioblastom widerspricht. Die Untersuchung der postulierten pro-invasiven Funktion von PDPN im Glioblastom setzte die Optimisierung eines dreidimensionalen Invasionsassays voraus, das auf organotypischen Hirnschnitten basiert. Die Verwendung von adulten Mäusehirnen sowie der Einsatz eines rot emittierenden fluoreszenten Farbstoffes verbesserte die Qualtität des Assays erheblich. Die Anwendung des optimierten Assays ergab, dass PDPN nicht zum Invasionsvermögen der Glioblastomzellen beiträgt. Auch die Analyse weiterer Tumorcharakteristika, wie Proliferation, Apoptose, oder Tumorvaskularisation, deutete auf eine fehlende maligne Funtion von PDPN im Glioblastom hin. Somit konnte diese Studie die Hypothese, dass PDPN eine tumor-, und insbesondere eine invasionsfördernde Rolle im

Glioblastom einnimmt, nicht bestätigen. Dennoch weisen die Ergbnisse darauf hin, dass die Expression von PDPN mit der Aggressivität der Gliomzellen korreliert, was den Einsatz von PDPN als klinischen Marker nahelegt. Die Erkenntnis dieser Studie ist daher ein wichtiges Puzzlestück in der Entwicklung neuer Glioblastomtherapien. Die bisherige Annahme, die funktionelle Inaktivierung von PDPN könnte als therapeutisches Mittel eingesetzt werden, wurde in dieser Studie zwar widerlegt, stattdessen könnte PDPN aber als Marker zur Prognose oder zur gezielten Einbringung von Zytostatika in Tumorzellen dienen.

TABLE OF CONTENTS

LIST OF FIGURES

INTRODUCTION

METHODS

RESULTS

DISCUSSION

SUPPLEMENT

LIST OF TABLES

INTRODUCTION

MATERIALS

METHODS

SUPPLEMENT

LIST OF ABBREVIATIONS

ABC	Avidin/biotin concentrate
ACK	Ammonium Chloride Potassium
AP-1	Activator protein 1
BBB	Blood brain barrier
bp	Base pair
BSA	Bovine serum albumin
Cas9	CRISPR-associated protein-9 nuclease
CD	Cluster of differentiation
cDNA	Complementary DNA, copy DNA
CNS	Central nervous system
CO_2	Carbon dioxide
CRISPR	Clustered Regularly Interspaced Short Palindromic Repeats
CT	Cycle of threshold
d	day(s)
DAB	3,3'-diaminobenzidine
DiD	1,1'-dioctadecyl-3,3,3',3'-tetramethylindodicarbocyanine, 4-chlorobenzenesulfonate salt
DiI	1,1'-dioctadecyl-3,3,3',3'-tetramethylindocarbocyanine
DMEM	Dulbecco's Modified Eagles Medium
DMSO	Dimethyl sulfoxide
DNA	Deoxyribonucleic acid
dNTP	Deoxynucleotide triphosphate
ECM	Extracellular matrix
EDTA	Ethylenediaminetetraacetic acid
EGF	Epidermal growth factor
EtOH	Ethanol
FACS	Fluorescence-activated cell sorting
FBS	Fetal bovine serum
FGFb	Basic fibroblast growth factor
FITC	Fluorescein isothiocynate
FRCs	Fibroblastic reticular cells
GBM	Glioblastoma multiforme
GEMMs	Genetically engineered mouse models

GFAP	Glial fibrillary acidic protein
GFP	Green fluorescent protein
GOI	Gene of interest
H_2O_2	Hydrogen peroxide
HCV	Hepatitis C virus
HEPES	4-(2-hydroxyethyl)-1-piperazineethanesulfonic acid buffer
HEPES	4-(2-hydroxyethyl)-1-piperazineethanesulfonic acid buffer
HIV	Human immunodeficiency virus
HKG	House keeping gene
HRP	Horseradish peroxidase
IARC	International Agency for Research on Cancer
Iba1	Ionized calcium-binding adapter molecule 1
i.c.	intracranial
ICAM	Intercellular adhesion molecule
IDH	Isocitrate dehydrogenase
IgG	Immunoglobulin γ
IHC	Immonohistochemistry
kDa	Kilodalton
KO	knockout
LECs	Lymphatic endothelial cells
M	Molar
MAPK	Mitogen-Activated Protein Kinase
MBP	Myelin basic protein
MDM2	Mouse double minute 2 homolog
MGMT	O-6-Methylguanine-DNA Methyltransferase
MEM	Minimum Essential Medium
NF-1	Neurofibromin 1
NHEJ	non-homologous end joining
o/n	Over night
PBS	Phosphate buffered saline
PCR	Polymerase chain reaction
PDPN	Podoplanin
PDGF	Platelet-derived growth factor
PDX	Patient-derived xenografts
PFA	Paraformaldehyde

pH	potential of hydrogen
PI3K	Hhosphatidylinositol-3-kinase
PTEN	Phosphatase and tensin homolog
qRT-PCR	Quantitative real-time PCR
RIPA	Radioimmunoprecipitation assay buffer
RNA	Ribonucleic acid
rpm	Rounds per minute
RT	Room temperature
SD	Standard deviation
SDS-PAGE	Sodium dodecyl sulphate –polyacrylamide gel electrophoresis
STAT	Signal transducer and activator of transcription
TBE	Tris/borate/EDTA (buffer)
TBS	Tris-buffered saline (buffer)
TCGA	The Cancer Genome Atlas
Th17	T helper 17 cells
TUNEL	Terminal deoxynucleotidyl transferase dUTP nick end labeling
U	Units
V	Volt
Vol%	Volume percent
v/v	Volume/volume
w/v	Weight/volume

1 INTRODUCTION

1 INTRODUCTION

1.1 **Glioblastoma** – the most malignant primary brain tumor

1.1.1 Classification, characteristics and therapeutic interventions

According to the International Agency for Research on Cancer (IARC) database, estimated 57.000 Europeans were newly diagnosed with central nervous system (CNS) tumors in 2012 (Ferlay et al., 2015). Tumors of the brain and CNS are categorized as either primary or secondary brain tumors. Primary brain tumors arise from tissue of the CNS whereas secondary brain tumors are defined as tumors that metastasized from a primary tumor outside the CNS into the brain. With more than 130 different subtypes, primary brain tumors comprise a large multitude of tumors (Figure 1.1) that differ in many phenotypic and, as recently introduced by the 2016 World Health Organization Classification, more objective molecular parameters (Louis et al., 2016). The introduction of genotypic parameters has particularly simplified the sub-classification of diffuse gliomas, the largest primary brain tumor group, into oligodendrogliomas (*IDH* mutation in combination with 1p/19q co-deletion) and astrocytomas (*IDH* wild-type or mutant) (Louis et al., 2016). Further sub-classification is mostly based on cytological and histological parameters and will assign the tumor to the group of oligodendroglioma, anaplastic oligodrendroglioma, diffuse astrocytoma, anaplastic astrocytoma, the new diagnostic entity diffuse midline glioma or glioblastoma.

Glioblastoma is the most malignant glioma subtype (grade IV). Furthermore, it represents the most frequent malignant brain tumor affecting nearly half of all adult primary brain tumor patients (Visser et al., 2015). Glioblastoma is characterized by an extremely poor prognosis. The five year relative survival of glioblastoma patients in Europe is below 10% (Stupp et al., 2009, Visser et al., 2015) and median survival of patients that have received current standard-of-care treatment has been reported to be 14.6 months (Stupp et al., 2009). The disease affects slightly more men than women (1.6:1) and a median age of diagnosis around 65 years makes glioblastoma an age-related pathology (Ostrom et al., 2013). A difference in the age distribution of patients has been reported for patients with primary and secondary glioblastoma. Patients with secondary glioblastoma are on average diagnosed significantly younger, at the age of 45 years (Ohgaki and Kleihues, 2005). This form of glioblastoma accounts for only approximately 10% of all glioblastomas and is termed secondary as it develops from lower grade glioma.

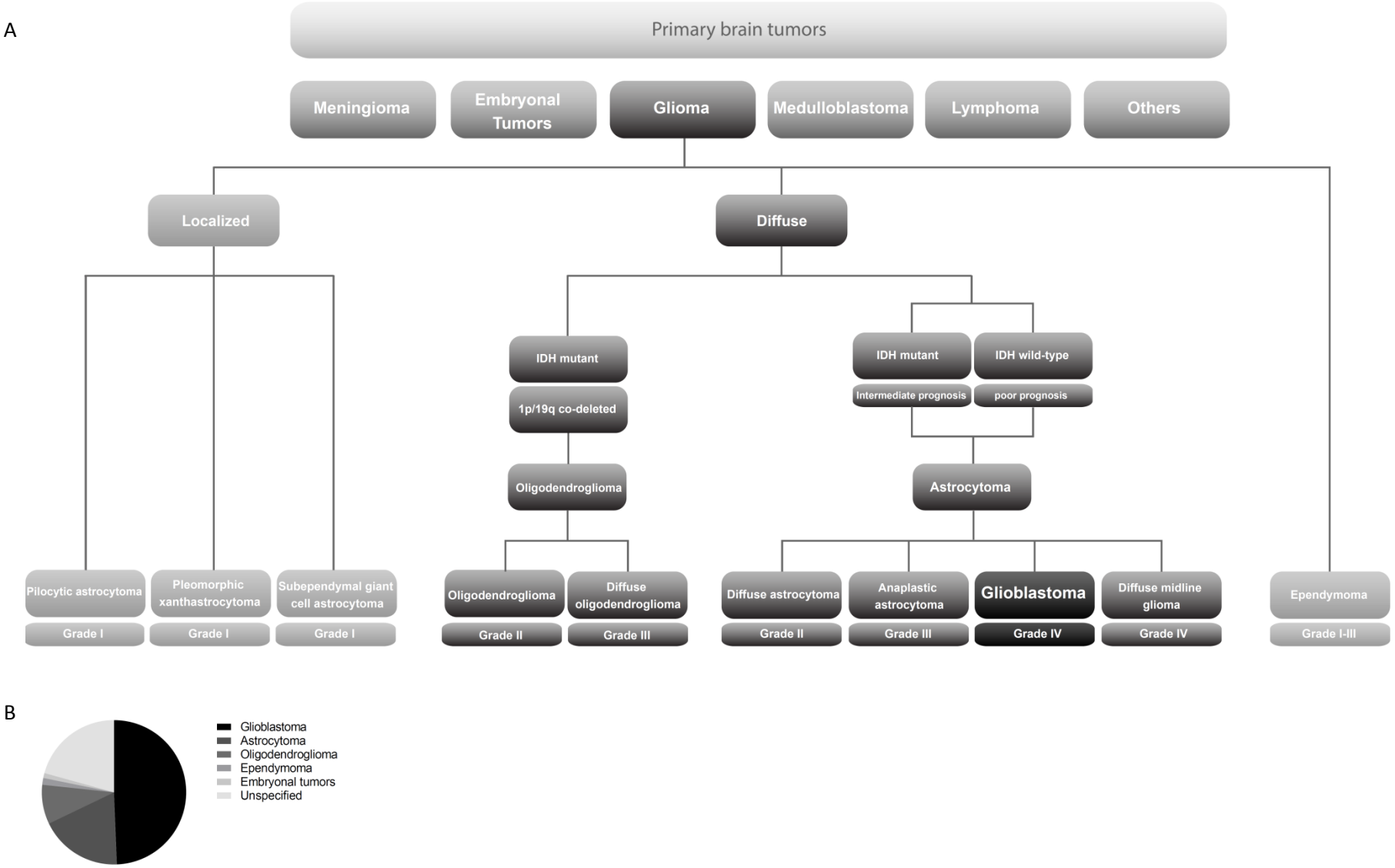

Figure 1.1 (A) Classification of brain tumors according to WHO 2016 (Louis et al., 2016) and (B) composition of neuro-epithelial tumors diagnosed in 2007 and 2011 (Visser et al., 2015).

In contrast, the vast majority of glioblastoma tumors develops *de novo* and is therefore called primary glioblastoma (Louis et al., 2016). In general, primary glioblastomas show a more rapid progression and confer a worse prognosis compared to secondary glioblastomas.

Histologically, glioblastoma distinguishes from all other grades primarily by a high mitotic index, hypervascularization and facultatively by the presence of necrosis and pseudopalisades, fencelike hypercellular arrangements of tumor cells that actively migrate from necrotic foci (Aldape et al., 2015, Brat et al., 2004). Although the histological class of glioblastoma consists of molecularly heterogeneous tumor types, they share some common aberrations in various molecular pathways. Oncogenic events such as amplification of the *EGFR* gene (40%), often accompanied with the constitutively active EGFRvIII mutation, activation or loss of suppression of the PI3K-AKT (50%) and/or RAS-MAPK signaling pathways are found in the majority of glioblastomas (Cancer Genome Atlas Research, 2008, Parsons et al., 2008). Concomitantly, tumor suppressor pathways such as NF1- (15%), PTEN- (30%), p53- (64%) and Rb-pathways (68%) are frequently disrupted (Cancer Genome Atlas Research, 2008, Parsons et al., 2008). The presence and activity of the tumor suppressors p53 and Rb is not only directly affected by mutations and deletions of their corresponding genes, but additionally by the deletion of upstream activators (p19 and p16 encoded by the *INK4A/ARF* locus) or by gene amplifications and transcriptional upregulation of their upstream repressors (Mdm2 and, respectively, Cdk4). The intention of sub-classifying glioblastoma tumors according to their genetic profiles has emerged as difficult challenge. In 2006 and 2010 three or respectively four major molecular signatures were identified: proneural, proliferative and mesenchymal (Phillips et al., 2006); or proneural, neural, classical and mesenchymal, respectively (Verhaak et al., 2010). The molecular sub-classification of glioblastoma tumors was intended to define a specific set of markers within each group that predict the response to different therapies. However, the specific subtypes could not be matched to efficient therapeutic options yet and thus have not been incorporated into clinical decision making.

One of the most clinically relevant discoveries in the past decade was the identification of mutations in the genes encoding for isocitrate dehydrogenase (*IDH*) 1 or 2 in the vast majority of gliomas (Parsons et al., 2008, Yan et al., 2009). IDH1 (R132) and IDH2 (R172) gain of function mutations are early oncogenic events, which shift the balance from the physiologic metabolite α-2-ketoglutarate to the oncometabolite 2-hydroxyglutarate (2-HG) (Dang et al., 2009). Elevated 2-HG levels result in the inhibition of various enzymes that are involved in the methylation and demethylation process of DNA presumably causing the Glioma CpG Island Methylation Phenotype (G-CIMP) (Christensen et al., 2011, Noushmehr et al., 2010). The discovery of this oncogenic gain

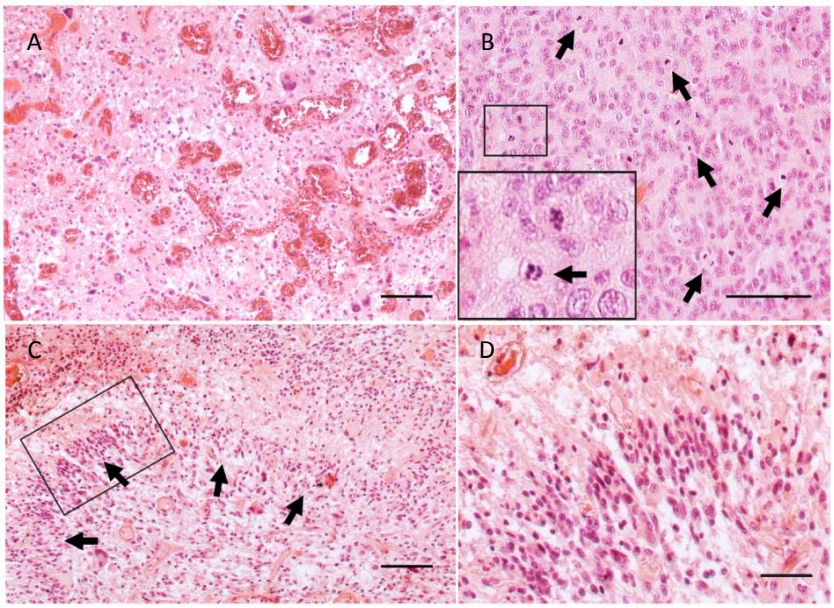

Figure 1.2 Histological features of glioblastoma.
Hematoxylin and eosin staining of human glioblastoma tumors that show characteristic (A) hypervascularization, (B) high mitotic activity (arrows indicate mitotic cells) and (C) pseudopalisades indicated by arrows. (D) Magnification of marked area in (C). Scale bars (A; B; C) 100 µm; (D) 50 µm.

of function mutation enables the development of novel therapeutic means such as a vaccine against the R132H neoantigen (Schumacher et al., 2014) or small molecular inhibitors that specifically target the mutated IDH protein (Rohle et al., 2013).

Importantly, although *IDH* mutations affect almost 70% of all gliomas, it is less abundant in grade IV glioblastomas. Here, *IDH* mutant tumors closely correspond to secondary glioblastoma (10% of all glioblastomas) which are, despite the oncogenic effects of mutant *IDH*, characterized by a significant better prognosis (Parsons et al., 2008, Yan et al., 2009, Sanson et al., 2009). This illustrates that, although histologically similar, primary and secondary glioblastomas are molecular distinct diseases that differ in progression, prognosis and therapeutic response (Wick et al., 2013).

In addition to the IDH status, the promoter methylation of the O-6-methylguanine-DNA methyltransferase (*MGMT*) is used as a prognostic and predictive marker for glioblastoma patients (Stupp et al., 2009, Wick et al., 2013). MGMT is involved in DNA repair where it removes alkyl groups from O6-position of guanine preventing base damage, subsequent mutations and double strand breaks. Glioma cells with a methylated *MGMT* promoter show decreased levels of MGMT protein, which in turn hampers the repair of alkylated DNA and results in the accumulation of DNA damages. This is exploited in glioma therapy where the alkylating agent temozolomide (TMZ), in combination with radiotherapy, is applied to introduce an intolerable level of DNA damage and thus cell death. As the accumulation of DNA damage by alkylating agents relies on

the decreased levels of MGMT, TMZ therapy is generally more effective in glioblastoma patients who exhibit hypermethylation of the *MGMT* promoter (approx. 40% of all glioblastoma patients) (Hegi et al., 2005). Importantly, it has been shown that the *MGMT* promoter methylation alone is not enough to predict a positive response to temozolomide treatment, but additionally requires the *IDH* wild type status, a fact that has mechanistically not been understood yet (Wick et al., 2013).

1.1.2 Glioblastoma cell invasion – one major hurdle in glioblastoma therapy

The standard-of-care treatment that comprises surgery and radiotherapy was extended by temozolomide treatment in 2005 in Europe and the United States. This change in therapy has improved median survival time from 12.1 to 14.6 months and increased the five year relative survival from 1.9% to 9.8% (Stupp et al., 2009). Despite this significant prolongation in survival, the absolute survival time for glioblastoma remains very dismal. This is a result of multiple causes, including the challenge of delivering chemotherapeutics in effective doses across the blood-brain barrier (BBB) and the intrinsic and acquired resistances against current standard therapies (Oberoi et al., 2016). Furthermore, the infiltrative growth of glioblastoma tumor cells impedes complete surgical resection and the continuance of remaining therapy resistant tumor cells results inevitably in recurrences. The ability of glioblastoma cells to extensively infiltrate the brain was already described in 1938 by the German neuropathologist Hans Joachim Scherer (Scherer, 1938). He reported that glioma cells migrate along pre-existing structures of the brain, including meninges and the subjacent subarachnoid space, blood vessels, myelinated nerve fibers and the extracellular space between neuronal or glial processes in the brain parenchyma. Furthermore, it has been described that glioma cells of one tumor are not restricted to the migration along one structure (Scherer, 1938). However, whether and how subpopulations of glioma cells prefer certain structures remains to be determined. These structures could provide the path of least resistance in the condensed mesh of extracellular matrix (ECM) and densely packed neuronal and glial cells in the brain; or tumor cells could be attracted by certain structures as their surfaces and microenvironment provide distinct advantages in the process of invasion (Cuddapah et al., 2014).

The fact that the invasive growth of glioblastoma results in recurrences has already been experienced early in history of glioblastoma therapy, when surgeons radically resected the entire tumor bearing hemisphere only to witness recurrences on the contralateral hemisphere (Dandy, 1928). Today the application of modern microsurgical techniques and gross-total resection has

improved the survival of glioblastoma patients (Stummer et al., 2008), however, recurrence at the contralateral hemisphere or even in close proximity to the resection cavity cannot be prevented. This highlights the urgent need of new and innovative therapeutic means that inhibit tumor cell invasion. Anti-invasive therapies are conceptually meant to contain the disease in order to improve the efficacy of local treatments. As glioblastoma cells have most likely invaded the brain at the time of diagnosis, anti-invasive therapies might first seem of limited value. However, targeting invading tumor cells remains an interesting approach for several reasons. Firstly, although the dissemination of glioblastoma cells within the brain tissue had most probably already commenced before diagnosis and treatment, it is of strong importance to restrain the continuous colonization of the brain reducing the number of potential recurrent lesions that can then be tackled by a combination of surgery and radiochemotherapy. Secondly, invasiveness unifies all glioblastoma cells that remain in the brain and escaped surgical resection and local radiotherapy. Hence, proteins involved in invasion could represent a common denominator and therapeutic targets e.g. for the delivery of cytotoxic compounds or as immunogenic targets. Thirdly, migrating glioblastoma cells that use blood vessels as preferred route of invasion have been reported to focally breach the BBB by disrupting astrocytic endfeet and degrading the basement membrane and tight junctions of endothelial cells (Watkins et al., 2014). Damaged BBB leads to uncontrolled leakage of serum components into the parenchyma resulting in edemas. This process that represents a strong burden to glioblastoma patients could be prevented by the inhibition of tumor cell invasion. And lastly, an inverse correlation of proliferation and invasion has been suggested, also referred to as the “go or grow hypothesis” which implies the reduced proliferation rate of invading tumor cells (Giese et al., 1996, Horing et al., 2012, Mariani et al., 2001). Since standard anti-cancer chemotherapy primarily targets dividing cells, therapy resistance of glioblastoma cells could be partially caused by their high invasiveness. The inhibition of invasion could thus restore susceptibility to chemotherapeutic approaches.

The development of novel anti-invasive therapies is a crucial step in the combat of glioblastoma and requires mechanistic insight into the biology of glioblastoma invasion. Most studies dealing with glioblastoma cell invasion involve easy-to-handle and inexpensive two-dimensional cell-based methods like *in vitro* wound healing assays. However, recent studies have shown striking differences in the function of proteins between two- and three-dimensional migration conditions (Khatau et al., 2012, Madsen et al., 2015, Skau et al., 2016). The alternative approach to assess invasion in a three-dimensional matrix of matrigel or collagen is unsatisfactory as these reagents do not reflect the complex composition of the brain ECM (for review see Barros et al., 2011). Furthermore, *in vivo* tumor cells are embedded in a three-dimensional environment that does not

only contain components of the ECM, but also other cell types that have been reported to substantially impact on tumor cell invasion (reviewed in Joyce and Pollard, 2009). Additionally, glioma cells encounter secondary structures, introduced above as the Scherer's structures, that serve as migration routes. Thus, the most reliable analysis of glioma cell migration is the monitoring of invasive cells in their natural environment in a living organism. This, however, requires the cutting-edge technique of intravital imaging. For this procedure, the cranial bone of a living animal is replaced by a glass coverslip (Askoxylakis et al., 2017). This chronic cranial window enables the live imaging of single fluorescently labeled tumor cells that leave the implanted tumor and invade the surrounding tissue (Osswald et al., 2015, Winkler et al., 2009). Intravital imaging however, is not the assay of first choice to analyze glioma cell invasion, as it is a very laborious and time consuming technique that requires the approval of *in vivo* experiments by local authorities and specialized equipment to install the cranial window and to perform subsequent high resolution imaging. This highlights the need of an invasion assay that unites advantages of both approaches in an easy and inexpensive assay that provides the environment glioma cells encounter *in vivo*. Obviously, the complex organization of brain tissue cannot simply be mimicked by co-cultivation of involved cell types and ECM components. Thus, inspired by the field of electrophysiology, glioma research has exploited the organotypic *ex vivo* cultivation of murine brain slices (for reviews see Huang et al., 2012, Lossi et al., 2009). The well-preserved tissue of these brain slice cultures is used as a three-dimensional invasion matrix in which fluorescently labeled tumor cells are implanted and imaged (Aaberg-Jessen et al., 2013, Jung et al., 2002, Xu et al., 2016). However, the reported methods were based on human brain slices or could not accurately reflect the high infiltration capacity of glioblastoma cells *in vivo*. Thus, further optimization is required in order to obtain an invasion assay that enables the reliable and quantitative measurement of glioma cell migration using the standard laboratory equipment.

1.1.3 Models of glioblastoma

In order to identify and validate novel key players in glioblastoma development and progression we depend on models that mimic the disease of the patient. The variety of *in vitro* and *in vivo* glioblastoma models is large and strengths and weaknesses of the different models have to be evaluated in order to choose the most suitable model for the respective research question. In general, glioma models can be categorized as (i) *in vitro* glioma cell cultures derived from human or animal gliomas, (ii) animal models, mostly rodents, in which gliomas are induced by carcinogens, (iii) genetically engineered mouse models (GEMMs) in which gliomas arise due to

genetic deletions or transgene expression, (iv) immunocompetent allograft models that serve as recipients for murine- or rat glioma cell lines or (v) xenograft models, again mostly rodents, that serve as recipients for patient-derived glioma cell transplants (patient-derived xenografts, PDX).

This chapter will focus on *in vivo* techniques involving rodents. As these models certainly confer disadvantages, more and more 'exotic' glioma models dealing with zebra fish and drosophila are emerging. Elaborating these rather novel models would go beyond the scope of this work, however, detailed information is provided here (Read, 2011, Vittori et al., 2015).
The carcinogen-based method of glioma formation has been developed in the 1970s and includes the intracranial injection of the alkylating agent 3-methylcholantrene or intravenous injection of pregnant animals with a single dose of N-ethyl-nitrosourea (Ausman et al., 1970, Russell et al., 1979). Although this model reflects the genetic heterogeneity of human glioma tumors and also involves an intact immune system, it is rarely used nowadays due to its poor reproducibility and thus costly and time-consuming studies with high numbers of animals (Lenting et al., 2017). Still, these models have been a valuable tool in glioma research since their unpredictable character of glioma formation has stimulated researchers to generate *in vitro* cell cultures, such as the murine cell line GL261 (Ausman et al., 1970) and its rat counterpart C6 (Benda et al., 1968). These murine and rat glioma cell lines have been established as a common tool for orthotopic transplantations into syngeneic and thus immunocompetent animals making them indispensable for the study of the glioma microenvironment or immunology.

GEMMs and PDX represent the two major state-of-the-art *in vivo* models in glioma research. GEMMs comprise a large amount of models that are predominantly based on the global or brain-specific inactivation of one tumor suppressor either in combination with the overexpression of an oncogene or with the additional deletion of other tumor suppressors (reviewed in Hambardzumyan et al., 2011, Miyai et al., 2017). In general, GEMMs are suitable models to study many aspects in glioma biology, in particular glioma immunology and the influence of the stromal contribution to glioma formation by crossing in the respective genetic background. However, many of these models confer disadvantages like the lack of intratumor heterogeneity observed in human patients (Patel et al., 2014) since the tumors consist of cells with a number of specific homogeneous genetic aberrations. Furthermore, specific combinations of target genes and the target cell can result in an inefficient penetrance and latency (Costa et al., Xiao et al., 2002). Generally, latency represents one obstacle in the application of GEMMs for example in therapeutic studies, as the time point of tumor initiation cannot be controlled unless tumor cell isolates derived from these models are used in allotransplantations.

Besides allotransplantations, the xenotransplantation of human glioma cells into immunodeficient mice is a common tool in glioma research. This approach resulted from the attempt to work with glioma cells that more closely reflect the tumor in patients. The transplantation of established glioblastoma cell lines results in reproducible tumor growth with high engraftment rates. However, the usage of human cell lines can also be disadvantageous as some hallmarks of glioblastoma including hypervascularization and diffuse infiltrative growth cannot be achieved (Huszthy et al., 2012, Mahesparan et al., 2003). Moreover, the adaptation to the adherent growth conditions in serum-containing media can induce gene expression alterations, clonal selection, and genetic drift (Clark et al., 2010) resulting in immense differences between established cell lines and primary glioblastoma tumors on genomic and transcriptional level (Ernst et al., 2009, Li et al., 2008). The approach to simply switch from established cell lines that have been cultivated for several decades to short-term cultivated patient material has not completely resolved the issue. As previously shown, even short cultivation times in the presence of serum alters the gene expression profile and reduces heterogeneity of the cells (Ernst et al., 2009, Hamer et al., 2008, Lee et al., 2006). This can be circumvented by the immediate implantation of feshly obtained surgical glioma specimens into the recipient mouse (Claes et al., 2008) – which rules out any experimental manipulation of the cells before intracranial injection. Thus, to overcome the disadvantages accompanying cultivation in the presence of serum, alternative cultivation methods have been developed. The application of serum-free growth media supplemented with epidermal growth factor (EGF), fibroblast growth factor (FGFb), and insulin or the serum substitute B27 induces sphere growth, the enrichment of tumor-initiating cells and has proven to be a very successful cultivation method for a variety of brain tumors, including glioblastoma (Ernst et al., 2009, Lee et al., 2006). Importantly, these glioblastoma spheroid cultures of human primary material were found to retain the characteristic profile of the original tumor on a genomic and transcriptional level (Ernst et al., 2009, Hamer et al., 2008, Lee et al., 2006). Besides the genomic and translational conservation of glioblastoma spheroids, they possess the great advantage of forming tumors that display hallmarks of primary glioblastoma tumors, especially strong infiltrative growth (Huszthy et al., 2012). Thus, cell-based assays as well as patient-derived xenotransplantations involving spheroid cultures of primary glioblastoma material represent a promising tool to identify novel candidates that are involved in glioblastoma cell invasion and progression. One candidate that has been associated with glioblastoma cell migration is the transmembrane protein podoplanin (Grau et al., 2015, Peterziel et al., 2012). Noteworthy, this protein has also been found to be overexpressed in the mesenchymal signature of primary glioblastoma tumors, a signature that correlates with a poor outcome (Phillips et al., 2006). Further information on this protein and preliminary data that indicates its involvement in glioblastoma progression and tumor cell invasion is presented in the following chapter.

1.2 Podoplanin

1.2.1 Podoplanin – a glycoprotein with many functions

Podoplanin (PDPN) is a type-I integral membrane protein with diverse distribution in human and rodent tissues (see Table 1.1). PDPN was named according to its function in shaping kidney podocytes (Breiteneder-Geleff et al., 1997), however, as the protein has simultaneously been described in a variety of biological contexts it has received multiple names: T1α as it is expressed in type I alveolar cells (Rishi et al., 1995), gp40/gp36 derived from the fact that it is a 40kDa large glycoprotein with a 36kDa murine homolog (Zimmer et al., 1995, Zimmer et al., 1997), PA2.26 according to an antibody that targeted the protein in epidermal keratinocytes during chemical carcinogenesis and wound healing (Gandarillas et al., 1997); and aggrus due to its platelet aggregation-inducing function (Kato et al., 2003). The function of PDPN in physiology and pathology has not been fully understood, however, knockout studies in mice have discovered an essential role for PDPN in development. *Pdpn* knockout mice suffer from multiple developmental defects, including malformation of the lungs due to dysregulated proliferation and differentiation of type I alveolar cells. This hampers the correct inflation of lungs, which results in respiratory failure and perinatal lethality (Ramirez et al., 2003). Aberrations in cardiac development, in particular hyperplasia of several cardiac components, have been proposed to result from the abnormal epithelial-to-mesenchymal transition (EMT), a critical process in cardiac development that is possibly regulated by PDPN (Douglas et al., 2009). Furthermore, the constitutive knockout of *Pdpn* induces hemorrhages in the embryonic brain (Lowe et al., 2015) and impairs the separation of the lymphatic and blood vascular system (Bertozzi et al., 2010, Fu et al., 2008, Uhrin et al., 2010). Interestingly, although the loss of PDPN in a rat nephrosis model has been described to cause an aberrant morphology of kidney podocytes (Breiteneder-Geleff et al., 1997), no anomalies in kidney morphology or function have been reported for the murine knockout model.

The molecular mechanism of PDPN within above described developmental processes has largely remained unclear, however, as PDPN lacks a catalytical domain, it has to mechanistically function by protein-protein interactions (for described interaction partners see Table 1.2 and Figure 1.3). These interactions can occur via the three different domains of the protein; the large extracellular domain which is followed by a membrane spanning domain and a short cytoplasmic tail of 9 amino acids. The ectodomains of the human 162-amino acids large protein and its corresponding 172-amino acids mouse homolog (Martin-Villar et al., 2005) are highly glycosylated, with sialic acid, α-2,3 linked to galactose being the most prominent post-translational modification (Breiteneder-Geleff et al., 1999). Due to this extensively glycosylated mucin-like domain, PDPN

Table 1.1 Podoplanin expression in human and/or rodent tissue

Tissue	Cell type	Reference
Heart	Myocardial cells	Gittenberger-de Groot et al. (2007)
Lymphoid organs	Lymphatic endothelial cells (LECs)	Wetterwald et al. (1996), Scholl et al. (1999), Breiteneder-Geleff et al. (1999)
	Fibroblastic reticular cells (FRCs)	Schacht et al. (2005)
	Follicular dendritic cells	Schacht et al. (2005)
	Thymic epithelial cells	Farr et al. (1992)
	Macrophages (subpopulation)	Hou et al. (2010), Kerrigan et al. (2012)
	Th17 cells	Peters et al. (2011)
Angiosarcoma	*Angiosarcoma cells*	Breiteneder-Geleff et al. (1999)
Kidney	Podocytes	Breiteneder-Geleff et al. (1997), Scholl et al. (1999)
	Parietal epithelial cells of Bowman's capsule	Scholl et al. (1999)
Renal carcinoma	*Clear cell renal cell carcinoma cells*	Xia et al. (2016)
Bone	Mature osteoblasts and newly formed osteocytes	Wetterwald et al. (1996)
Osteosarcoma	*Osteosarcoma cells*	Wetterwald et al. (1996)
Cartilage	Chondrocytes	Smith and Melrose (2011)
Chondrosarcomas	*Chondrosarcoma cells*	Huse et al. (2007)
Brain	Cells of the ependyme and choroid plexus	Wetterwald et al. (1996), Scholl et al. (1999)
	Neural stem cells	Kotani et al. (2003)
	Glutamatergic neurons	Kotani et al. (2003)
	Reactive astrocytes	Kolar et al. (2015)
Brain cancer	*Glioma, ependymal tumor, and meningioma cells*	Mishima et al. (2006), Shibahara et al. (2006), Peterziel et al. (2012)
Lung	Alveolar type I cells	Rishi et al. (1995), Dobbs et al. (1988), Wetterwald et al. (1996), Scholl et al. (1999)
Lung cancer	*Lung squamous cell carinoma cells*	Kato et al. (2005)
Skin	Basal keratinocytes during cutaneous wound healing	Gandarillas et al. (1997)
	Dermal fibroblasts during cutaneous wound healing	Gandarillas et al. (1997)
	basal cells of sebaceous glands	Honma et al. (2012)
	hair follicles	Honma et al. (2012)
Skin cancer	*differentiated papillomas and skin carcinomas*	Gandarillas et al. (1997)
	Skin squamous cell carcinoma	Schacht et al. (2005), Martin-Villar et al. (2005)
Mesothelium	Pleural, pericardial and peritoneal mesothelial cells	Scholl et al. (1999), Ordonez (2005)
Mesothelioma	*Epithelioid mesothelioma cells*	Ordonez (2005), Kimura and Kimura (2005)
Others	*Germ cell tumors*	Schacht et al. (2005)
	Head and neck squamous cell carcinoma	Martin-Villar et al. (2005)
	Cancer associated fibroblasts	Kawase et al. (2008), Kitano et al. (2010)

has early been suggested to act as a receptor for selectins and lectins mediating anchoring of the cell in the ECM (Breiteneder-Geleff et al., 1999). In fact, one decade later PDPN has been identified to interact with galectin-8 facilitating the adhesion of lymphatic endothelial cells (LECs) to the ECM (Cueni and Detmar, 2009). Recently in a mouse model of corneal allogeneic transplantation, the interaction between PDPN and galectin-8 has been reported to induce pathological lymphangiogenesis in a complex interplay with vascular endothelial growth factor c (VEGFc) and integrins (Chen et al., 2016). Another lectin that has been identified to interact with PDPN is the C-type lectin-like receptor CLEC-2. This interaction is probably the best described one and revealed a function for PDPN in platelet aggregation and the development of the lymphatic vascular system. CLEC-2 is a type II transmembrane receptor that has originally been identified in immune cells (Colonna et al., 2000, Sobanov et al., 2001) and subsequently found to be expressed in platelets where it acts as the receptor for rhodocytin and PDPN (Suzuki-Inoue et al., 2006, Suzuki-Inoue et al., 2007). Binding between CLEC-2 and PDPN is facilitated by the sialylated platelet aggregation-stimulating (PLAG) domain, a conserved amino acid sequence (EDxxVTPG) in the extracellular domain of PDPN. In particular, it has been shown that the sialylation at Thr52 within the PLAG domain is critical for CLEC-2 and PDPN interaction and subsequent signaling events (Kaneko et al., 2007). The intercellular binding of platelet CLEC-2 and its ligand PDPN on the surface of LECs induces CLEC-2 multimerization and a subsequent phosphorylation cascade by SRC and SYK kinases that results in the activation of phospholipase C (PLC)γ2 and aggregation of platelets (Hughes et al., 2010, Suzuki-Inoue et al., 2006). The induction of platelet aggregation upon contact with LECs is a critical step in the separation of the lymphatic from the blood circulatory system during embryonic development. Mice harboring a global knockout of *Pdpn*, *Clec-2* or a hematopoietic-specific knockout of *Slp7* (involved in the downstream cascade of activated CLEC-2) have been reported to exhibit defects in lymphatic vessel patterning, lymphedema and disorganized and blood-filled lymphatic vessels at birth (Bertozzi et al., 2010, Fu et al., 2008, Uhrin et al., 2010). Furthermore, mice deficient for *Pdpn* exhibit neurovascular hemorrhages which are presumably unrelated to the defective lymphatic development because the lymphatic system is absent in the brain parenchyma (Louveau et al., 2015) and the cerebrovascular defects are observed before the manifestation of the global vascular separation failure (Lowe et al., 2015). Still, the correct maturation and integrity of the developing neurovasculature is based on the interaction of CLEC-2 and PDPN, as the authors have observed the same indistinguishable phenotype of cerebral hemorrhaging in both knockout animal models. *Pdpn* is widely expressed on neuro-epithelial cells in the developing neural tube and presumed to activate CLEC-2-dependent platelet aggregation during initial vascularization of the neural tube, which plugs the newly formed vessel walls and prevents hemorrhages. In

addition, the authors proposed that platelets-derived secreted molecules recruit pericytes and matrix components to stabilize and mature developing vessels (Lowe et al., 2015). Furthermore, the interaction between CLEC-2 and PDPN has been reported to play an important role in immunity, in particular in the interaction of dendritic cells and the lymph node microarchitecture. The interplay of CLEC-2 on activated dendritic cells and PDPN on LECs and fibroblastic reticular cells (FRCs) that are central elements of the lymph node, has been reported to promote dendritic cell migration and to decrease PDPN-mediated contractility in FRCs resulting in FRC relaxation and reduced tissue stiffness in favor of efficient T-cell trafficking (Acton et al., 2012, Astarita et al., 2015). In this respect, this finding revealed the novel and interesting fact that the CLEC-2-PDPN interaction also induces signaling in the *Pdpn* expressing cell and does not only impact on the *Clec-2* expressing compartment. Mechanistically, CLEC-2 has been proposed to compete with a lateral interaction partner for binding the extracellular domain of PDPN, which inhibits signaling activation of key contractility regulators in the *Pdpn* expressing cell (Astarita et al., 2015). Although the lateral binding partner that induces contractility in absence of CLEC-2 has not been identified, the authors suggested the transmembrane proteins CD9 and CD44 that have previously been described to interact with PDPN (Astarita et al., 2015).

CD9, a tetraspanin protein, has been shown to form multimeric complexes with intergrins, and other proteins including PDPN, acting context- and cell type- dependent on intergrin signaling, cell adhesion and cell migration (for review see Zoller, 2009). In a tail vein injection model, ectopic expression of *CD9* in PDPN positive HT1080 fibrosarcoma cells has been shown to decrease the formation of pulmonary metastases (Nakazawa et al., 2008). Although CD9 has been reported to not directly affect the binding between PDPN and CLEC-2, CD9 expression clearly decreased the platelet aggregation capacity of the tumor cells, presumably by the inhibition of CLEC-2 multimerization. As coverage by aggregated platelets protects circulating tumor cells from shear stress and facilitates adhesion of cancer cell clusters to the vascular endothelium for extravasation, the suppression of the metastatic growth is most likely based on the decreased platelet aggregation capacity of the *CD9* and *PDPN* co-expressing tumor cells.

The standard isoform of CD44, which is expressed in a great variety of cell types in physiology and pathology, has been reported to interact with the ectodomain of PDPN (Martin-Villar et al., 2010). This interaction has furthermore been shown to promote directional migration of MDCK cells, however, the underlying molecular mechanisms have not been unraveled.

Table 1.2 Interaction partners of podoplanin

Interaction	PDPN$^+$ cell	Interacting cell	Interaction partner	Reported function	Reference
trans	LECs	Platelets	CLEC-2	Platelet activation	Suzuki-Inoue et al. (2006), Suzuki-Inoue et al. (2007)
				Separation of blood and lymphatic endothelial system	Uhrin et al. (2010), Bertozzi et al. (2010)
trans	LECs	Neuro-epithelium	CLEC-2	Cerebrovascular integrity	Lowe et al. (2015)
trans	FRCs, LECs	Dendritic cells	CLEC-2	Motility and homing of dendritic cells,	Acton et al. (2012)
				Relaxation of lymph node	Astarita et al. (2015)
trans	LECs	Unknown, ECM	Galectin-8	LECs anchoring into the surrounding ECM	Cueni and Detmar (2009)
				Pathological lymphangiogenesis	Chen et al. (2016)
cis	LECs	-	CCL21	Perilymphovascular CCL21 gradient formation required for the directed migration of CCR7+ cells	Kerjaschki et al. (2004)
cis	MDCK (ectopic expr.)	-	CD44	Directional cell migration	Martin-Villar et al. (2010)
cis	HT1080 fibrosarcoma cell line	-	CD9 (ectopic expr.)	Inhibition of platelet aggregation and metastasis formation	Nakazawa et al. (2008)
cis	MDCK (ectopic expr.)	-	ERM	Connection to cytoskeleton/EMT	Martin-Villar et al. (2006)

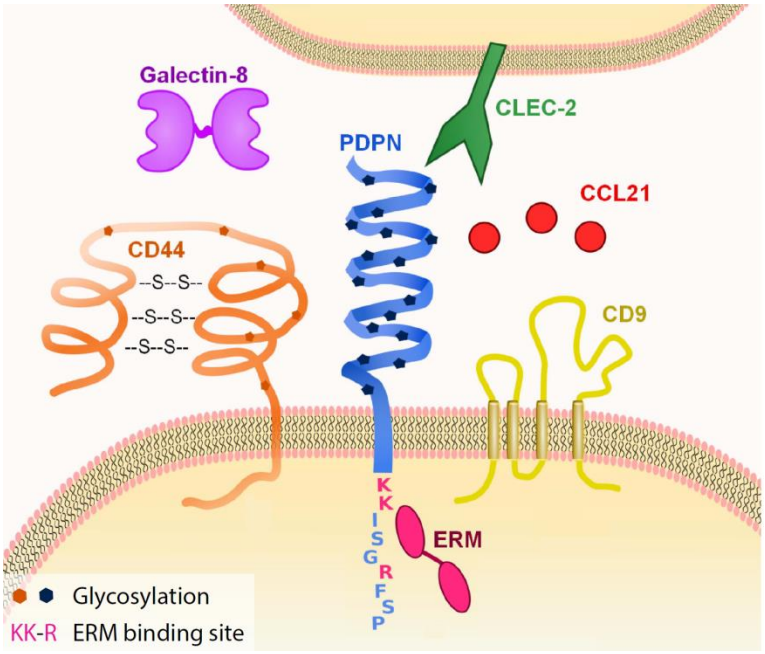

Figure 1.3 Schematic illustration of podoplanin and its interaction partners.
PDPN has been shown to interact via different domains with several proteins including CLEC-2, galectin-8, CD44, CD9, CCL21 and ERM proteins. Depending on the cell type and interaction partner, the binding can occur in a cis- or trans-acting manner presumably affecting both involved cell types.

Adapted from Astarita et al. (2012).

The chemokine CCL21 has been reported as another interaction partner of PDPN. In the rejection process of human kidney transplants, PDPN has been shown to form complexes with CCL21 on the basal cell membrane of LECs that are shed into the perivascular stroma forming a perilymphovascular CCL21 gradient for the attraction of CCR7 positive immune cells (Kerjaschki et al., 2004). The authors have not elaborated on the mechanism of shedding, however, the extracellular domain of PDPN has predicted cleavage sites for trypsin, elastase, calpain-2, and metalloproteases (MMPs), most of which are protected by O-glycans from proteolytic degradation (Pan et al., 2014, Yurrita et al., 2014). In addition to the ectodomain, the transmembrane domain of PDPN has been reported as a proteolytic target (Yurrita et al., 2014). The metalloprotease-mediated cleavage of the extracellular domain generates a truncated membrane-bound fraction that is further cleaved by the presenilin-1/γ-secretase within the transmembrane domain (Yurrita et al., 2014). As the intracellular domain of PDPN is released into the cytosol it has been speculated to act as a signaling molecule, like notch or CD44, whose intracellular domains function as co-transcription factors, when released by γ-secretase cleavage (Thorne et al., 2004). However, this process would be expected to be a highly regulated event. Though, the authors have shown that the proteolytic processing of PDPN is not induced by an external signal, but occurs instead constitutively in HEK293T and MDCK cells. This suggests that γ-secretase-dependent proteolysis is involved in regulating the stability and half-life of PDPN rather than in generating an intracellular/intranuclear signaling peptide. Comprising nine amino acids, the intracellular domain of PDPN is rather short, still it contains a basic recognition pattern that has been shown to play an essential role in the recruitment of ezrin and radixin, members of the ezrin, radixin and moesin (ERM) protein family (Martin-Villar et al., 2006). The recruitment of ezrin and moesin is followed by the local increase and activation of RhoA. The increased RhoA activity and concomitant activation of the RhoA-associated kinase (Rock) has been reported to induce the phosphorylation and stabilization of PDPN attached ERM proteins in an open and active conformation. Activated ERM proteins remodel the actin cytoskeleton by linking it to the membrane-bound PDPN protein preparing the cell for migration. Besides the impact on the actin cytoskeleton, the binding of ERM proteins to PDPN has been shown to be essential for the RhoA-mediated induction of EMT in MDCK cells, which further accelerates cell migration (Martin-Villar et al., 2006). However, the intracellular domain of PDPN has also been shown to inhibit cell migration. Results from recent studies have indicated that phosphorylation of serine residues in the cytoplasmatic tail by cyclin dependent kinase 5 (CDK5) and protein kinase A (PKA) inhibit cell motility (Krishnan et al., 2013, Krishnan et al., 2015). Whether these phosphorylation events interfere with the recruitment of ERM proteins or whether migration is suppressed by another mechanism has not been explored.

1.2.2 Transcriptional regulation of podoplanin

As PDPN is present in a variety of cell types, its expression is expected to be regulated by multiple tissue- and context-specific signaling pathways and transcription factors. Indeed, studies on the human, rat and murine promoter of podoplanin revealed binding sites for numerous transcription factors (as reviewed in Renart et al., 2015). *In vitro*, multiple factors have been found to be involved in the transcriptional control of podoplanin, including normal differentiation transcription factors as well as pro-tumorigenic signaling pathways and pro-inflammatory cytokines.

Under physiological conditions, PROX1, a master regulator in the program of lymphatic endothelial cell differentiation, has been shown to induce *Pdpn* expression in LECs (Hong et al., 2002). The discovery of PROX1 positive, but PDPN negative endothelial cells of a lymphatic-like drainage canal in the eye (Schlemm's canal) however questioned whether PROX1 is sufficient for *Pdpn* expression (Kizhatil et al., 2014).

In malignant conditions, *Pdpn* seems to be primarily regulated by the activator protein 1 (AP-1) transcription factor (Durchdewald et al., 2008, Kunita et al., 2011, Peterziel et al., 2012). *Pdpn* upregulation in src-transformed murine brain cells has been reported to result most likely from the activation of AP-1 downstream of the adapter protein cas (Shen et al., 2010). In human glioblastoma samples, it has been shown that the AP-1-mediated activation of *PDPN* expression is dependent on the loss of *PTEN*, which negatively regulates the PI3K-AKT-AP-1 axis (Peterziel et al., 2012). Aberrant activation of PI3K as well as overexpression of *PDPN* signaling has been found in the majority of glioblastoma tumors (Cancer Genome Atlas Research, 2008, Ernst et al., 2009), which suggests that the transcriptional regulation of *PDPN* in glioblastomas largely occurs via the PI3K-mediated activation of AP-1. Alternatively, *PDPN* expression can be controlled on the epigenetic level as the hypermethylation of the *PDPN* promoter has been found to repress *PDPN* in glioblastoma (Peterziel et al., 2012). Studies on fibrosarcoma and human keratinocytes have showed a SMAD-mediated increase in *PDPN* expression upon TGF-β1 treatment (Honma et al., 2012, Suzuki et al., 2008). Furthermore, *PDPN* expression in keratinocytes (during wound healing or in psoriasis) has been shown to be controlled by the signal transducer and activator of transcription 3 (STAT3) that is activated in response to interferon γ (IFNγ). Similarly, STAT3 has been reported to induce *Pdpn* expression in glioblastoma (Priester et al., 2013). Considering the frequent aberrant activation of STAT3 in glioblastoma that contributes to tumor cell proliferation (Sherry et al., 2009) and TMZ resistance (Kohsaka et al., 2012), STAT3 appears together with AP-1 transcription factors as a major regulator of *PDPN* in malignant glioma.

1.2.3 Podoplanin in the physiologic and neoplastic brain

High PDPN protein levels have been detected in the developing nervous system of the mouse, particularly in the early neural tube, reaching its peak at about embryonic day 16. Subsequently, gene expression has been reported to be down regulated in neural tissue (Williams et al., 1996), with the exception of the choroid plexus, the ependyme (Tomooka et al., 2013, Williams et al., 1996), neural stem cells and glutamatergic neurons (Kotani et al., 2003). The function of PDPN in the developing neural tissue has recently been identified as introduced above; the presence of PDPN in the embryonic neuro-epithelium induces CLEC-2-dependent platelet aggregation in newly formed vessels, which contributes to the sealing of the vessel walls and recruitment of pericytes (Lowe et al., 2015). However, the role of PDPN in the adult brain, specifically in the choroid plexus, the ependyme and neural stem cells, has not been unraveled yet. Ependymal cells are ciliated glial cells that line the ventricles of the brain and the central canal of the spinal cord, circulating the cerebrospinal fluid (CSF) within the ventricular system, subarachnoid space and spinal cord. Together with cells of the choroid plexus, a specialized ependymal tissue, they produce the CSF and regulate the intracranial pressure (for review see Jimenez et al., 2014). Interestingly, PDPN is also abundant in the ciliary epithelium of the rat eye and thus, PDPN has been speculated to modulate the process of active ion transport and water fluxes or cilia movement (Williams et al., 1996). Yet, no study has investigated the role of PDPN in ependymal or other ciliated cells. Similarly, the expression of *Pdpn* in neural stem cells has not been pursued further. However, preliminary results from our research group have shown that also the motile neural progenitor cells express *Pdpn*. These neuronal precursor cells migrate along the rostral migratory stream to the olfactory bulb in order to differentiate into GABAergic (PDPN negative) interneurons constituting the highly developed olfactory sense in rodents. Considering previous publications that associated PDPN with cell migration (Martin-Villar et al., 2006, Wicki et al., 2006, Scholl et al., 1999), PDPN could promote migration of the highly motile progenitor cells.

Astrocytes have been reported to be negative for *Pdpn* expression (Kotani et al., 2003), unless they become activated by CNS insults like injury, ischemia or tumor growth (Kolar et al., 2015). The reactive state of astrocytes is characterized by changes in the morphology, metabolism and the repertoire of secreted messenger molecules. Together with activated microglia, reactive astrocytes are, dependent on the grade of the stimulus, frequently organized in a dense mesh around the insult. The function of this glial scar is context dependent and can have both beneficial and detrimental effects on the course of the disease (for reviews see Burda and Sofroniew, 2014, Pekny et al., 2016). How PDPN influences the reactive state and function of astrocytes has not been addressed yet and presents an interesting and relevant research topic, as reactive astrocytes

are involved in multiple CNS pathologies like stroke, migraine, neuroinflammation, epilepsy and brain tumors. Reactive astrocytes are not the only cells in the brain tumor microenvironment that have been identified to express *Pdpn*. Tumor-associated myeloid cells have been shown to express podoplanin (Engler et al., 2012, Szulzewsky et al., 2015). In addition to tumor-associated myeloid cells also subsets of inflammatory myeloid cells have previously been shown to be PDPN positive (Hou et al., 2010, Kerrigan et al., 2012), however, the function has not been further investigated.

Besides cells of the brain tumor microenvironment, CNS neoplasms themselves have been shown to express *PDPN* (Mishima et al., 2006, Scrideli et al., 2008, Shibahara et al., 2006) – like multiple other cancer types (Table 1.1). We and others have recently shown a correlation between high *PDPN* expression, the grade of astrocytoma tumors and poor survival (Ernst et al., 2009, Mishima et al., 2006, Peterziel et al., 2012). Specifically, a strong *PDPN* expression has been detected in 85% of primary glioblastomas, whereas secondary glioblastomas and the majority of grade II and III gliomas have shown weak or no expression (Ernst et al., 2009). Furthermore, the effect of RNA interference (RNAi)-mediated down-modulation (Ernst et al., 2009, Peterziel et al., 2012) or ectopic overexpression (Grau et al., 2015) of *PDPN* on invasion and proliferation has been examined. Although several publications have reported contrary or no effects on proliferation, they have consistently shown a pro-migratory effect of PDPN in glioblastoma cells using two-dimensional-wound healing and three- dimensional collagen invasion assays (Ernst et al., 2009, Grau et al., 2015, Peterziel et al., 2012). This is in line with previous observations of other tumor entities like lobular breast cancer and squamous cell carcinomas, where up to 80 % have been reported to express *PDPN* predominantly at the invasive front (Martin-Villar et al., 2005, Wicki et al., 2006). Despite the fact that PDPN has been associated with *in vitro* migration of different cell lines (Grau et al., 2015, Li et al., 2015, Martin-Villar et al., 2010, Peterziel et al., 2012) and the correlation of high *PDPN* expression with poor survival in malignant glioma and oral squamous cell carcinoma (OSCC) (Mishima et al., 2006, Nakashima et al., 2013, Peterziel et al., 2012), no *in vivo* study has been conducted to ultimately proof the role of PDPN in invasion and malignant progression. The only published functional *in vivo* study has dealt with the ectopic expression of *Pdpn* in a pancreatic carcinoma model which has resulted in a higher incidence of invasive tumors (Wicki et al., 2006). However, the relevance of this study seems controversial since *PDPN* expression has not been reported for pancreatic carcinoma.

To conclude, the function of PDPN in the adult brain, where it is expressed by specific cell types and neoplasms, has not been clarified yet. *In vitro* studies involving cell lines of glioblastoma and

other tumor entities have indicated a pro-migratory function for PDPN. Experimental animal work necessary for a clear statement about the pathological function of PDPN as well as its clinical suitability for cancer therapy is currently missing.

1.3 Aim of the study

Previous work of the past decades has revealed an indispensable role for PDPN in the embryonic and perinatal development and certainly provided mechanistic insight into the formation and function of lymphatic tissue. Still, the detailed function of PDPN remains unclear for many tissues and cancer entities including malignant glioma. As the correlation of *PDPN* expression with malignant progression of gliomas implies, the protein is especially abundant in high grade glioblastoma tumors. Few studies have investigated PDPN in glioblastoma and associated the protein with a migratory and proliferative cell behavior. As cell invasion remains a major hurdle in glioblastoma therapy, the interest in PDPN as a therapeutic target has raised. However, necessary *in vivo* validations of its proposed migratory function as well as mechanistic studies are still lacking. Recent efforts to unravel the molecular downstream processes in the *PDPN* expressing cell were mostly based on overexpression studies in tumor cells of other entities. However, it is important to critically evaluate whether the obtained data can be reliably extrapolated to other cell types and moreover to the *in vivo* situation. As we lack detailed insight into the biological and mechanistic function of PDPN in glioblastoma cells, this study aimed at closing this gap of knowledge.

(i) For this purpose, serial xenotransplantations and fluorescence activated cell sorting experiments of primary human glioblastoma material were performed to validate the previously published correlation of PDPN and malignant progression and to identify underlying mechanisms.

(ii) In a functional approach, this study pursued the question whether PDPN represents an attractive therapeutic target. Therefore, the impact of PDPN on survival, tumor growth and tumor cell invasion was investigated by the CRISPR/Cas9-mediated deletion of *PDPN* in human glioblastoma cells and subsequent orthotopic xenotransplantations.

(iii) Moreover, due to the lack of a reliable and standardized invasion assay, this work optimized the co-cultivation of tumor cells and organotypic brain slices which represent an invasion matrix that closely mimics the *in vivo* situation and allows for a reliable assessment of glioblastoma cell invasion.

2 MATERIALS

2 MATERIALS

2.1 Equipment

Agilent 2100 Bioanalyzer	Agilent Technologies, Berlin
Binocular M10	Leica, Wetzlar
Cell culture sterile hood	Hera Safe Thermo Fisher Scientific, USA
Cell incubator	Heraeus, Hanau; Binder, Tuttlingen
Centrifuge Megafuge 1.0	Heraeus, Hanau
Centrifuge Varifuge 3.0 R	Heraeus, Hanau
Centrifuge Biofuge 13	Heraeus, Hanau
Centrifuge Heraeus Fresco17	Thermo Fisher Scientific, USA
Centrifuge Megafuge 3.0R	Heraeus, Hanau
Cold light source KL1500	Schott, Mainz
Cryo freezing container	Nalgene; Thermo Fisher Scientific, USA
Developer Classic E.O.S.	Agfa, USA
Electrophoresis chamber for agarose gels	PeqLab, Erlangen
Electrophoresis chamber for SDS-PAGE	Bio-Rad Laboratories, Munich
Embedding machine	Vogel, Gießen
FACSAria™ I cell sorter	Becton Dickinson Biosciences, Heidelberg
FACSAria™ II cell sorter	Becton Dickinson Biosciences, Heidelberg
FACSAria™ Fusion cell sorter	Becton Dickinson Biosciences, Heidelberg
FACS Calibur™	Becton Dickinson Biosciences, Heidelberg
Fine scales	Mettler Toledo, Gießen
Gooseneck lamp	Th. Geyer, Renningen
Hamilton syringe Nanofil	World Precision Instruments, Berlin
Hamilton syringe 701N, 10µl, 26s/51/3	Hamilton, USA
Heating mat	Conrad Electronic, Mannheim
Magnetic stirrer/heat plate	Sigma-Aldrich, Munich
Magnetic stirrer/heat plate MR 3001K	Heideloph, Schwabach
Microplate reader Clario Star	BMG Labtech, Ortenberg
Microscope Nikon Eclipse Ti	Nikon, Düsseldorf
Microscope Olympus IX81	Olympus, UK
Microscope Leica DMLB	Leica, Wetzlar

Microtome RM 2155	Leica, Bensheim
Minishaker Ika® Model MS1	Sigma-Aldrich, Munich
NanoDrop 1000 Spectrophotometer	PeqLab, Erlangen
Needle, 34 gauge beveled	World Precision Instruments, Berlin
Orbital shaker, Minishaker MS1	Ika Labortechnik, Staufen
pH-meter	Knick, Berlin
Pipets, Pipetman	Gilson, USA
Pipettor Pipetboy acu	Integra Biosciences, Switzerland
Pipettor accujet pro	Brand, Wertheim
Platform shaker Polymax 2040	Heidolph, Schwabach
Power supply Power Pac 300/3000	Bio-Rad Laboratories, Munich
Robot Stereotaxic	Neurostar, Tübingen
Rotator/Shaker	Rotoshake Genie Scientific Industries, USA
Scales	Sartorius, Göttingen
Shaker Multitron	Infors, Bottmingen, Schweiz
StepOnePlus Real-time PCR system	Applied Biosystems, UK
Surgical tools	Fine Science Tools, Heidelberg
Thermocycler PTC-200	MJ Research, USA
Thermocycler MJ Mini	Bio-Rad Laboratories, Munich
Thermomixer 5437	Eppendorf, Hamburg
Water baths	GFL, Burgwedel
Wet blot transfer system	Sigma, Deisenhofen

2.2 Consumables

Bone wax	Braun, Melsungen
Cell culture plates	Corning, USA and Greiner, Frickenhausen
Cell culture vessels	Sigma Aldrich, USA
Cell strainer (70 µm)	Becton Dickinson Biosciences, Heidelberg
Conical centrifuge tubes 15ml, 50ml	Corning, USA
Cover glasses	Menzel-Gläser, Braunschweig
Cryo vials	Thermo Fisher Scientific, USA
Disposible scalpel	Feather, Japan

Filter pipet tips 10 µl, 20 µl, 200 µl, 1000 µl	Neptune, USA; Nerbe plus, Winsen/Luhe
Hydrophobic Barrier PAP Pen ImmEdge	Vector Laboratories, USA
Insuline syringe U-100	Becton Dickinson Biosciences, Heidelberg
MicroAmp 96-Well Optical Adhesive Film	Applied Biosystems, UK
MicroAmp® fast optical 96-well reaction plate	Applied Biosystems, UK
Millicell Cell Culture Insert, PTFE, 0.4 µm	Merck, Darmstadt
Needles (23G, 25G, 26G, 27G)	Dispomed Witt oHG, Gelnhausen; Braun, Melsungen
Object slides SuperFrost Plus	Thermo Fisher Scientific, USA
Octenisept alcohol free disinfectant	Schülke, Nordersted
Opitran BA-S83 Nitrocellulose membrane	GE Helthcare, Munich
Parafilm PM996	Bemis flexible packaging, USA
Pasteur pipets	WU, Mainz
PCR reaction tubes (8-well stripes)	Nerbe plus, Winsen/Luhe
Pipets plastic 5 ml, 1 ml,	Sigma Aldrich, USA
Pipet tips 10 µl, 20 µl, 200 µl, 1000 µl	Steinbrenner, Wiesenbach
Pre-cast SDS RunBlue protein gels 10%	Expedeon, USA
Reaction tubes 1.5 ml, 2 ml	Eppendorf, Hamburg
Round-bottom 96-well plates	Greiner Bio-one, Frickenhausen
Sugi swabs	Kettenbach, Eschenburg
Surgical suture 3/8 circle, DS12mm, USP 6/0	SMI, Belgium
Syringe filters 0.22 µm	Renner, Darmstadt
Syringe filters 0.45 µm	TPP, Switzerland
Western blot membrane Optitran BA-S83	Schleicher & Schüll, Dassel
Whatman 3 MM paper	Whatman, Dassel
X-ray films	Fuji, Düsseldorf

2.3 Software

Adobe Illustrator	Adobe Systems, USA
BD CellQuest ProTM	Becton Dickinson Biosciences, Heidelberg
BD FACSDiva™ Software	Becton Dickinson Biosciences, Heidelberg
CRISPR design tool, http://crispr.mit.edu/	Feng Zhang group at MIT Boston, USA

EndNote v.X7	Adept Scientific GmbH, Frankfurt
FlowJo v.10	Tree Star, Inc., Ashland, USA
Graphpad Prism	GraphPad Software, Inc., La Jolla, USA
ImageJ	National Institutes of Health, USA
NIS Elements AR 4.13.04	Nikon, Darmstadt
Office 2010	Microsoft, USA
Primer blast, https://www.ncbi.nlm.nih.gov/tools/primer-blast/	National Institutes of Health, USA
StepOne Software v.2.2.2	Life Technologies, Darmstadt

2.4 Chemicals and reagents

Agarose	Roth, Karlsruhe
Bacto agar	Roth, Kalsruhe
Boric acid	Sigma-Aldrich, Munich
Bovine serum albumin fraction V	PAA, Austria
β-Mercaptoethanol	Merck, Darmstadt
Calcium chloride	Merck, Darmstadt
Citric acid	Sigma-Aldrich, Munich
Desoxynucleotide triphosphates	Bioron, Ludwigshafen
Dimethylsulfoxide (DMSO)	Sigma-Aldrich, Munich
Disodium phosphate (Na_2HPO_4)	Sigma-Aldrich, Munich
Enhanced Chemiluminescence Substrate	PerkinElmer, USA
Eosin B	Merck, Darmstadt
Ethanol (EtOH)	Fisher Scientific, UK
Ethanolamine	Merck, Darmstadt
Ethidiumbromide	AppliChem, Darmstadt
Ethylenediamine-tetraacetate (EDTA)	Roth, Karlsruhe
Eukitt	Kindler, Freiburg
Gelatine	Merck, Darmstadt
Glycerol	Roth, Karlsruhe
Glycine	AppliChem, Darmstadt
Hematoxylin	Roth, Kalsruhe

HEPES	Sigma-Aldrich, Munich
Hoechst 33342	Biomol, Hamburg
Hydrogen peroxide	Merck, Darmstadt
Isopropanol (2-Propanol)	Sigma-Aldrich, Munich
Jasplanikolide	Cayman Chemicals, USA
Lithium dodecyl sulfate sample buffer RunBlue 4x	Expedeon, USA
Manganese(II) sulfate ($MnSO_4$)	Sigma-Aldrich, München
Methanol	Merck, Darmstadt
Milk powder	Roth, Karlsruhe
Monosodium phosphate (NaH_2PO_4)	Sigma-Aldrich, Munich
Nuclease-free water	Invitrogen, Kalsruhe; Qiagen, Hilden
Paraffin	Vogel, Giessen
Paraformaldehyde	Roth, Karlsruhe
Polyethylenimin, linear, MW 25.000	Alfa Aesar, USA
Potassium chloride (KCl)	Roth, Karlsruhe
Qiagen RNeasy Mini-Kit	Qiagen, Hilden
SDS Run Buffer RunBlue 20x	Expedeon, USA
Sodium chloride (NaCl)	Fluka Chemicals, Switzerland
Sodium dodecylsulfate (SDS)	Gerbu Biotechnik, Gaiberg
Sodium deoxycholate	Sigma-Aldrich, Munich
Sodium hydroxyde (NaOH)	VWR, Belgium
Tris-base	Roth, Karlsruhe
Tris-hydrochloride (Tris-HCl)	Roth, Karlsruhe
Triton-X-100	AppliChem, Darmstadt
Trypan blue	Sigma-Aldrich, Munich
Tween-20	AppliChem, Darmstadt
Vectastain Elite-ABC-Peroxidase	Vector Laboratories, USA
Xylene	AppliChem, Darmstadt

2.5 Biomolecular reagents and enzymes

Cyanase	Serva GmbH, Heidelberg
DNAse I	Sigma-Aldrich, München

GeneRuler 100 bp DNA ladder	Thermo Fisher Scientific, USA
GeneRuler DNA ladder mix	Thermo Fisher Scientific, USA
Goat serum	Vector Laboratories, USA
Oligo(dT) primers	Thermo Fisher Scientific
PeqGOLD protein marker IV, pre-stained	PeqLab, Erlangen
Phosphatase inhibitor mix II	Serva GmbH, Heidelberg
Power SYBR Green PCR Master Mix	Applied Biosystems, UK
Protease inhibitor cocktail	Roche, Mannheim
Proteinase K	Sigma-Aldrich, Munich
Random hexamers	Thermo Fisher Scientific, USA
RNase ZAP	Sigma-Aldrich, Munich
Revertaid M-MuLV Reverse Transcriptase	Thermo Fisher Scientific, USA
Revertaid M-MuLV buffer	Thermo Fisher Scientific, USA
Ribolock RNase inhibitor	Thermo Fisher Scientific, USA
RQ1 RNase-free DNase	Promega, Mannheim
RQ1 RNase-free DNase buffer	Promega, Mannheim
Terminal deoxynucleotidyl transferase	New England Biolabs, USA

2.6 Buffers and solutions

Table 2.1 Composition of buffers

Buffer	Composition
FACS buffer	1% BSA/PBS
IHC blocking buffer	0.1% BSA/PBS 5% goat serum
IHC antigen retrieval citrate buffer	1.8 mM citric acid 8.2 mM sodium citrate
PBS, 10x (pH = 7.2)	1.5 M NaCl 27 mM KCl 82 mM Na_2HPO_4 x 2 H_2O 17 mM NaH_2PO_4 x H_2O
RIPA buffer	50 mM Tris-HCl, pH 8.0 150 mM NaCl 0.1 % SDS 0.5% sodium deoxylacid 1% NP-40
TBE, 10x	1 M Tris 1 M Boric acid 20 mM EDTA
TBS, 10x (pH = 7.6)	61 g Tris base 160 g NaCl

Western Blot blocking buffer	5% milk/PBS 0.5% Tween
Western Blot transfer buffer	25 mM glycine 0.15% ethanolamine 25% methanol

2.7 Oligonucleotides

Table 2.2 Primers used for qRT-PCR

Target	Sequence	Efficiency	Reference
PDPN_FW	TGACTCCAGGAACCAGCGAAG	1.87	Inoue et al. (2012)
PDPN_RV	GCGAATGCCTGTTACACTGTTGA		
IPO8_FW	TGCATATTGTAGCTCGGCTCT	1.87	
IPO8_RV	AATGAACCACCCCTTGGTTG		
TBP_FW	GAGCTGTGATGTGAAGTTTCC	2.02	Valente et al. (2009)
TBP_RV	TCTGGGTTTGATCATTCTGTAG		
APOE_FW	CTTGAGTCCTACTCAGCCCC	1.75	
APOE_RV	AATCCCAAAAGCGACCCAGT		
BNIP3_FW	TGGACGGAGTAGCTCCAAGA	1.82	
BNIP3_RV	AAAGAGGAACTCCTTGGGGG		
DKK3_FW	ACAGCCACAGCCTGGTGTA	1.89	Gu et al. (2011)
DKK3_RV	CCTCCATGAAGCTGCCAAC		
H19_FW	TGCTGCACTTTACAACCACTG	1.95	Matouk et al. (2007)
H19_RV	ATGGTGTCTTTGATGTTGGGC		
MGP_FW	ATGAATCACATGAAAGCATGGAA	1.94	
MGP_RV	GAGCGTTCTCGGATCCTCTC		
COL20a1_FW	TGACCACCAAGAAAGCTCCC	1.76	
COL20a1_RV	ATCTGGTAGACAAGCACGCC		
SPP1_FW	CCCACAGACCCTTCCAAGTA	1.86	
SPP1_RV	GCAGGTCCGTGGGAAAATCA		
CD44_FW	TACAGCATCTCTCGGACGGA	1.90	
CD44_RV	CACCCCTGTGTTGTTTGCTG		
NRCAM_FW	TGAAGACTTGGTACAGCCTCC	1.74	
NRCAM_RV	CTCAGCTTTCCCTTCGCTCA		
TIAM2_FW	GAGCTTGTGGACACAGAGAAGT	1.95	
TIAM2_RV	AGAGCCTCCAAGGGAAAACAG		
SNAI2_FW	TGCGATGCCCAGTCTAGAAA	1.88	Schrader et al. (2015)
SNAI2_RV	AAAAGGCTTCTCCCCCGTGT		

Table 2.3 Sequences of guide RNAs

Target	Sequence 5’ - 3’
PDPN exon 2	CACCG**AGACTTATAGCGGTCTTCGC**
Renilla luciferase	CACCG**GGTATAATACACCGCGCTAC**

Table 2.4 Sequences of short hairpin RNAs

Target	Sequence 5' - 3'
PDPN (sh5αPDPN) (TRC-61926)	CCGGCAACAACTCAACGGGAACGATCTCGAGATCGTTCCCGTTGAGTTGTTGTTTTTG
Non-target	Sigma #SHC002V

2.8 Plasmids

Table 2.5 List of plasmids

Name	Company
MISSION® pLKO.1-puro	Sigma-Aldrich, USA
lentiCRISPR v2	Addgene #52961
pCMV-VSV-G	Addgene #8454
psPAX2	Addgene #12260

2.9 Antibodies

2.9.1 Primary antibodies

Table 2.6 Antibodies used for flow cytometry

Antigen	Clone	Concentration	Company/catalog number
PDPN	NC-08	5 µl/million cells	Biolegend; #337008
HLA	W6/32	5 µl/million cells	Biolegend; #311413; 311414
CD11b	M1/70	1:100	BD Pharmingen #5533121
PDGFRβ	18A2	5 µl/million cells	Biolegend #323608
CD31	WM59	5 µl /million cells	ebioscience #11-0319
CD45	HI30	5 µl /million cells	Biolegend #304018

Table 2.7 Antibodies used for Western blotting

Antigen	Species	Dilution	Company/catalog number
PDPN	mouse	1:1000	Covance; #SIG-3730
Cyclophilin A	rabbit	1:1000	Cell signaling; #2175S

Table 2.8 Antibodies used for immunohistochemistry and immunofluorescence

Antigen	Species	Dilution	Antigen retrieval	Company/catalog number
PDPN	mouse	1:100	EDTA/citrate	Covance; #SIG-3730
Stem121	mouse	1:1000	EDTA	Cellartis/Takara; #Y40410
Ki67	rabbit	1:500	EDTA	Abcam; #ab15580
Laminin	rabbit	1:100	Proteinase K	Progen; #10765

2.9.2 Secondary antibodies

Table 2.9 Secondary antibodies used for Western blotting

Antigen	Species	Dilution	Conjugate	Company/catalog number
Mouse IgG	horse	1:5000	HRP	Cell Signaling; #7076S
Rabbit IgG	goat	1:5000	HRP	Cell signaling; #7074S

Table 2.10 Secondary antibodies used for immunohistochemistry and immunofluoresence

Antigen	Species	Dilution	Conjugate	Company/catalog number
Mouse IgG	goat	1:500	biotin	Vector Laboratories; #BA-9200
Rabbit IgG	goat	1:500	biotin	Vector Laboratories; #BA-1000

2.10 Cell lines and primary cultures

Table 2.11 Primary human glioblastoma cultures

Name	Provenience	Comment
NMA7	Martín-Villlalba lab, DKFZ Heidelberg	Long-term primary culture
NMA50	Martín-Villlalba lab, DKFZ Heidelberg	Long-term primary culture
NMA59	Martín-Villlalba lab, DKFZ Heidelberg	Long-term primary culture
NMA65	Martín-Villlalba lab, DKFZ Heidelberg	Long-term primary culture
GBM10	Martín-Villlalba lab, DKFZ Heidelberg	Long-term primary culture
GBM13	Martín-Villlalba lab, DKFZ Heidelberg	Long-term primary culture
GBM30	Martín-Villlalba lab, DKFZ Heidelberg	Long-term primary culture
T1132	Apogenix, Heidelberg	Long-term primary culture
MNOF1300	Mittelbronn lab, Edinger-Institute, Frankfurt	Primary culture
GBMF1	Angel lab, DKFZ Heidelberg	Primary culture
GBMF2	Angel lab, DKFZ Heidelberg	Primary culture
GBMF3	Angel lab, DKFZ Heidelberg	Primary culture
GBMF5	Angel lab, DKFZ Heidelberg	Primary culture
GBMF6	Angel lab, DKFZ Heidelberg	Primary culture
GBMF8	Angel lab, DKFZ Heidelberg	Primary culture
GBMF9	Angel lab, DKFZ Heidelberg	Primary culture
GBMF10	Angel lab, DKFZ Heidelberg	Primary culture

Table 2.12 Established cell lines

Name	Species	Tissue
HEK293T	human	Embryonic kidney
U87MG	human	Glioma
U251MG	human	Glioma
LN308	human	Glioma
LN319	human	Glioma

2.11 Cell culture media and supplements

Table 2.13 Cell culture reagents

Name	Company/catalog number
Accutase	Sigma # A6964
Papain	Sigma #P3125
ACK lysis buffer	Lonza #10-548E
Leibovitz medium	Thermo Fisher Scientific #21083027
DNase I	Sigma #D4527-20KU

Table 2.14 Cell culture conditions

Cells	Condition	Medium	Supplements	Company/catalog number
Cell lines	37°C, 8% CO_2	DMEM		Sigma #D5671
			10% FBS	Sigma #F7524
			2 mM L-glutamine	Sigma #G7513
			100 U/ml penicillin/ streptomycin (P/S)	Sigma # P4333
Primary cultures	37°C, 5% CO_2	Neurobasal		Thermo Fisher Scientific #10888022
			1x B27	Thermo Fisher Scientific #17504044
			20 ng/ml EGF	Promokine #C-60170
			20 ng/ml bFGF	Promokine #C-60240
			2 µg/ml heparin sodium salt	Sigma #H3149
			2 mM L-glutamine	Sigma #G7513
			100 U/ml P/S	Sigma # P4333

Table 2.15 Brain slice culture conditions

Tissue	Condition	Medium	Supplements	Company/catalog number
Brain slices	37°C, 5% CO_2	MEM		Sigma #M2279
			25% horse serum	Life Technologies # 26050070
			25 mM HEPES	Sigma # H0887
			5 mg/ml glucose	Sigma #G8769
			1 mM L- glutamine	Sigma #G7513
			100 U/ml P/S	Sigma # P4333

2.12 Mouse strains

Table 2.16 Immunocompromised mouse strain

Name	Abbreviation	Full name	Company
Scid/beige	CBSCBG	C.B-*Igh1*<b>/GbmsTac-*Prkdc*^{scid}-*Lyst*^{bg}N7	Taconic

3 METHODS

3 METHODS

3.1 Gene expression profiling

3.1.1 Isolation of RNA

$PDPN^{high}$ and $PDPN^{low}$ FAC-sorted glioblastoma cells of six samples each (NMA7; NMA50; NMA59; NMA65; GBM10; GBM30) were spun down and RNA isolated from cell pellet using the Qiagen RNeasy Mini Kit according to the manufacturer's instruction. DNase digestion was directly performed on column as suggested by the manufacturer.

3.1.2 Measurement of RNA quantity and RNA quality control

RNA concentration was measured using a Nanodrop Spectophotometer (ND-1000 UV-VIS, PeqLab). Ratios of absorption 260/280 or 260/230 were used as indicators of contamination for proteins and aromatic compounds, respectively. In particular, preparations with 260/280 ratio of 1.8 – 2.0 and 260/230 ratio greater than 2.0 were considered of good quality, and used for further analysis. RNA was stored at -80°C until further processing. For microarray analysis, RNA was delivered to the DKFZ Genomics and Proteomics core facility were RNA quality was validated using Agilent 2100 Bioanalyzer (Agilent Technologies) according to the manufacturer's instructions.

3.1.3 Microarray analysis and data processing

Gene expression was analyzed using an Illumina HumanHT-12v4 Expression BeadChip. RNA quality control, reverse transcription with labeling, chip hybridization and calculation of mean averages was conducted by the DKFZ Genomics and Proteomics core facility according to the manufacturer's protocol. Chipster was used for quantile normalization of the raw microarray data. Differential gene expression was analyzed by Dr. Annette Kopp-Schneider, head of the biostatistics division, DKFZ. The ratios for the six samples were averaged and compared. Gene annotation enrichment analysis was performed using DAVID Bioinformatics Resources software (Huang et al., 2009).

3.2 Molecular biology methods

3.2.1 Isolation of RNA

As described in 3.1.1, RNA was isolated from FAC-sorted cells by Qiagen RNeasy Mini Kit (incl. on-coloumn DNase treatment).

3.2.2 Measurement of RNA quantity and RNA quality control

As described in 3.1.2 RNA was measured and potential contamination assessed by Nanodrop Spectophotometer (ND-1000 UV-VIS, PeqLab).

3.2.3 Reverse Transcription PCR (RT-PCR)

For cDNA synthesis, 250 ng or 500 ng of RNA were pre-heated for 5 min at 65°C with a mixture of oligo-dT primers and random hexamers and then transcribed into cDNA (1 h; 42°C) using RevertAid M-MuLV reverse transcriptase (Thermo Fisher Scientific). Transcribed cDNA was stored at -20°C.

Table 3.1 Composition of RT-PCR reaction mix

Reagent	Quantity
RNA	500 ng
5 ng/µl oligodT/random hexamers	1 µl
H_20	Fill up to 6.25 µl
5x RT-Buffer	2 µl
25 mM dNTPs	0.4 µl
RiboLock RNase inhibitor	0.25 µl
RevertAid enzyme	0.5 µl
H_20	0.6 µl
Total	10 µl

3.2.4 Quantitative real-time RT-PCR (qRT-PCR)

For quantitative gene expression analysis, 40 cycles of real-time PCR was performed on the StepOnePlus real-time detection system (Applied Biosystems). Every PCR reaction was carried out in duplicates with 2.5 ng of cDNA in a final volume of 12.5 µl Power SYBR® Green PCR Master Mix (Applied Biosystem). Since AmpliTaq polymerase (present in Master Mix) is optimized to work at 60°C, primers had been designed accordingly by using primerBlast.

Table 3.2 Composition of qRT-PCR reaction mix

Reagent	Quantity
1 ng/µl cDNA	2.5 µl
Power SYBR® Green PCR Master Mix	6.25 µl
5 µM forward Primer	0.75 µl
5 µM reverse Primer	0.75 µl
H_20	2.25 µl
Total	12.5 µl

Table 3.3 qRT-PCR program

Step	Temp.	Time
Activation of polymerase	95°C	10 min
Denaturation	95°C	15 s
Annealing	60°C	30 s
Elongation	72°C	30 s
Melt curve	95°C	15 s
	60°C	1 min
	+1°C (up to 95°C)	15 s

StepOneTM Software v2.2 was used for data analysis. To calculate the relative expression of a gene of interest (GOI), the ΔΔCT method was used, which normalizes the cycle of threshold (CT) measured for the GOI to the CT measured for a housekeeping gene (HKG) taking into account the primer efficiency. Normalizing to a house keeping gene corrects variations in the initial amount of cDNA used. Importin-8 (*IPO8)* and TATA-Box binding protein (*TBP)* have been identified to exhibited high expression stability throughout all glioma grades (Kreth et al., 2010) and were thus used as HKG to normalize target gene expression. One of the cDNA samples was used as internal reference for the fold induction calculation of the transcript level of the other samples. The calculation can be summarized in the following formula (Pfaffl, 2001):

$$\text{Calculation of relative expression} = \frac{E(GOI)^{\Delta CT(GOI)\ (mean(control) - mean\ (sample))}}{E(HKG)^{\Delta CT(HKG)\ (mean(control) - mean\ (sample))}}$$

E(GOI) = Real-time PCR efficiency of GOI transcript
E(HKG) = Real-time PCR efficiency of HKG transcript
ΔCT(GOI) = CT-deviation of GOI transcript between control and sample of interest
ΔCT(HKG) = CT-deviation of HKG transcript between control and sample of interest

3.2.5 Validation of qRT-PCR primers

Primer efficiency was measured performing a reaction with consecutive 1:10 dilution series ranging from 0.01 ng to 100 ng of a cDNA mixture of multiple glioblastoma samples. Primer efficiencies between 1.7 and 2.2 were considered of good quality. Primer specificity was evaluated by analysis of the melting curve and by separation on an agarose gel for fragment size determination. Primer sequences are provided in Table 2.2. Primer efficiency was calculated as follows:

$$\text{Efficiency} = E = 10^{\left(\frac{-1}{\text{slope}}\right)}$$

slope = derived from standard curve of CT vs. log(cDNA input) plot

3.2.6 Agarose gel electrophoresis

PCR amplicons were separated according to their size by electrophoresis using 2% agarose gels containing 5 µl ethidium bromide. Prior to loading, DNA samples were mixed with 6x loading buffer. 100 bp DNA Ladder (100 - 1000 bp, Thermo Fisher Scientific) was used as a reference for size estimation of separated DNA fragments. Electrophoresis was carried out at constant voltage of 120 V.

3.3 Protein biochemistry methods

3.3.1 Isolation of whole cell protein extracts

Cells were washed with ice cold PBS and lysed in RIPA cell lysis buffer freshly supplemented with phosphatase and protease cocktail inhibitors (1:100; Serva/Roche), 25 U cyanase (Serva) and 6 mM $MnSO_4$. After 10 min incubation on ice, the extracts were centrifuged for 15 min at 13000 rpm (Eppendorf) at 4°C. The supernatant was transferred to new Eppendorf reaction tubes and stored at -20°C.

3.3.2 Determination of protein concentration

The yield of isolated proteins was determined according to the Bradford assay. Protein lysates were diluted 1:5 in H_20. A BSA standard was prepared with concentrations ranging from 0.125 mg/ml to 2 mg/ml. 5 µl of each sample were pipetted in duplicates into a 96-well plate and 200 µl Bradford MX solution (expedeon) added. After 5 min incubation time, the resulting colorimetric

reaction was measured at 595 nm in a microplate reader (BMG). The BSA dilution series was used to create a standard curve and to quantify protein concentration.

3.3.3 SDS polyacrylamide gel electrophoresis (SDS-PAGE)

Sodiumdodecylsulfate polyacrylamide gel electrophoresis (SDS-PAGE) was used to separate proteins according to their molecular weight. 15 µg or 25 µg protein lysates were mixed with 4x Loading buffer (expedeon), boiled for 10 min, cooled down for 5 min on ice, spun down and loaded onto the 10% SDS polyacrylamide gel (expedeon). SDS-PAGE was run in 1x SDS running buffer at 120 V for approximately 40 min until the running front reached the bottom of the gel. For protein size estimation, a prestained protein marker (Peqlab) was run in parallel.

3.3.4 Transfer of proteins to nitrocellulose membranes (Western Blot)

Denatured proteins resolved by SDS-PAGE were transferred onto nitrocellulose membranes (Optitran BA-S83) using a wet blotting system (Bio-Rad; Sigma). The separation gel and nitrocellulose membrane were embedded in three sheets of Whatman 3MM paper on either side pre-incubated in Western blot transfer buffer. The assembled blot was inserted with the correct orientation in the blotting system containing the Western blot transfer buffer. Transfer was performed at 300 mA for 2 h at 4°C. After disassembling the apparatus, the membrane was washed in PBS and incubated in blocking buffer for 30 - 60 min at RT while shaking. Subsequently, the membrane was incubated with the diluted primary antibody in blocking buffer o/n at 4°C while shaking. The membrane was then washed three times in washing buffer at RT while shaking. After washing, the membrane was incubated with the diluted secondary antibody coupled with horse radish peroxidase (HRP) in blocking buffer for 30 – 60 min hour at RT. The membrane was washed as described before, and incubated for 1 min with enhanced chemiluminescence solution (PerkinElmer). Finally, signals were detected using x-ray films and the Developer Classic E.O.S (Agfa). All antibodies used for Western Blot analysis are listed in Table 2.7 and Table 2.9.

3.4 Cell culture

3.4.1 Isolation and cultivation of primary human glioblastoma cells

Human glioblastoma biopsies were freshly obtained on ice from the operation room of the university hospital Frankfurt. All following preparation steps were conducted under sterile conditions. Tissue was minced in a cell culture dish using a scalpel. The tissue was then

transferred to a falcon containing 5 ml Leibovitz-L15 (Thermo Fisher Scientific) solution that had been pre-incubated with 60 U papain (Sigma) for 15 min at 37°C. 1000 U DNase I (Sigma) and 0.5 mM EDTA were added, incubated for 25 min at 37°C and inverted every 5 - 10min. After the incubation time, the suspension was resuspended well with additional 10 ml neurobasal-A medium (Thermo Fisher Scientific) using 10 ml and 5 ml sterile pipettes. The suspension was then filtered using to a 70 µm cell strainer. After a centrifugation step at 1000 rpm for 4 min at RT, the pellet was incubated for 2 min at RT with ACK lysing buffer (Lonza) to eradicate erythrocytes. The solution was filled up with neurobasal medium to 15 ml and centrifuged like previously described. After two additional washing steps the pellet was resuspended in supplemented neurobasal culture medium, transferred to a T75 cell culture vessel and cultivated at 37°C and 5% CO_2. The medium was refreshed the next day and then every 2 - 3 days.

For cultivation of the primary human glioblastoma material, cells were grown as spheroids in neurobasal medium. When spheroids reached a diameter of approximately 500 µm, they were spun down and resuspended in 1 ml accutase. Thorough resuspension resulted in dissociation of the spheroids into single cell suspensions which were washed with neurobasal medium before subcultivation or further processing for cell-based experiments.

3.4.2 Cultivation of cell lines

Human glioma cell lines were cultivated in supplemented DMEM (Sigma) under adherent conditions. Medium was refreshed every 2 - 3 days and cells were split when confluency was reached. For passaging the cells were washed with PBS to remove serum-containing medium and detached using 0.25% trypsin/0.6 mM EDTA in PBS.

3.4.3 Contamination control of primary cells

To have the primary human cells tested for infections of human immunodeficiency virus (HIV) and human hepatitis C virus (HCV), 8 ml of cell culture supernatant that had been cultured for at least 3 days were sent in to a diagnostic laboratory (Labor Limbach, Heidelberg). All tested samples were negative for HIV and HCV.

3.4.4 Determination of doubling time

To determine the proliferation rates of primary cells and cell lines, 2 x 10^6 cells were plated. After a specific time point (dependent on cell line), cells were dissociated or trypsinized, counted and

again 2 x 10^6 cells seeded. This process was repeated at least two times. Based on these numbers the doubling time was calculated.

$$\text{doubling time} = \frac{\text{duration (hours)} \times \log(2)}{\log(\text{finalcell number}) - \log(\text{initial cell number})}$$

3.4.5 Viral transduction of cells

Primary human glioblastoma cells were lentivirally transduced in order to stably transfer the desired RNAi or CRISPR/Cas9 construct. For the production of lentivirus that carried the transfer vectors given in Table 2.5; 4.5 x 10^6 HEK293T cells were seeded per 10 cm dish and transfer vector. After cells had firmly attached, the medium was exchanged to neurobasal medium. The medium was renewed after 24 h (10 ml medium/dish). The transfection was conducted mixing 4 µg pPAX2; 2 µg pCMV-VSV-G and 8 µg transfer vector with 200 µl OPTIMEM medium, then 42 µl polyethyleneimine (PEI; 1 mg/ml) were added. After 10 - 15min incubation at RT the transfection mix was pipetted drop by drop to the cells while slowly swirling the culture dish. 12 h post transfection the medium was renewed (7 ml/dish) and 24 h later the virus particle-enriched supernatant collected. The supernatant was filtered through 0.45 µm filter in order to remove HEK293T cells and cell debris and stored at 4°C. New medium (7 ml/dish) was added to the virus producing HEK293T cells and the harvest repeated 24 h later. The filtered supernatant from both days was pooled and 2 ml used to resuspend a pellet of 0.5 x 10^6 target cells. 8 µg/mL polybrene was added to increase infection efficiency. The medium was renewed 24 h later.

Established cell lines were transduced similarly, only HEK293T cells were continuously cultured in DMEM medium throughout the procedure. Cell lines were infected by transferring the filtered virus particle-containing supernatant to adherent cells of approximately 40% confluency. 8 µg/mL polybrene was added to increase infection efficiency; the medium was renewed 24 h later.

3.4.6 Flow cytometry and fluorescence activated cells sorting

Single cell suspensions were prepared as described above. Cells were manually counted using a Neubauer Chamber and trypan blue to exclude dead cells. For flow cytometry, 5 x 10^5 cells in 100 µl 1% BSA/PBS were stained with the appropriate amount of antibody (given in Table 2.6). After an incubation time of 20 min at 4°C in the dark, cells were washed with PBS and resuspended in 400 µl 1% BSA/PBS for analysis using BD FACSCalibur™.

For fluorescence activated cell sorting (FACS), single cell suspensions were additionally stained with 0.5 µg/ml propidium iodide (PI) to identify dead cells. Stained and washed cells were filtered through a 70 µm strainer and kept in high density (up to 10 x 10^6 cells/ml) in 1% BSA/PBS in order to ensure a fast sorting process. Cells were sorted into 15 ml falcons containing 2ml cultivation medium using a FACSAria™ I, FACSAria™ II or FACSAria™ Fusion cell sorter with 100 µm nossle. After the sorting process cells were spun down and lysed for RNA isolation or resuspended in fresh culture medium for subcultivation. In case of subsequent intracranial injection within the frame of serial transplantations cells were kept maximal 3 days in culture. Cells sorted for $PDPN^{high}$ and $PDPN^{low}$ expression were for logistic reasons kept 1 day in culture before intracranial injection.

3.5 Invasion assay using *ex vivo* organotypic brain slice cultures

3.5.1 Preparation of brain slices

After euthanizing a 6 - 8 weeks old C57BL/6 wild-type mouse, the brain was isolated and the cerebellum removed with a scalpel. Using insect forceps the brain was transferred to the vibratome (Leica) platform where it was stuck by a drop of superglue. The lateral short side of the brain was placed facing the blade, in order to reduce mechanical stress. 350 µm thick coronal slices were cut with a maximal speed of 0.2 mm/s. Up to three slices were gathered per filter (Millipore). The transfer of the slices was facilitated by a brush and addition of brain slice medium (for composition see Table 2.15) on top of the filter. For cultivation at 37°C and 5% CO2 the medium was removed from the filter and 1 ml of fresh brain slice medium was added to the well. The medium was refreshed after 18 - 24h and then every other day. Brain slices were cultivated air-exposed. To prevent dehydration the tissue was moistened with a drop of medium every day, and remaining excess medium removed. Although the brain slices can be cultivated for at least one week, experiments were performed at day 2 and, due to the high migratory capacity of glioma cells, terminated on day 4.

3.5.2 Preparation of fluorescently labeled spheroids

Glioma cell lines cultivated in serum-containing medium were trypsinized and counted. 1 x 10^6 cells/ml PBS were incubated with 5 µl lipophilic dye DiD (1 mg/ml in DMSO, Biotium) or 5 µl DiI (Biotium) for 30 min at 37°C. After two washing steps 500 cells/well were seeded a flat-bottom 96-well plate coated with 50 µl low melt agarose (1% in PBS; Genaxxon). Most glioma cell lines

formed spheroids under the described conditions. However, U251MG and LN319 were kept in neurobasal medium in order to obtain compact spheroid formation. Primary glioblastoma cells were cultivated as spheroids in serum-free neurobasal medium. After dissociation cells were labeled as described above and seeded into agarose-free U-bottom 96-well plates (Greiner). Due to the different growth rates of the tumor cells used in the experiments and the difficulty of precisely measuring the number of cells in an established spheroid, a fixed number of 500 cells were seeded and implanted when the spheroids reached a diameter of approximately 150 µm.

3.5.3 Spheroid implantation

Approximately ten spheroids per brain slice were manually implanted using a blunt Hamilton syringe (701N; 10 µl; 26s/51/3) and a binocular microscope. The proper implantation depth of the spheroid is essential to obtain maximal invasion. The spheroid must be implanted within the tissue, as release of the spheroid below or on top of the brain tissue will not result in tumor cell invasion but in proliferation or in some cases in collective migration along the tissue surface. Furthermore, tissue integrity is an essential factor for correct implantation. Dehydration of brain slices impedes penetration of the tissue with the needle tip, as the tissue surface becomes too rigid. Conversely, excessive immersion of the brain slice in medium results in tissue degeneration and disintegration upon penetration with the needle tip. Thus, brain slices were moistened every other day, followed by removal of excessive medium. Following implantation, medium was refreshed and the slices cultivated at 37°C and 5% CO_2. Experiments were terminated 2 days after implantation unless otherwise stated. For fixation brain slice medium was removed and 1 - 2ml 4% PFA added on top of the filter for 2 h at RT or o/n at 4°C. Fixed slices were transferred with a spatula from the filter into a new 6-well plate containing 2 ml PBS/well. Although the slices can be stored in the parafilm-sealed plate for at least three months in the dark at 4°C, slices were imaged by epi-fluorescence or confocal microscopy as soon as possible.

3.5.4 Tumor cell and brain slice treatment with jasplakinolide

500 DiD labeled SMA560 glioma cells were seeded in spheroid-forming conditions per well of a 96-well plate. 18 h prior to implantation, spheroids or brain slices were treated with 1 µM jasplakinolide (Cayman) or DMSO (Sigma). 24 h after implantation, brain slices were fixed and imaged by confocal microscopy. Cell viability *in vitro* was measured with trypan blue staining (Sigma). To test whether the assessed invasion was significantly affected in the jasplakinolide-treated groups, Welch's t-test was performed. Differences in the grade of invasion were

considered significant if $p < 0.05$. Bonferroni correction (for multiple comparisons) of p-values was applied.

3.5.5 Imaging and quantification of invasion

For epi-fluorescence imaging the slices were kept in 6-well plates containing PBS. For confocal imaging slices were transferred with a spatula onto an object slide and loosely covered with a coverslip. Z-stack images were transformed to a maximum projection image by using ImageJ (Schneider et al., 2012). Image quality was optimized by adjusting brightness, contrast and gamma. Migratory cells were visible as spikes emerging from the bulk of the spheroids that had been formed by cells establishing an infiltration path. These invasion sprouts were traced from the center of the mass to the tip using the freehand tool. The radius of the spheroid body (if not determinable spheroid body radius from day 0) was subtracted from the measured sprout length. Subsequently, the average cumulative sprout length was calculated by adding up the length of all sprouts of a spheroid and dividing this sum by the number of analyzed spheroids. This statistic integrates sprout length and the number of sprouts to estimate the migratory capacity of the cells. Calculation of the cumulative sprout length is a common tool in angiogenesis research, where it is used as reliable quantification of cell movement and proliferation in a three-dimensional environment (Heiss et al., 2015, Weber et al., 2008). Statistical analysis was performed using student's t-test or Welch's t-test in case of unequal standard deviations.

3.6 Animal experiments

3.6.1 Housing of animals

Scid/beige animals were purchased from Taconic and kept in the experimental animal facility of the DKFZ under specific pathogen-free conditions and controlled temperature (21°C), light cycles and humidity (50 - 60 %). Food and drinking water were offered *ad libitum*.

3.6.2 Intracranial injections

Single cell suspensions were prepared as described above. Cells were manually counted using a Neubauer chamber and trypan blue to identify dead cells. PBS cell suspensions of 1×10^7 primary cells/ml or 5×10^7 cells/ml of established cell lines were prepared and stored on ice until intracranial injection.

The 6 - 10 weeks old scid/beige mouse was given 200 mg/kg metamizol pain killer by subcutaneous injection. The animal was anesthetized by isoflurane (3 vol%, gradually decreased to 1.5 vol%) and fixed with the head into the mounting brackets of the stereotaxic device (Neurostar). Eyes were protected from dehydration by application of eye ointment and the body temperature of the mouse was maintained using a 37°C warm heat map. A Hamilton nanofil syringe with 34 gauge needle (World Precision Instruments) was filled with the cell suspension and mounted to the device. The disinfection of the animal's head was followed by a small incision of the skin. The syringe's needle tip was aligned 2 mm lateral (right) of the bregma and inserted 3 mm deep after manually drilling the skull with a 23 gauge needle. 2 µl cell suspension was injected with a speed of 0.2 µl/min. The needle was retracted after additional 5 min to allow the injected cell suspension to be resorbed by the tissue. The skull was sealed with bone wax and the skin closed using non-absorbable suture. The mouse was kept warm until recovery from anesthesia.

All animal experiments were approved by the responsible authority for animal experiments (Regierungspräsidium Karlsruhe, Germany) and performed in conformity with the German Law for Animal Protection.

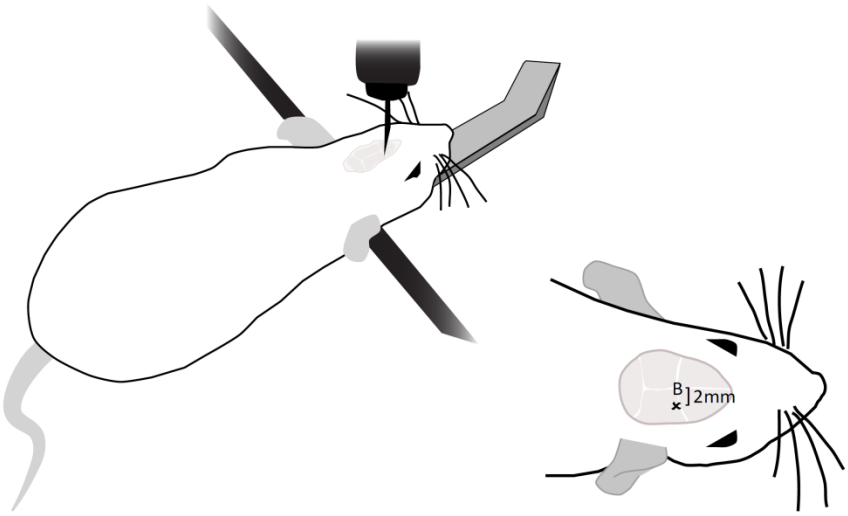

Figure 3.1 Schematic representation of intracranial injection site.
Using a stereotaxic device, tumor cells were injected in 3 mm depth, 2 mm lateral from the bregma (B).

3.6.3 Magnetic resonance imaging

Animals were measured by the small animal imaging core facility of the DKFZ. For this, animals were anaesthetized as described above and imaged in a 1 Tesla MRI scanner. Animal preparation, imaging and image analysis was conducted by the core facility.

3.6.4 Sacrificing mice and sample preparation

Mice used for organ extraction or experimental mice that showed termination criteria were euthanized by CO_2 inhalation, and death was determined by evaluation of the toe and the eye reflex. After sacrifice, brain was isolated and either processed for *ex vivo* brain slice cultures, fixed in 4% PFA/PBS for histological examinations or used for tumor cell isolation.

3.7 Histological methods

3.7.1 Fixation and embedding of tissue in paraffin

Immediately after sacrificing the mouse, the brain was isolated and fixed in 4% paraformaldehyde in PBS at 4°C for at least 48 h. Samples were washed in PBS and transferred to 70% ethanol. Samples were then stored at 4°C until proceeding with the subsequent stages required for paraffin embedding. Therefore, the brains were transferred in tissue cassettes, and treated according to the program given in Table 3.4. For embedding in paraffin, the samples were transferred from the tissue cassette into a metal well, which was then filled with liquid paraffin and subsequently cooled down to 4°C. When the paraffin blocks were completely solid, they were removed from the metal wells and stored at RT until sectioning.

Table 3.4 Tissue preparation for paraffin embedding

Step	Temp.	Time	Cycles
70% EtOH	35°C	45 min	1
80% EtOH	35°C	90 min	1
90% EtOH	35°C	90 min	2
96% EtOH	35°C	90 min	2
100% Isopropanol	35°C	90 min	2
Xylene	40°C	150 min	2
Paraffin	60°C	45 min	4

3.7.2 Preparation of sections from paraffin-embedded samples

Paraffin blocks were cut in 6 µm sections using the microtome RM2155, and transferred on SuperFrost object slides. The sections were dried at 42°C o/n, and stored at RT. This procedure was performed by Angelika Krischke and Sabrina Lohr.

3.7.3 Hematoxylin and eosin staining of paraffin-embedded tissue sections

Tissue sections were incubated twice in xylene for 10 min to remove paraffin, and rehydrated by the application of a dilution series of ethanol (ranging from 100% - 50% EtOH). Slides were incubated in each dilution for 2 min, then stained in hematoxylin solution for 8 min and washed in distilled H_2O twice for 2 min. Prior to eosin staining, the sections were washed in 70% EtOH/0.05% HCl for 20 s and in distilled H_2O for 10 min. Staining in 0.1% eosin was conducted for 5 min. Stained sections were dehydrated by short incubations in 70%; 90%; 100% EtOH and xylene before mounting with Eukitt. The hematoxylin and eosin (H&E) staining was performed by Angelika Krischke.

3.7.4 Immunohistochemistry staining of paraffin-embedded tissue sections

Sections were deparaffinized and rehydrated as described above. Depending on the applied antibody one of the antigen retrievals given in Table 3.5 was conducted.

Table 3.5 Overview of different antigen retrieval methods

Method	Reagent	Temp.	Time
Heat-mediated	1 mM EDTA, pH = 8	95°C	15 min
Heat-mediated	10 mM citrate buffer, pH = 6	95°C	15 min
Enzyme-mediated	1 mg/ml proteinase K	RT	10 min
	20 µ/ml proteinase K	37°C	15 min

After antigen retrieval, sections were rinsed with PBS for 5 min, and incubated with 3% H_2O_2 in tap water in the dark for 10 min at RT. After washing in PBS, sections were incubated in blocking solution containing 5% goat serum (Vector Laboratories) and 0.1 % BSA in PBS for 30 min. Sections were subsequently incubated with primary antibody appropriately diluted (as indicated in Table 2.8 and Table 2.10) in blocking solution o/n at 4°C. After a washing step sections were incubated with the appropriate biotin-coupled secondary antibody diluted 1:500 in blocking buffer for 30 min at RT. In the meantime, an avidin/horse radish peroxidase containing solution (ABC kit, Vector Laboratories) was prepared in 0.1% BSA/PBS, and incubated for 30 min at RT. After the incubation with the secondary antibody sections were washed in PBS incubated in ABC solution for 30 min at RT. Subsequently, sections were washed in PBS. The staining was developed with DAB reagent (Vector Laboratories) until a brown signal of the desired intensity and localization appeared. To stop this colorimetric reaction, sections were immersed in tap water. Sections were then counterstained with hematoxylin solution for 4min, and rinsed in tap water for 6 min.

In case of laminin staining, no hematoxylin staining was performed in order to facilitate automated analysis of the stained area. This analysis was conducted using image J software and a macro that was written by Dr. Barbara Costa and Dr. Damir Krunic.

3.7.5 TUNEL assay on paraffin-embedded tissue sections

Apoptotic cells on paraffin-embedded sections were detected by visualizing fragmented DNA, a key feature of (late) apoptotic cells. Therefore, sections were deparaffinized and rehydrated as described above. Antigen retrieval was performed by incubation of the slides with 20 µg/ml proteinase K for 15 min at 37°C. After washing and blocking steps (as described above), samples were incubated with TUNEL labeling solution (Sigma) and 20 U terminal deoxynucleotidyl transferase (NEB) for 1 h at 37°C. During this incubation step the terminal transferase attaches fluorescently labeled nucleotides in a template-independent manner on free hydroxyl termini of damaged DNA (present in apoptotic cells). After a washing step the samples were counterstained with Hoechst and mounted. Samples treated with 10 U DNase I for 15min at 37°C served as a positive control. Samples incubated with labeling solution without terminal transferase were used as a negative control.

3.8 Statistical analysis

To identify a potential difference between the survival times of two groups, Kaplan-Meier curves were plotted and the two survival curves statistically compared by application of the log-rank test. To assess whether the difference between the means of two groups (knockout and control group) reached statistical significance, student's t-test or Welch's t-test in case of unequal variations was performed. In case of multiple comparisons, p-values were corrected according to Bonferroni.
Additional details of statistical analysis are given in the methodology description of the respective experiment. Graphpad Prism 7 (Graphpad Software, Inc.) was used for plotting and analyzing data. Statistical advice was given by Dr. Anette Kopp-Schneider for the analysis of the brain slice invasion assay. Dr. Kopp-Schneider also performed the analysis of the microarray data.

4 RESULTS

4 RESULTS

4.1 Optimization of a glioma cell invasion assay based on organotypic brain slice cultures[1]

Previous publications have indicated a pro-migratory function for PDPN using standard migration assays (Grau et al., 2015, Martin-Villar et al., 2005, Peterziel et al., 2012, Wicki et al., 2006). However, false-positive and false-negative results have been reported for conventional two-dimensional migration assays (Jensen et al., 2017, Scott et al., 2010), which might be due to discrepancies in protein function between two- and three-dimensional assays (Khatau et al., 2012, Skau et al., 2016), and the lack of the three-dimensional tumor microenvironment (Joyce and Pollard, 2009, Pampaloni et al., 2007). In order to assess the potential involvement of PDPN in tumor cell invasion most faithfully, this work devoted substantial effort to move from traditional two-dimensional migration assays to an elaborate three-dimensional system that more closely recapitulate the *in vivo* glioma microenvironment. Organotypic brain slice cultures, which have mainly been used to study developmental, structural and electrophysiological aspects of neuronal circuits (for reviews see Huang et al., 2012, Lossi et al., 2009), represent an optimal matrix to study tumor cell invasion as they preserve essential features of the host tissue. However, previous attempts to use organotypic brain slices in a novel *ex vivo* invasion assay were accompanied with certain disadvantages: Reported methods were based on human brain slices (Jung et al., 2002), included upright confocal imaging (Chadwick et al., 2015), which may both not be universally

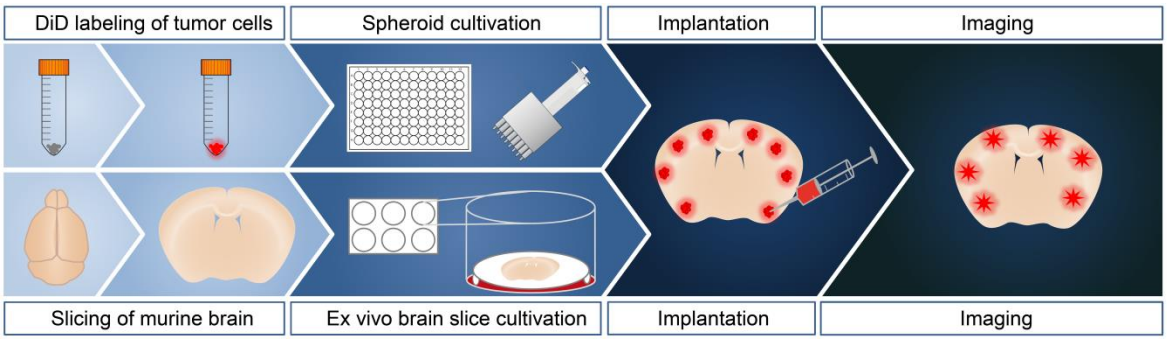

Figure 4.1 Schematic representation of the *ex vivo* invasion assay.
DiD labeling of tumor cells is followed by seeding into 96-well plates for spheroid formation. Adult murine brain slices of 350 µm thickness are prepared by vibratome and cultivated air-exposed for 2 days until implantation. Tumor cell spheroids are then manually implanted into the cortex. Depending on the invasive capacity of the cells, the assay is terminated after 1 - 4 days by fixation.

1 The text of the following section has been taken and partially modified from Eisemann et al. (2017) which had originally been written by myself

available, or the extent of invasion observed was rather low (Aaberg-Jessen et al., 2013, Petterson et al., 2016, Xu et al., 2016), not reflecting the high infiltration capacity of glioblastoma cells *in vivo*. Thus, several optimization steps had to be established to meet the demands for a reproducible protocol of glioma cell invasion assay based on organotypic brain slice cultures. A schematic overview of the assay is presented in Figure 4.1.

4.1.1 Adult slice cultures retain the cytoarchitecture of the brain

The majority of previous publications utilized brain slices from perinatal donors that show a high degree of resistance to mechanical trauma during the slice preparation (Cho et al., 2007). However, high grade gliomas are most common among adult patients, and neonatal slices do not structurally reflect adult brains as in rodents the ECM is substantially remodeled starting from 2 weeks after birth. This remodeled and thus significantly firmer ECM is subsequently maintained

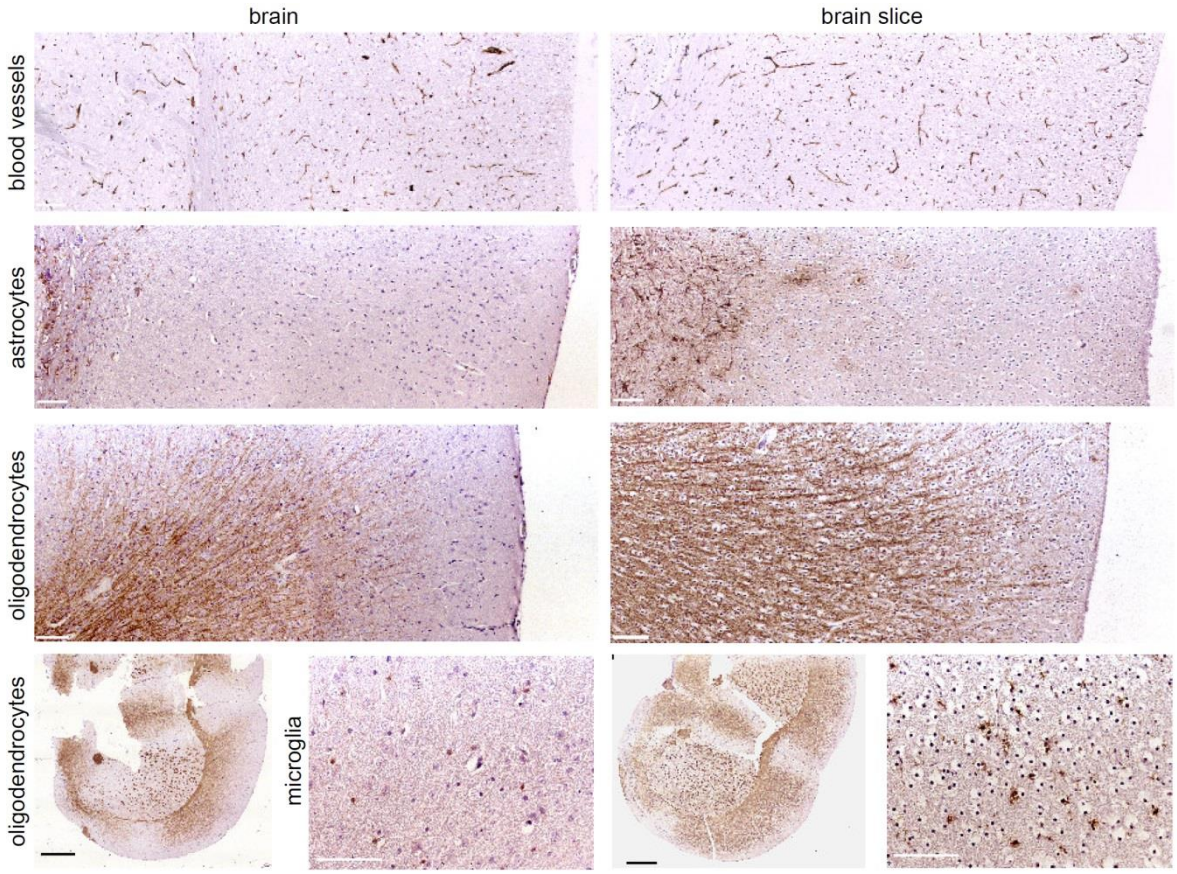

Figure 4.2 Organotypic brain slice cultures maintain characteristic features of adult brain tissue. Immunohistochemical stainings of murine brain and brain slices cultivated for four days show comparable patterns of blood vessels (laminin) and myelinating oligodendrocytes indicated by MBP staining. Astrocytes (GFAP) and microglia (Iba1) seem to be slightly activated in the brain slice. White scale bars 100 µm, black scale bars 1 mm.

throughout adulthood (Zimmermann and Dours-Zimmermann, 2008). Similarly, myelination of nerve fibers occurs predominantly postnatally and can be extended to adulthood (Semple et al., 2013). Hence, absent or incomplete myelination and the immature and loose extracellular matrix are profound differences between neonatal and mature adult brain tissue. In order to reflect the age-related disease of adult glioma, adult brain slices were used that exhibit a mature myelination pattern and ECM composition. Immunohistochemical stainings were performed on adult brain slices embedded 4 days after preparation to determine the integrity of the cytoarchitecture.These stainings revealed that blood vessels and myelinated fiber tracts (indicated by laminin and myelin basic protein, MBP, respectively) were present and morphologically intact; astrocytes and microglia (indicated by glial fibrillary acidic protein, GFAP, and ionized calcium binding adaptor molecule 1, Iba1, respectively) were slightly activated within the brain slice, presumably induced by the mechanical trauma of cutting (Figure 4.2). In contrast to the survival of astrocytes, microglia and endothelial cells, neuronal survival in brain slices has been reported as a major challenge, especially for slices prepared from adult donors (Humpel, 2015). This is partly attributed to the fact that neuronal cell death is induced by axotomy during the process of tissue slicing. Yet, the structure of myelinated nerve tracts remains intact providing the same structural surfaces glioma cells encounter *in vivo*. Taken together, the cytoarchitecture of the brain slice closely resembles that of the adult murine brain, thus, providing an authentic surface for glioma cell migration.

4.1.2 DiD labeling of tumor cells improves fluorescence imaging

Although previous studies have used ectopic GFP expression or the carbocyanine dye DiI for membrane labeling and tracing of cell invasion (Aaberg-Jessen et al., 2013, Jung et al., 2002, Xu et al., 2016), I experienced high autofluorescence of the brain slice and a poor contrast between tissue and tumor cells when imaged with short excitation/emission wavelengths, especially at the epi-fluorescence microscope (Figure 4.3 A). In order to reduce autofluorescent background, the lipophilic carbocyanine dye DiD was used, an analog of DiI with markedly red-shifted fluorescence excitation and emission spectra. As autofluoresence decreases dramatically at longer wavelengths, DiD labeling resulted in strikingly sharper images compared to the usage of DiI (Figure 4.3) and is moreover preferable for live cell imaging applications due to reduced photodamaging effects. Thus, the application of DiD strongly improves the imaging of invaded fluorescent tumor cells and even enables epi-fluorescence microscopy as a good alternative to confocal imaging.

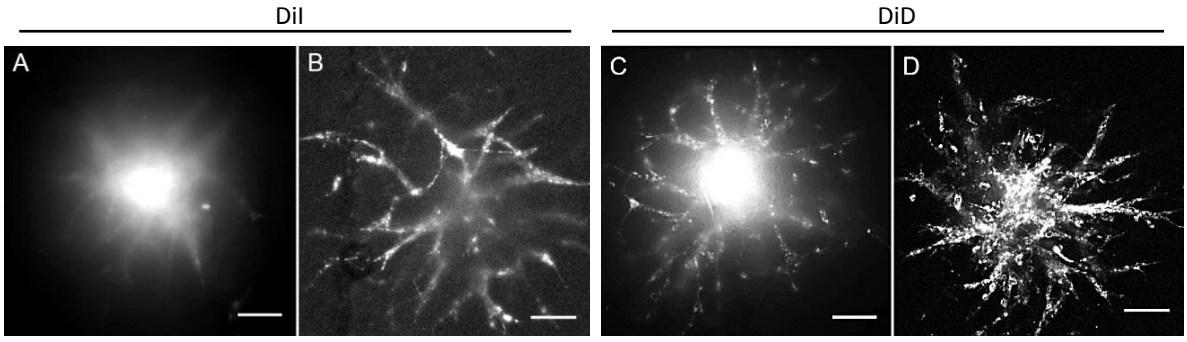

Figure 4.3 Improved image quality by confocal imaging and DiD labeling.
Representative pictures of epi-fluorescent (A,C) and confocal microscopy (B,D). Usage of DiD (C,D) improves picture quality compared to DiI labeling of SMA560 cells (A,B). Scale bars 100 µm, image quality was optimized by the adjustment of brightness, contrast and gamma.

4.1.3 Human and murine glioblastoma cells extensively migrate in adult murine brain slices

In order to show that this protocol for the *ex vivo* invasion assay allows glioma cells to invade to a high degree, a panel of DiD labeled human and murine glioma spheroids were manually implanted into adult brain slices that had been cultivated for 2 days. 48 h after implantation the slices were fixed and imaged by confocal microscopy. As illustrated in Figure 4.4 a strong invasion of all implanted glioma cells into the surrounding tissue could be observed. Thus, using this *ex vivo* invasion assay protocol the invasive capacity of different tumor cells can be reliably assessed and compared.

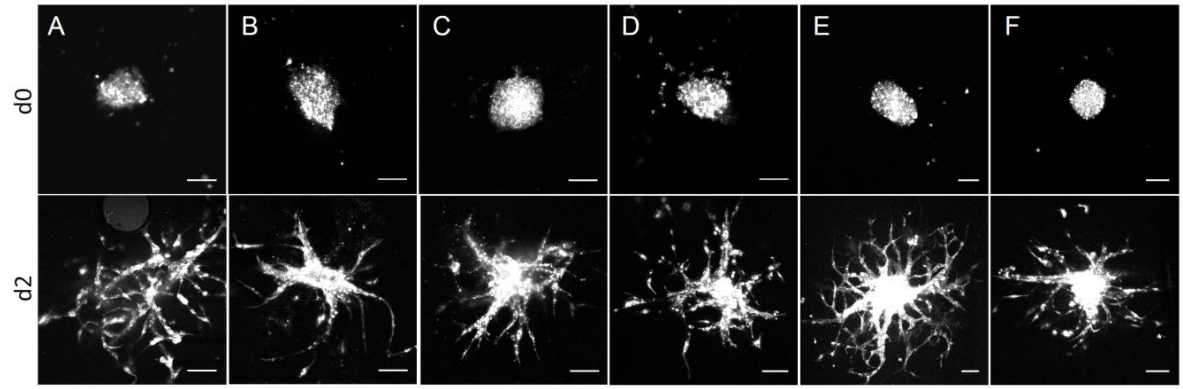

Figure 4.4 Strong invasion of glioblastoma cells in organotypic brain slice cultures.
Representative confocal images of DiD labeled primary glioma cells (human (A), murine (B)) and established glioma cell lines (murine SMA560 (C) and human LN319 (D), U87MG (E) and U251MG (F)) implanted in adult brain slice cultures. Images were acquired at day 0 (top) and day 2 (bottom). Scale bars 100 µm, image quality was optimized by adjustment of brightness, contrast and gamma.

4.1.4 The *ex vivo* invasion assay as a quantitative tool

Furthermore it was evaluated whether this system enables the detection of differences in the extent of migration. As a proof of principle, either tumor spheroids or brain slices were treated before implantation with the direct inhibitor of actin depolymerization and known inhibitor of migration, jasplakinolide (Ivkovic et al., 2012, Ponti et al., 2004). Indeed, tumor cell treatment with 1 µM jasplakinolide for 18 h significantly blocked tumor cell invasion (Figure 4.5 B) without inducing cell death (Figure 4.5 E). Moreover, similar results were obtained when treating the brain slice 18 h prior to implantation with 1 µM jasplakinolide (Figure 4.5 C). Observed invasion was quantified by the determination of the cumulative sprount length. The assessment of the cumulative sprout length is an established analysis method in angiogenesis research to quantify three-dimensional sprouting and tube formation of endothelial cells (Heiss et al., 2015, Korff and Augustin, 1999). This quantification implies the great advantage that not only spike length but also the number of spikes is considered. The quantifications given in Figure 4.5 reflect the extent of invasion visually observed in the brain slice (illustrated by given representative images). These results confirm that this *ex vivo* invasion assay facilitates the quantitative measurement and comparison of invasion between different groups. It furthermore highlights the suitability of this method for drug discovery and preclinical evaluation where it could permit the robust selection of compounds affecting tumor cell invasion before ultimate *in vivo* testing.

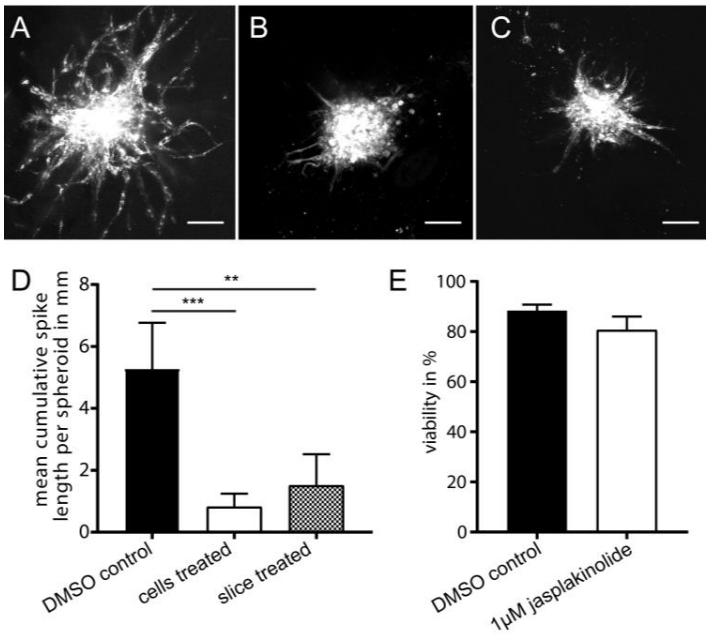

Figure 4.5 The *ex vivo* invasion assay as a tool to identify invasion modulating compounds.
18 h prior to implantation SMA560 spheroids or brain slices were treated with 1 µM jasplakinolide. 24 h after implantation brain slices were fixed and imaged by confocal microscopy. In contrast to the highly invasive control-treated SMA560 (A), the treatment of the tumor cells (B) or brain slices (C) with jasplakinolide significantly reduced their ability to invade without inducing cell death as examined by trypan blue staining (E). (D) Quantification of invasion. Error bars show 95% confidence interval, (A) n = 12; (B,C) n = 7; (E) n= 3; **p<0.001; ***p≤0.0001; Welch's t-test, p-values Bonferroni corrected.

4.2 The role of podoplanin in glioblastoma progression

Multiple models are available to study glioblastoma, as elaborated in the introduction section (see chapter 1.1.3; page 9). Although genetically engineered mouse models (GEMMs) confer many advantages in modeling glioblastoma, there are some drawbacks that were considered when choosing the appropriate model for this project. GEMMs involve numerous technical disadvantages including the long generation time of the genetic background (tissue-specific deletion of an established combination of tumor-suppressors and *Pdpn*), and the potentially long latency. Moreover, as all tumors are composed of cells with a number of specific homogeneous genetic changes, they cannot reflect the high intratumoral genomic and phenotypic heterogeneity found in human tumors. In contrast, patient-derived xenografts (PDX) retain the genetic and chromosomal makeup of the original tumor reflecting the biological properties and cellular heterogeneity of the patients' tumors. Moreover, this xenotransplantation model results in strong invasion and other characteristic features of glioblastoma. Thus, although facing the disadvantage of neglecting the impact of the immune system by the required usage of immuodeficient mice, this project focused on the application of patient-derived xenotransplants to study the function of PDPN in glioblastoma progression and invasion.

4.2.1 Podoplanin is expressed in primary glioblastoma

As PDPN has been proposed as a major driver for glioblastoma progression and especially for glioblastoma cell invasion, this study aimed at investigating this hypothesis. As a first step, the expression of *PDPN* in primary human glioblastoma samples was validated. For this purpose, paraffin-embedded human glioblastoma biopsies were immunohistochemically stained for PDPN (Figure 4.6). Due to the lack of a unique glioblastoma or astrocyte marker, PDPN expression cannot be exclusively ascribed to tumor cells but could also derive from reactive (tumor-associated) astrocytes. However, all tumor biopsies showed intermediate to high PDPN levels with an inter- as well as intratumoral variability of PDPN expression. Many samples showed foci of high PDPN expression (Figure 4.6 A, B, C, G), which were in most cases perivascularly located. Although few samples contained non-neoplastic tissue (determined by morphology), high levels of PDPN expression were not restricted to the invasive front of the tumor (Figure 4.6 F). Additionally, freshly isolated cells from eight human glioblastoma tumors were examined by flow cytometry. This served not only for the verification of *PDPN* expression in glioblastoma tumors, but was furthermore intended to determine the number of PDPN positive tumor cells. Detailed instructions

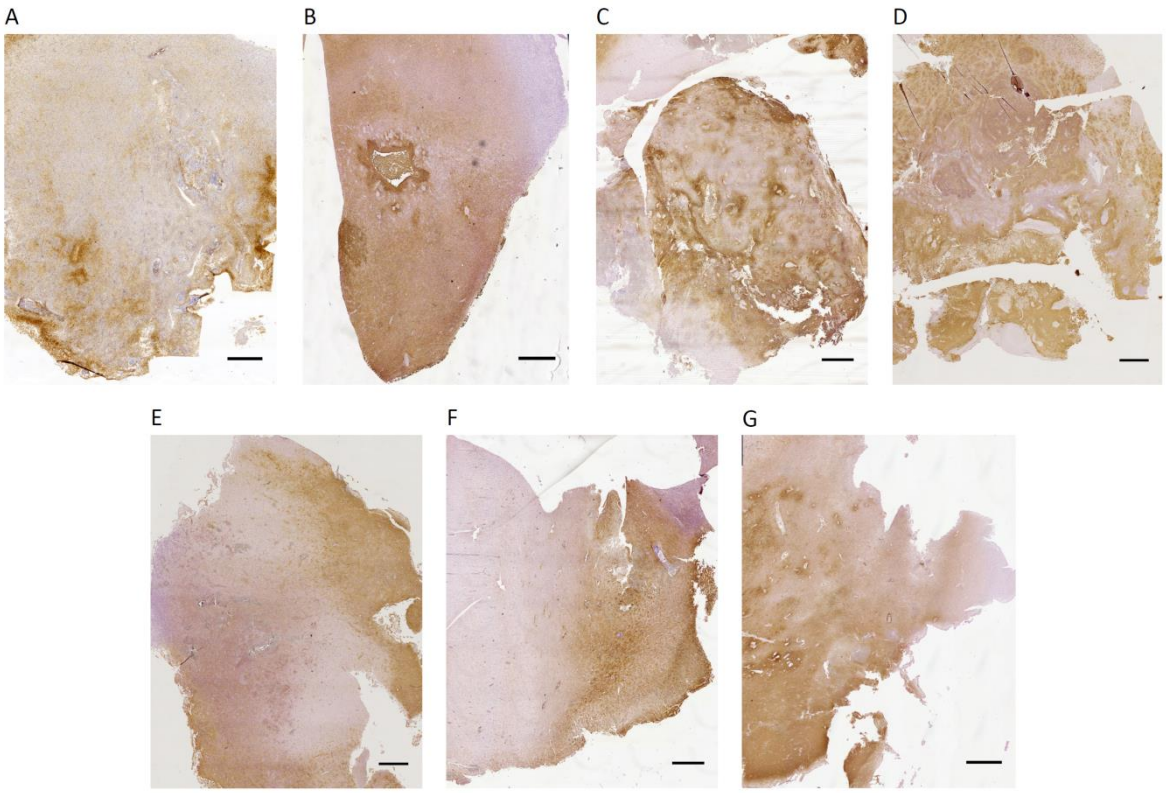

Figure 4.6 Podoplanin immunohistochemistry staining of primary human glioblastoma biopsies.
Primary human glioblastoma sections show variable *PDPN* expression. Some biopsies show focal increase in *PDPN* expression (A, B, C, G), primarily in perivascular areas. Due to the lack of glioblastoma/astrocyte markers, PDPN cannot clearly be allocated to tumor cells or reactive astrocytes. (A) GBMF1; (B) GBMF2; (C) GBMF3; (D) GBMF9; (E) GBMF10; (F) 341/09; (G) 531/14; scale bars 1 mm.

for tumor cell isolation are listed in the section 3.4.1, page 41. Briefly, after human glioblastoma biopsies had been obtained from the operating room on ice, the tissue was gently digested with papain, erythrocytes were lysed and residual cells cultivated in neurobasal medium. Importantly, in line with the report of PDPN beeing a substrate for calpain-1 (Martin-Villar et al., 2009), a cysteine proteases of the papain superfamily, I found the protein to be cleaved upon papain treatment (Figure 4.7). As the papain-based dissociation is a standard method to isolate glioblastoma cells (Bao et al., 2008, Eyler et al., 2011, Patel et al., 2014) and I experienced a good yield of tumor cells, we decided to follow the papain-based isolation protocol despite the cleavage of PDPN. Thus, to enable the reconstitution of the protein on the cell surface, isolated cells were cultivated for two days before flow cytometric analysis. Furthermore, this short cultivation period served to deplete non-neoplastic cells as the applied culture conditions are tailored for tumor cell cultivation. Yet, it could not be excluded that some undesired cells would survive and bias the flow cytometric analysis. Thus, as no glioblastoma cell marker exists, an

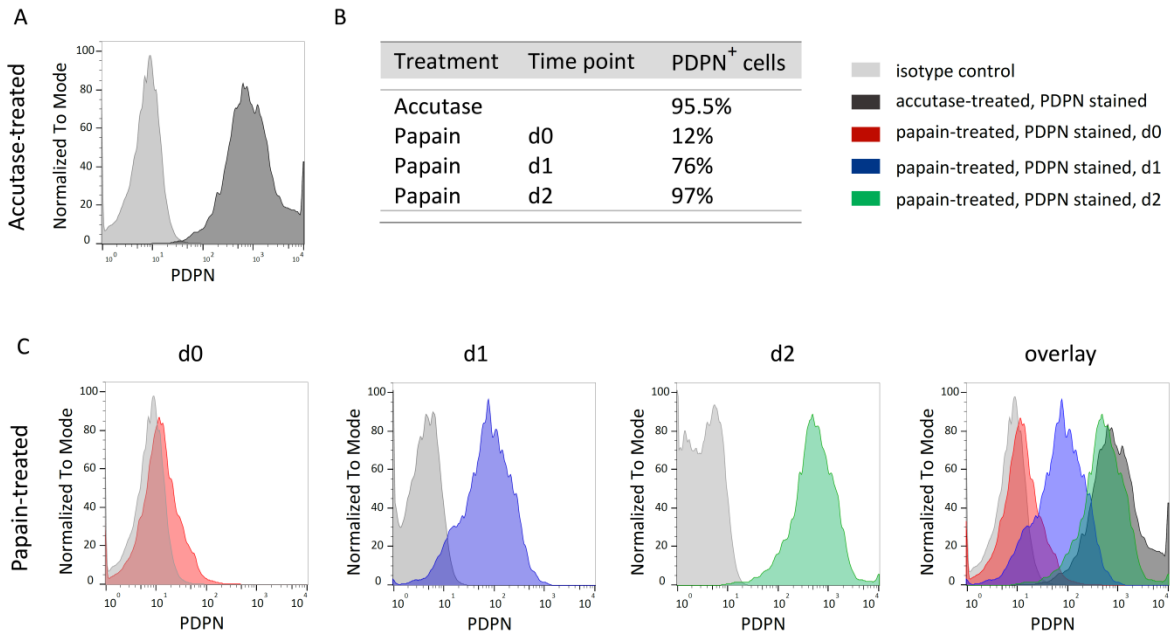

Figure 4.7 PDPN is a substrate for papain enzyme.
Primary human glioblastoma tumorspheres (T1132) were dissociated with either (A) accutase or (C) papain and analysed for PDPN expression by flow cytometry. Mild treatment with accutase resulted in almost 100% positive PDPN staining. PDPN protein levels and the number of PDPN positive cells were dramatically reduced after papain treatment. PDPN was gradually re-exposed on the cell surface over time (C) and fully reconstituted after two days. (B) Overview of PDPN positive cells per group.

elimination strategy was applied to distinguish tumor cells from non-neoplastic cells. Stainings were performed to identify endothelial cells (CD31), pericytes (PDGFRβ) and immune cells (CD45). As the cultivation of neurons and oligodendrocytes is very challenging, a potential contamination of the tumor cell cultures by these cell types was excluded. With the exception of GBMF9, that harbored a great proportion of immune cells, the number of non-neoplastic cells was generally low (Figure 4.8 A), indicating that the isolation process and cultivation conditions resulted in cultures strongly enriched for tumor cells. However, due to the extensive overlap of astrocytes and tumor cells in their protein repertoires, it was not possible to determine the presence of astrocytes in the tumor cell isolates. The presence and numbers of non-neoplastic cells were considered when calculating the percentage of PDPN positive tumor cells (Figure 4.8 C). As subsets of immune cells have been reported to express *PDPN*, isolated cells of five tumor samples were co-stained for CD45 and PDPN in order to determine the non-neoplastic cell proportion within the PDPN positive cells. With the exception of GBMF6 (33%), immune cells constituted less than 5%, or in the case of GBMF9 8%, of all PDPN positive cells and were thus considered negligible (Figure 4.8 B). In summary, all examined human glioblastoma samples have shown *PDPN* expression and immune cell infiltration, albeit at variable extent.

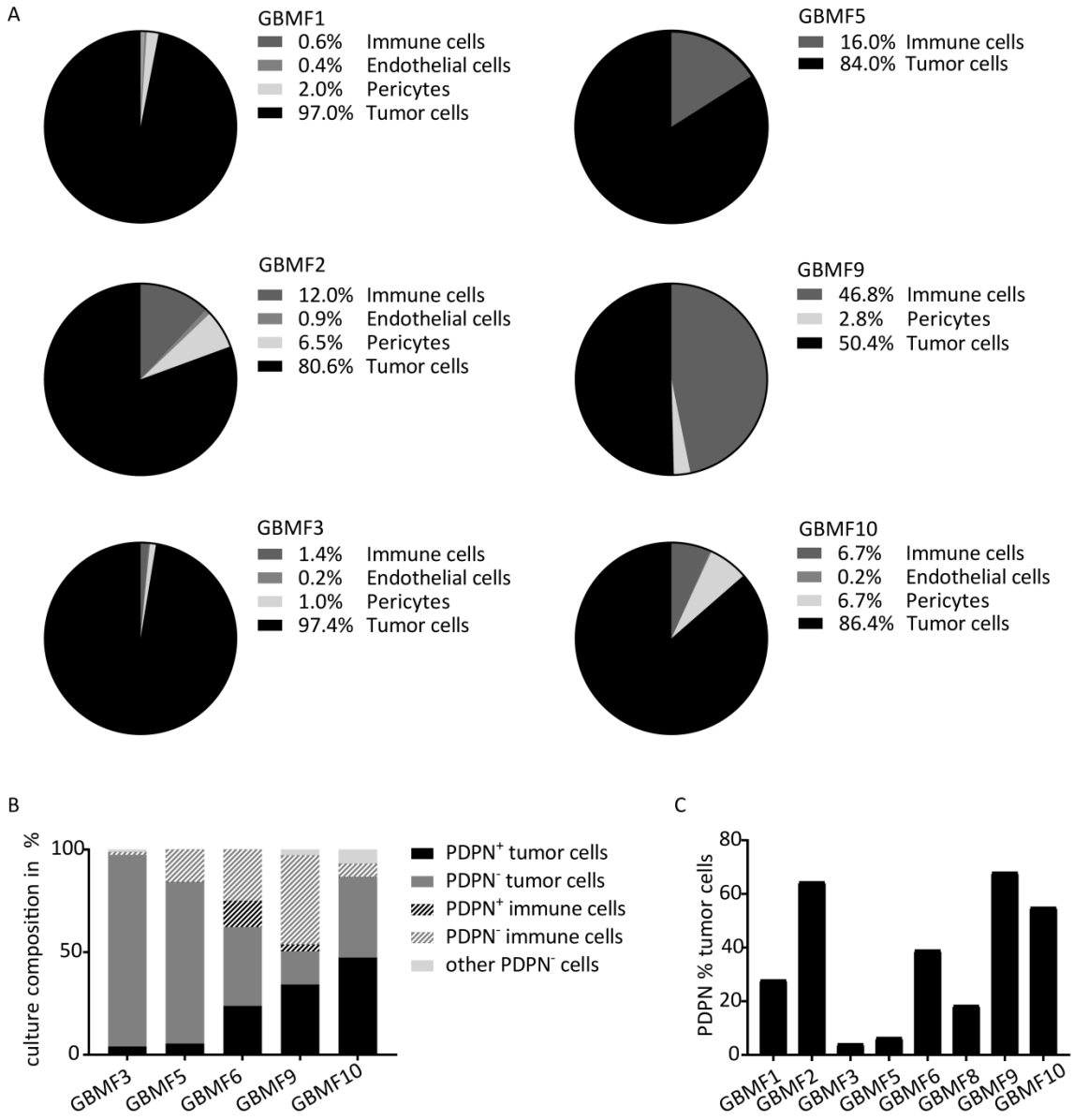

Figure 4.8 Composition of primary human glioblastoma cultures

Two days after tumor cell isolation, cultures were analysed by flow cytometry. (A) tumor cell cultures primarily consist of tumor cells. Major residual non-neoplastic cell types are immune cells. (B) Five primary cultures were co-stained for CD45 and PDPN. With the exception of GBMF6, PDPN positive immune cells represent a negligible population. (C) Primary human glioblastoma cultures express PDPN to various extents.

4.2.2 High podoplanin expression is associated with a malignant gene signature

In order to investigate whether glioma cells that express high levels of PDPN are enriched with tumor promoting properties, $PDPN^{high}$ and $PDPN^{low}$ subpopulations of six long-term patient-derived glioblastoma cultures were sorted, RNA isolated and a microarray analysis performed.

The microarray was validated by quantitative real-time (qRT-) PCR. The expression of selected genes that were either up- or downregulated in PDPN^{high} cells was analysed by qRT-PCR and reflected the results obtained from the microarray analysis (Figure 4.9 B). Gene annotation enrichment analysis was performed to determine whether defined sets of genes associated with a specific biological or molecular function were differentially expressed between the two groups. The analysis revealed a significant higher expression of genes functionally associated with cell adhesion and cell motility, negative regulation of apoptosis and angiogenesis in PDPN^{high} glioma cells compared to PDPN^{low} cells (Figure 4.9 A). As these gene ontologies are associated with tumor development and progression, obtained results indicate that high PDPN expression is part of the malignant gene signature in glioblastoma.

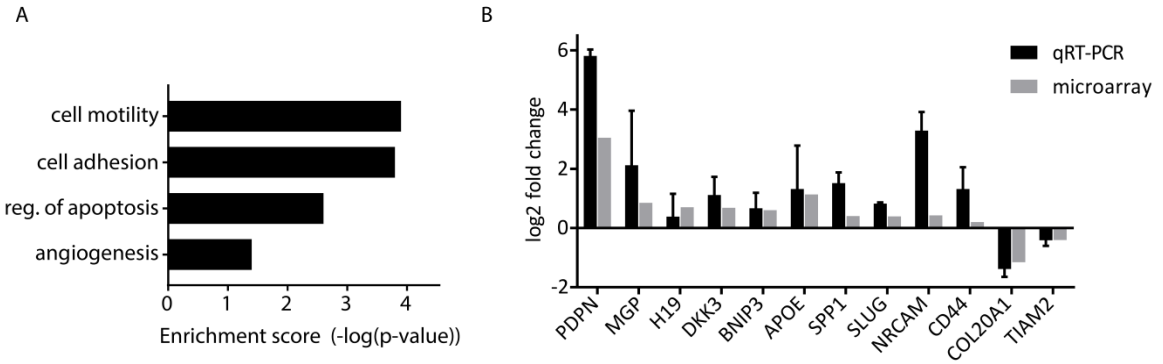

Figure 4.9 Differential gene expression between PDPN^{high} and PDPDN^{low} glioblastoma cells.
(A) Gene annotation enrichment analysis. DAVID-based functional annotation analysis of differentially expressed genes obtained by comparison of PDPN^{high} versus PDPN^{low} glioblastoma cells. Depicted gene ontologies were found to be significantly overrepresented in PDPN^{high} cells. (B) Genes differentially expressed in PDPN^{high} cells. Quantitative RT-PCR validated the microarray results of selected genes most of which are associated with malignancy or cell migration.

4.2.3 Shortened survival correlates with increased podoplanin expression in serial xenotransplantations

As serial transplantations of tumor material result in an increased tumor growth rate and enhanced invasion (Visvader and Lindeman, 2008, Yano et al., 2016), this experimental approach was used to model the malignant progression of glioblastoma. For this purpose, three serial transplantations of five human primary glioblastoma tumors into murine immunocompromised mice were conducted. To gain insight into the expression pattern of *PDPN* during the malignant progression, its expression level was monitored through the course of the disease by flow

cytometry after every isolation step (for schematic overview see Figure 4.10 A). In addition to the analysis of *PDPN* expression, tumor cells isolated from murine recipients were sorted by flow cytometry for a human marker (human leukocyte antigen, HLA) to avoid re-transplantation of residual murine non-neoplastic cells. Although five human tumor samples had initially been used for serial transplantations, in only three cases (GBMF2; GBMF3; GBMF10) I could successfully isolate sufficient tumor cells for the next transplantation round. The survival of the recipents, which is negatively correlated with the aggressiveness of the tumor, was reduced with every stage of transplantation (Figure 4.10 B-D). Concomitant, glioblastoma tumors GBMF2 and GMF3 showed an increased PDPN expression in the successive recipients (Figure 4.10 E, F). The number of PDPN positive cells in the tumor GBMF10 increased drastically in the first recipients reaching almost 100% (Figure 4.10 G). The proportion of PDPN expressing tumor cells settled close to this value and could thus not steadily increase as observed for the other tumors.

Taken together, the decreased survival time of successive recipients and associated aggresiveness of the tumors was parralleled by an increased number of *PDPN* expressing tumor cells. These correlative data suggest the involvement of PDPN in the gain of tumor aggressiveness and thus in malignant progression of glioblastoma.

4.2.4 Podoplanin^{low} sorted glioma cells regain PDPN expression *in vivo*

In order to test whether the aggressiveness of glioma cells depends on their PDPN levels, PDPN^{high} and PDPN^{low} tumor cells from three freshly isolated human primary glioblastoma cultures were sorted and intracranially injected into immunocompromised mice. According to the hypothesis PDPN drives malignant progression of glioblastoma, mice that received tumor cells with low PDPN expression levels were supposed to exhibit an extented survival time compared to mice that received tumor cells with a strong expression of PDPN. However, I did not observe differences in the survival time of the two groups (Figure 4.11 A). When animals had to be sacrificed, brains were either fixed and embedded in paraffin for histological examination or dissociated for flow cytometric analysis of PDPN levels. Interestingly, although sorting of PDPN^{high} and PDPN^{low} cells was efficient (Figure 4.11 B), histological sections and flow cytometry analyses of re-isolated tumors revealed a strong increase in PDPN expression of initially PDPN^{low} cells (Figure 4.11 C, D). It seems likely that this assimilation of PDPN levels accounts for the similar survival times of both groups, which impedes a clear statement about the effect of high PDPN expression on survival. However, the upregulation of *PDPN* expression in all tumors that developed from PDPN^{low} cells suggests that high levels of PDPN are necessary for tumor outgrowth.

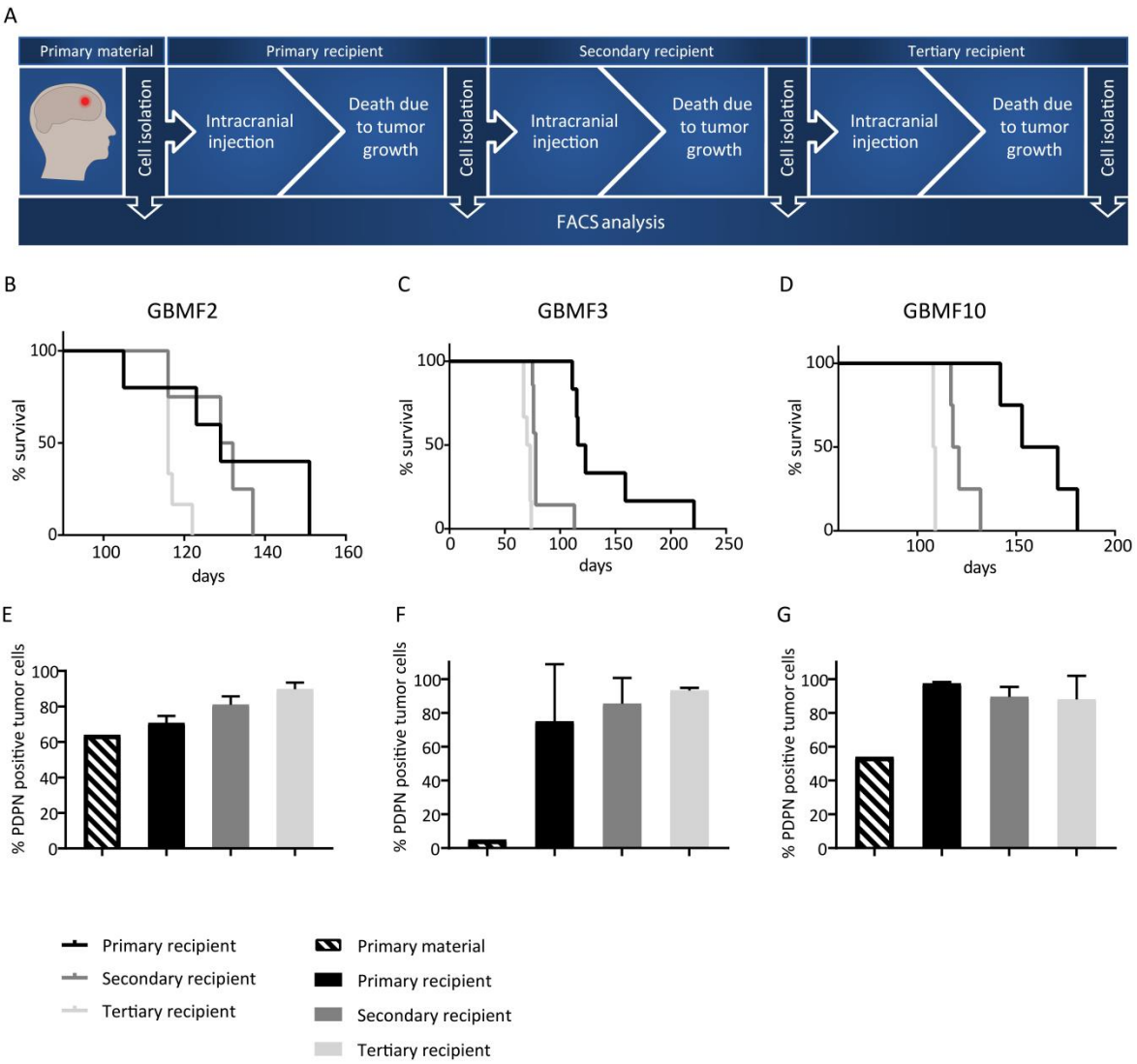

Figure 4.10 Serial transplantations of glioblastoma cells.
(A) Schematic illustration of the transplantation and analysis process. (B-G) *In vivo* passaging of human glioblastoma cells results in shortened survival paralleled by an increase in PDPN expressing tumor cells. Survival of primary, secondary and tertiary recipients of (B) GBMF2, (C) GBMF3 and (D) GBMF10. (E-G) The number of PDPN positive tumor cells (determined by human marker HLA) increases with every stage of transplantation of tumor (E) GBMF2 and (F) GBMF3 or reaches almost 100% with the first transplantation round as observed for (G) GBMF10.

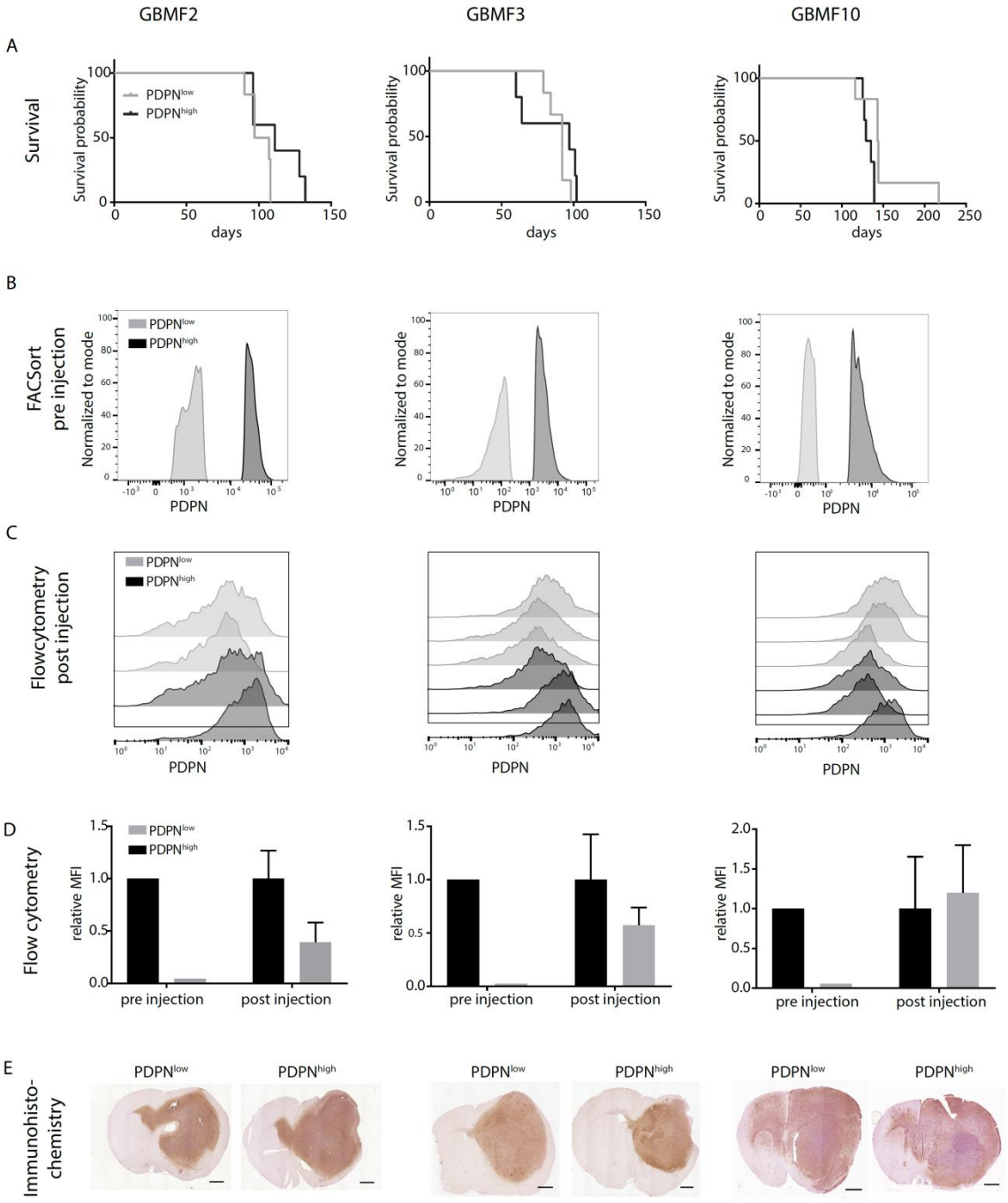

Figure 4.11 PDPN^{low} sorted glioblastoma cells regain high PDPN expression.
Three primary glioblastoma tumors were sorted into PDPN^{high} and PDPN^{low} subpopulations and injected i.c. into six recipients each. (A) Survival of recipients that received PDPN^{low} cells (grey) or PDPN^{high} cells (black) did not significantly differ. (B) PDPN expression level of PDPN^{high} and PDPN^{low} sorted cells. (C) Flow cytometric PDPN analysis of cells that had originally been sorted for low (grey) or high (black) PDPN expression and underwent *in vivo* passaging. (D) Relative change of PDPN expression before and after *in vivo* passaging illustrates the regain of PDPN expression in PDPN^{low} sorted cells. Data normalized to mean fluorescence intensity (MFI) values of PDPN^{high} cells. (E) PDPN immunohistochemistry staining of tumors originated from PDPN^{low} or PDPN^{high} cells. Scale bars 1 mm.

4.2.5 Deleting podoplanin in glioblastoma cells

Above described results were based on descriptive and correlative approaches that showed the expression of *PDPN* throughout all examined glioblastoma tumors and furthermore, indicated a correlation of high PDPN levels and malignant progression of the disease. However, to conclude on the causality of PDPN expression and glioblastoma development functional experiments were required. For this purpose, a loss-of-function approach was taken. In an initial experiment, primary human glioblastoma cells were transduced with a leniviral vector to induce an RNA interference (RNAi)-based knockdown. The usage of only one short hairpin RNA directed against PDPN (sh5αPDPN) resulted in a satisfactory knockdown (Figure 4.12). A FACSort would have additionally been required to eradiacate residual $PDPN^{high}$ cells. To select for stable integration of the RNAi construct prior to a FACSort, cells were treated with puromycin for one week. After a short recovery period of one week cells were reanalysed by flow cytometry. This analysis of PDPN levels revealed a regain in PDPN expression, indicating the instable knockdown of the protein over time. The gradual loss of the PDPN knockdown, even in the presence of puromycin, was also observed in human glioblastomas cell lines (data generated by other group members).

Thus, as the short hairpin-mediated knockdown turned out to be transient, especially in primary material, an alternative approach was taken and PDPN constitutively ablated by usage of the CRISPR/Cas9 system. Therefore, primary glioblastoma cultures, long-term glioblastoma cultures and established glioblastoma cell lines were transduced with the lentiviral vector lentiCRISPRv2 that encodes the endonuclease Cas9 and a guide RNA that either specifically targets PDPN or, as a control, renilla luciferase. The CRISPR/Cas9-induced knockout strategy is based on generation of indels by the error-prone non-homologous end joining (NHEJ)-mediated repair of CRISPR/Cas9-introduced double strand breaks (Ran et al., 2013). Although NHEJ repair is the principle means by which those breaks are repaired, it does not result in a pure knockout population due to in-frame indels, heterozygous deletions or due to the alternative and error-free homology-directed repair. To purify the PDPN knockout ($PDPN^{KO}$) population, all cultures were FAC-sorted to avoid the generation of single cell clones and related clonal artifacts, and to moreover retain the heterogeneity of the primary glioblastoma cultures. Subsequent xenotransplantations of the four $PDPN^{KO}$ and control long-term glioblastoma cultures, revealed that long-term cultivation (> 20 passages) stongly affects tumorigenicity as only two out of 48 injected mice developed tumors (see supplementary Figure 7.1). Thus, long-term cultures were excluded from this and subsequent experiments. Importantly, for some primary (short-term) glioblastoma cultures the viral transduction, FACSort, knockout validation, and especially recovery and propagation periods emerged as a very lengthy procedure. This does not

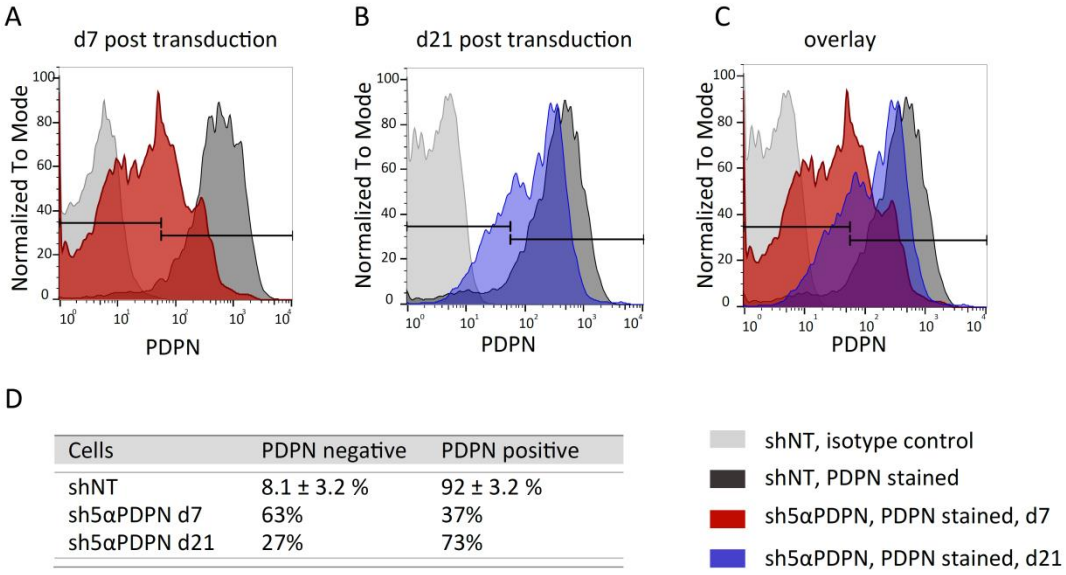

Cells	PDPN negative	PDPN positive
shNT	8.1 ± 3.2 %	92 ± 3.2 %
sh5αPDPN d7	63%	37%
sh5αPDPN d21	27%	73%

Figure 4.12 The short hairpin-mediated knockdown of PDPN declines over time.
(A) Flow cytometric analysis of primary human glioblastoma cells (MNOF1300) that express a non-target (shNT) or a PDPN-specific short hairpin RNA (sh5αPDPN). (B) After additional two weeks (including one week of puromycin treatment) reanalysis showed an increase in PDPN expression. (C) For better illustration PDPN expression levels of sh5αPDPN-cells at the two different time points are shown in one plot. (D) Percentages of PDPN negative and PDPN positive cells as analyzed by flow cytometry.

only disagree with the idea of primary cultures (that should be exposed to *in vitro* culture conditions as briefly as possible), but moreover endangers the risk of loss of tumorigenicity as observed for long-term cultures. Thus, only the two primary knockout and control cultures with shortest cultivation times (GBMF2; GBMF3), and additionally two established human glioma cell lines (LN308; LN319) were used for subsequent loss-of-function studies.

Sorted PDPN^{KO} and control cells were analysed by flow cytometry and Western blotting in order to validate the absence or, respectivley, presence of the protein. In general, high levels of PDPN were expressed in nearly 100% of the control cells, wheras almost no (<1%) PDPN positive cells could be detected in the GBMF2 and LN308 knockout lines. GBMF3 PDPN^{KO} cells contained a PDPN positive population of approxaimately 5%. Although this population could have been erradicated by an additional FACSort, this procedure was omitted to keep the cultivation period as short as possible. This residual small proportion of 5% PDPN positive cells was considered negligible, especially as they did not expand over time *in vitro*. Similary, the LN319 PDPN^{KO} line retained a small population of approximately 6% PDPN positive cells. Taken together, using the CRISPR/Cas9 system PDPN^{KO} cultures were generated that are deficient for PDPN protein.

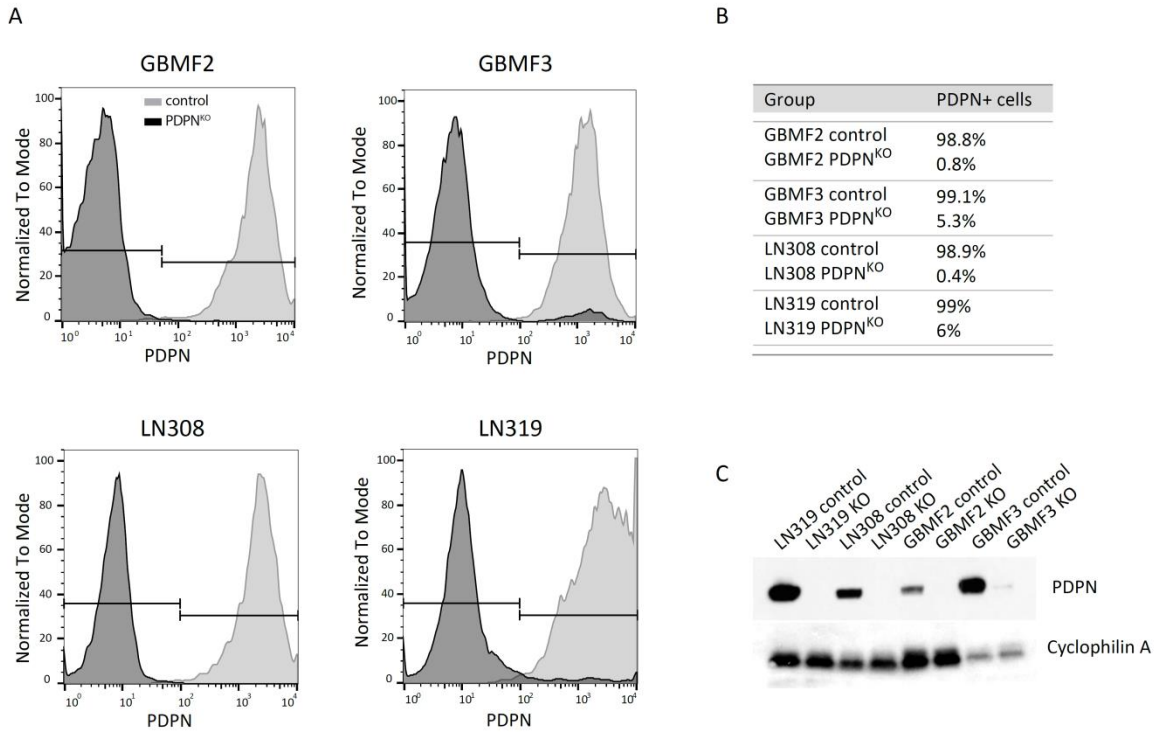

Figure 4.13 PDPN knockout cultures generated by the CRISPR/Cas9 technology.
(A) Flow cytometric analysis of PDPN levels of knockout and control cultures. (B) PDPN positive proportions of analyzed cultures. (C) PDPN levels assessed by Western blot.

4.2.6 Podoplanin deletion in glioblastoma cells does not affect tumor growth

The four control and knockout cell pairs (GBMF2; GBMF3; LN308; LN319) were intracranially injected into six immunocompromised mice per group in order to assess differences in tumor outgrowth and overall survival of the recipients. Tumor growth was regularly monitored by magnetic resonance imaging (MRI). Tissues and body structures are visualized by MRI due to differences in their proton densities and resonance properties in an applied magnetic field. In glioma patients, highest image quality of brain tumors is achieved by a T1-weighted imaging in combination with the intravenous administration of a contrast agent. The contrast agent, mostly gadolinium, enriches in the cancerous tissue due to disruption of the blood-brain barrier and helps to accurately determine the tumor volume. However, T1-weighted tumor volume determination of glioblastomas in mice failed here, presumably due to an intact blood-brain barrier and failure of contrast agent enrichment. Alternatively, brain tumors in mice were analyzed by a T2-weighted imaging, which allows for a gross visualization of the tumor. However, when used for volume determination, it has to be considered that glioblastomas are highly infiltrating and have poorly defined and irregular borders, which probably results in an underestimation of the overall tumor size. To compare the tumor growth of PDPN^{KO} and control

groups, two to three animals per group were regulary anaylzed by MRI, and tumor volumes as determined by T2-weighted images were plotted over time. Figure 4.14 shows tumor growth of two groups (GBMF3; LN319) that could continously be analyzed despite challenging volume determination by T2-weighted images. LN319 PDPN^{KO} and control tumor growth assessed by MRI volume analysis showed no obvious differences (Figure 4.14 B), whereas GBMF3 PDPN^{KO} may have a slight growth delay at later stages compared to the respective control tumors (Figure 4.14 A). However, due to the low number of replicates and the imprecise T2-weighted volume determination, this trend requires validation by other parameter such as survival of the mice. Taken together, these data suggest that PDPN deletion in glioblastoma cells might slightly decelerate tumor growth *in vivo*, however PDPN may not be a major driver for tumor growth.

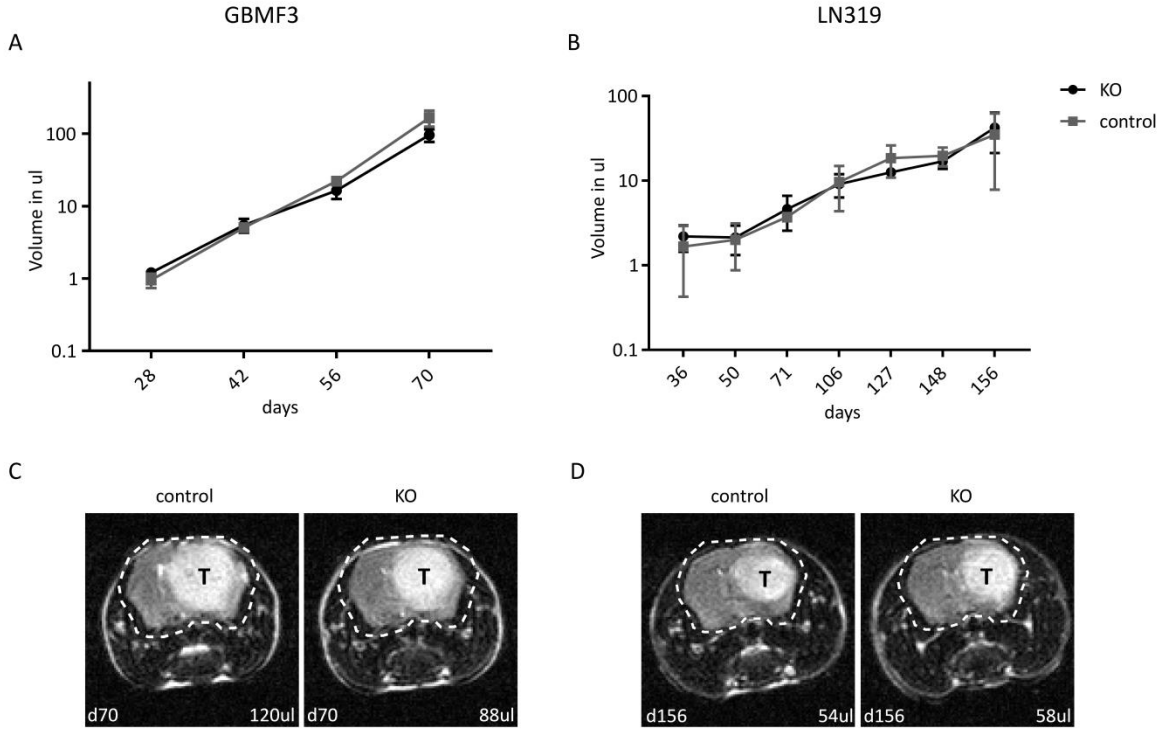

Figure 4.14 Podoplanin deletion has no major impact on tumor growth as analyzed by T2-weighted MRI. Tumor volume of (A) GBMF3 and (B) LN319 PDPN^{KO} and control groups over time, mean and standard deviation depicted. MR image of (C) GBMF3 or (D) LN319 PDPN^{KO} and control tumors. **T** indicates tumor area, the brain is marked by a dashed line, time point after tumor cell injection and determined tumor volume are given at the image bottom.

4.2.7 Survival of glioblastoma bearing mice is not affected by podoplanin deletion

The assessment of the median survival is a common tool to estimate the effect of a treatment or a genetic manipulation of the tumor cells. Thus, I determined the survival rates by the Kaplan-Meier method and analysed differences in the survival of the mice that received PDPN^{KO} or control cells

by the log-rank test. Although the deletion of PDPN did not result in a significant prolongation of survival, all mice bearing PDPN^{KO} tumors showed a slightly increased median survival (Figure 4.15). In general, however, survival curves of PDPN^{KO} and control tumor bearing mice were very similar, questioning the biologcial relevance of this marginal prolongation. Thus, the obtained data suggest that the deletion of PDPN in glioblastoma cells has no considerable impact on survival.

After animals had to be sacrificed, brains were fixed and embedded in paraffin to perform immunohistochemistry stainings. Sections of PDPN^{KO} and control tumors were stained for PDPN in order to validate the CRISPR/Cas9-induced kockout. As I was dealing with xenografts, namely human derived tumors that developed in rodent recipients, I could make use of a human-specific PDPN antibody that only recognizes human, and thus tumor cell-derived PDPN. As shown in Figure 4.16 B, all examined PDPN^{KO} tumors were negative for PDPN, whereas control tumors derived from primary human glioblastoma cells uniformly expressed PDPN. The human glioma cell lines LN308 and LN319 showed a heterogenous expression pattern of PDPN as the largely PDPN positive tumors harbored areas with low or no PDPN expression. Considering that nearly 100% of LN308 and LN319 control cells express PDPN *in vitro*, the focal loss of PDPN in tumors *in vivo* indicates its dispensability as its endogenous silencing did not result in a selective disadvantage of the tumor cells.

The high grade of invasion, especially in tumors generated from primary material, made the tumor mass (of PDPN^{KO} tumors) difficult to precisely determine. Thus, sections of all groups were stained for a human marker (stem121), which served in this case as a tumor cell marker and revealed a large tumor volume and strong invasion into the contraleteral hemisphere in all groups (Figure 4.16). This result illustrates that the deletion of PDPN did not inhibit tumor outgrowth.

4.2.8 The loss of podoplanin does neither affect tumor cell proliferation, nor apoptosis or tumor vascularization

Previous results did not indicate a decisive role of PDPN in glioblastoma progression, as the deletion of *PDPN* did neither affect survival nor tumor outgrowth. However, PDPN could still have a mechanistic function in specific features of glioblastoma, which do not directly affect survival.

Previously, high PDPN expression was associated with a malignant gene signature in glioblastoma (see chapter 4.2.2, page 61), in particular with a gene signature that favors angiogenesis, negative regulation of apoptosis and cell motility. Thus, I performed a number of stainings on PDPN^{KO} and control tumors to dissect the involvement of PDPN in these typical malignant features in more

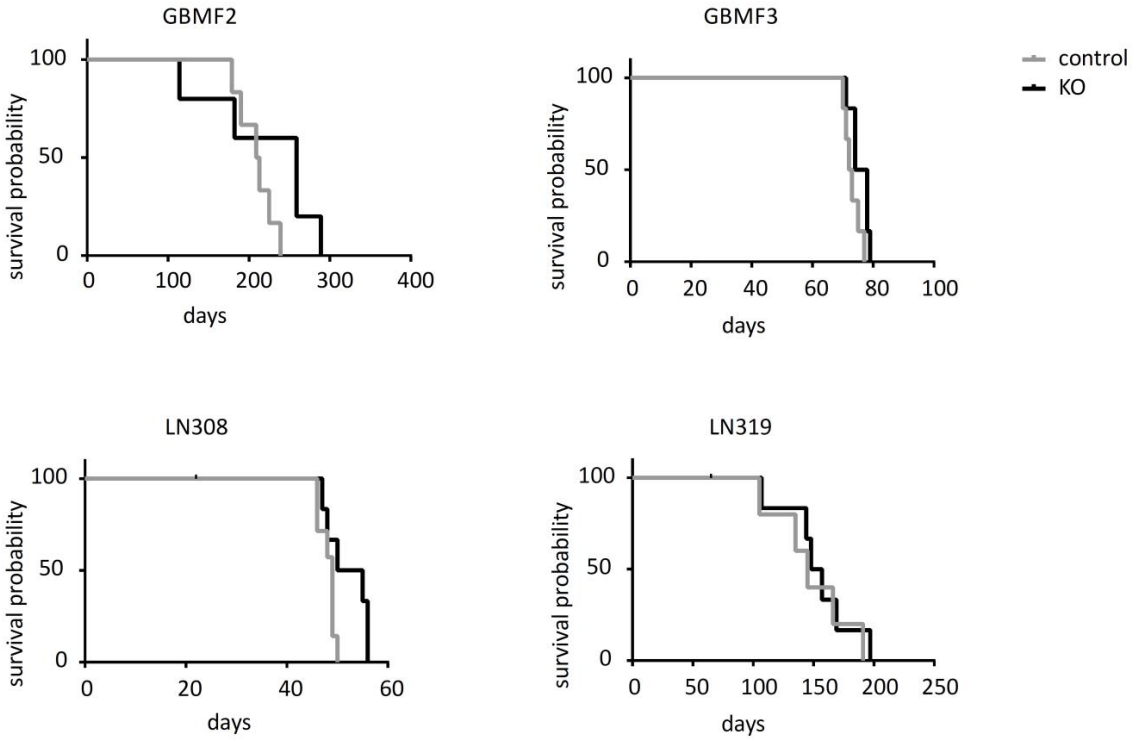

Group	Median survival	p-value
GBMF2 control GBMF2 PDPN^{KO}	211 days 259 days	0.157
GBMF3 control GBMF3 PDPN^{KO}	72.5 days 76 days	0.065
LN308 control LN308 PDPN^{KO}	49 days 52.5 days	0.064
LN319 control LN319 PDPN^{KO}	145 days 152.5 days	0.592

Figure 4.15 Survival is not significantly altered by deletion of PDPN in glioblastoma cells.
Survival curves of mice injected with PDPN^{KO} and control cells, and overview of median survival times of all groups. Log-rank test showed no significant difference in median survival times.

detail. Firstly, vascularization of the tumors was analyzed in order to identify changes in the angiogenic potential upon loss of PDPN. Blood vessel coverage of the tumors as determined by laminin staining was not altered between PDPN^{KO} and control tumors (Figure 4.17 A, B). This result suggests that PDPN expression is not causal for the angiogenic capacity of glioblastoma cells. Secondly, the role of PDPN on apoptosis was investigated. TUNEL staining was performed to analyze whether the loss of PDPN in glioma cells increases the number of apoptotic cells in the tumor. The rate of cell death within the tumor was generally low, and no significant increase in

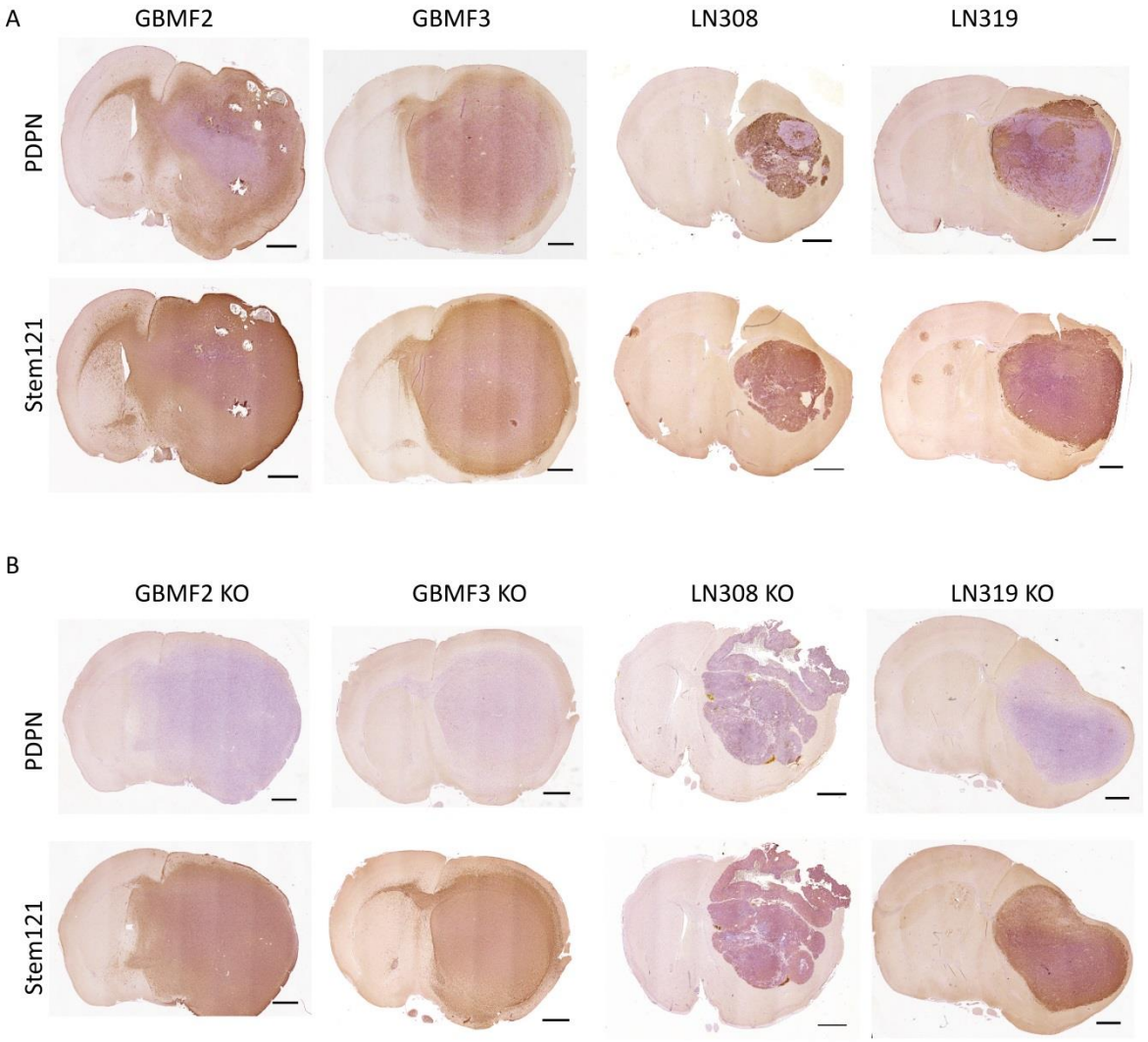

Figure 4.16 Immunohistochemistry staining confirms absence of PDPN in PDPN^{KO} glioblastoma cells.
(A) Control tumors stained for PDPN and stem121, a human marker. (B) Knockout tumors are present, as confirmed by stem121 staining, and remain negative for PDPN. Scale bars 1 mm.

apoptosis in the PDPN^{KO} group was observed (Figure 4.17 C, D). Additionally, cycling cells were identified by Ki67 staining. The staining did not reveal any alterations in tumor cell proliferation induced by the deletion of PDPN (Figure 4.17 E, F), which corresponds to the results of the *in vitro* doubling times of PDPN^{KO} and control cells (Figure 4.17 G). These findings indicate that PDPN does neither influence tumor cell apoptosis nor tumor cell proliferation. Taken together, the examination of PDPN^{KO} and control tumor sections has shown that PDPN is dispensable for tumor vascularization, regulation of apoptosis, and tumor cell proliferation in human glioblastoma.

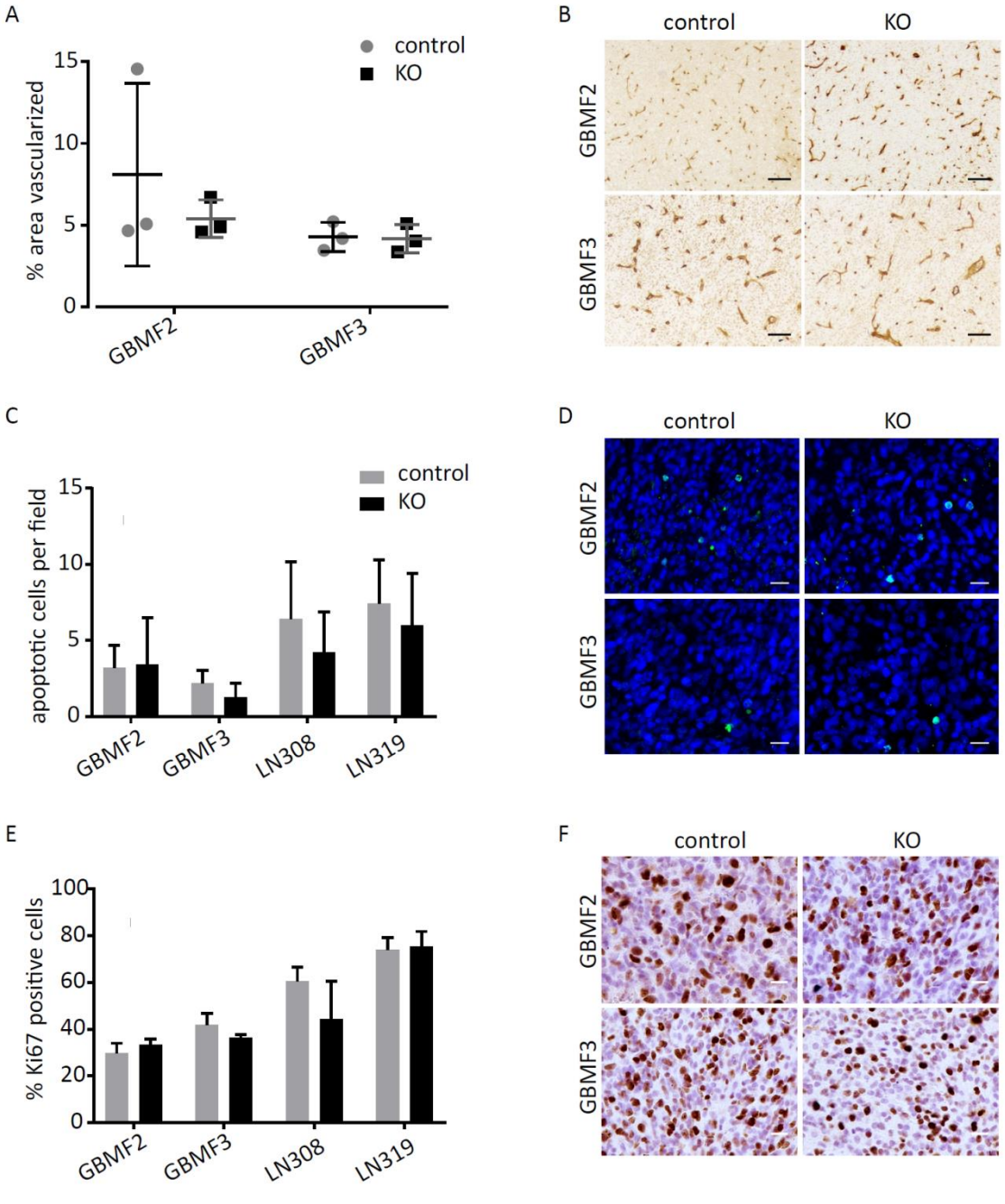

Figure 4.17 The deletion of PDPN does not affect specific tumor features.

(A) Tumor area covered by blood vessels (quantified by laminin staining, B) is not altered between control and PDPN^{KO} groups, 4 - 5 fields of each 3 tumors were analyzed. (C) Quantification of apoptotic cells per field showed no difference between control and knockout tumors, 5 fields per group were analyzed. (D) Representative pictures of TUNEL staining, apoptotic cells with fragmented DNA are indicated in green. (E) The deletion of PDPN did not influence tumor cell proliferation *in vivo,* 5 fields per group were analyzed. (F) Representative pictures of Ki67 staining. (G) *In vitro* doubling time was not altered by PDPN deletion. Black scale bars 100 µm, white scale bars 20 µm.

4.2.9 Glioblastoma cell invasion is podoplanin-independent

Invasion is a key feature of glioblastoma tumors and has been hypothesized to be driven by PDPN. This assumption was based on several findings, including the above reported co-expression of PDPN and genes associated with cell migration and adhesion in glioblastoma cells (see chapter 4.2.2, page 61) and several published *in vitro* studies that reported on the causality of PDPN and glioma cell migration (Ernst et al., 2009, Grau et al., 2015, Peterziel et al., 2012). These studies, however, used established cell lines, which due to their low invasive capacity may not constitute the best model to study glioblastoma cell invasion. Moreover, migration/invasion was examined using two-dimensional scratch or three-dimensional collagen invasion assays, which do not correctly reflect the *in vivo* situation. Thus, to investigate whether PDPN impacts on glioblastoma cell invasion, a three-dimensional invasion assay based on organotypic brain slices was performed. The advantages of this method and optimization steps that were established within the frame of this work were explained in more detailed in chapter 4.1, page 53. In this assay, only primary glioblastoma cultures were examined which exhibit highly invasive behavior *in vivo*. GBMF2 and GBMF3 $PDPN^{KO}$ and control cultures were fluorescently labeled and manually implanted into *ex vivo* cultured murine brain slices. After 2 days the assay was terminated by fixation of the brain slices. Fluorescently labeled glioblastoma cells within the slice were imaged by confocal microscopy. As depicted in Figure 4.18 A, PDPN deletion in the primary tumor cells did not influence their capacity to invade. This finding is in line with microscopic observations of tumor sections. Tumor cells engrafted in the murine brain could be visualized by immunohistochemistry staining using the human marker stem121. Representative pictures given in Figure 4.18 C-J indicated that both, control and knockout cells were able to migrate along common routes of migration, desribed as Scherer's structures. Independent of their PDPN status, glioblastoma cells were found to invade the brain tissue through the brain parenchyma, below the meninges, along blood vessels, and nerve fibers of the *corpus callosum*. In combination with the quantitative assessment of the invasive capacity of $PDPN^{KO}$ and control cells in the *ex vivo* brain slice assay, these data suggest that PDPN is not required for glioblastoma cell invasion.

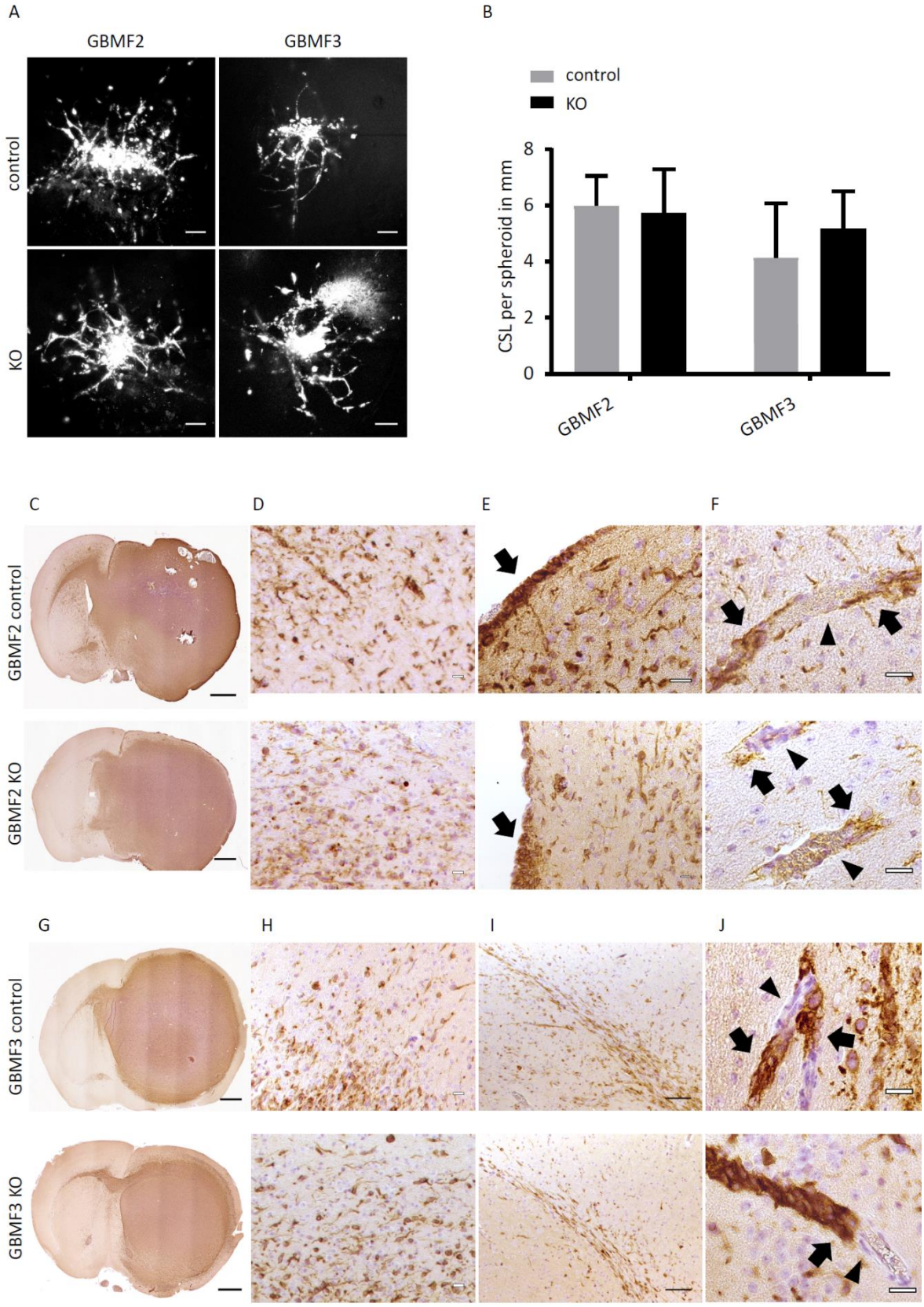

Figure 4.18 PDPN is not required for glioblastoma cell invasion.
(A) Representative pictures of glioblastoma cell invasion assessed by the *ex vivo* brain slice assay. Both, implanted PDPN^{KO} and control cells showed strong invasion into the surrounding brain tissue. Scale bars 100 µm, image quality was optimized by adjustment of brightness, contrast and gamma. (B) Quantification of invasion, represented as cumulative sprout length (CSL) in mm. (C)-(J) Stem121 immunohistochemistry

staining of control and knockout tumors. Stem121 marks human and thus tumor cells in the murine recipient brain. (D) and (H) show diffuse infiltration of the brain parenchyma, (E) depicts tumor cells that migration below the meninges (indicated by arrows). Migration along blood vessels is observed in (F) and (J), arrows indicate tumor cells, arrow heads indicate blood vessels. (I) shows infiltration of the contralateral hemisphere along the *corpus callosum*. Scale bars in (C) and (G) 1 mm, in (I) 100 µm. White scale bars 20 µm.

5 DISCUSSION

5 DISCUSSION

The identification of novel therapeutic targets to improve current treatment measures continues to be a major focus in glioblastoma research. Genes that are mutated, inactivated or overexpressed in neoplastic compared to physiological tissue represent candidates that are potentially involved in the development or progression of cancer. PDPN has been identified as one gene that is overexpressed in high grade gliomas. Accordingly, high PDPN expression has been found to correlate with poor prognosis among all glioma patients (Ernst et al., 2009, Peterziel et al., 2012). Moreover, among all glioblastoma subtypes, PDPN has been reported to be the most expressed in the mesenchymal subtype of glioblastoma. The molecular subtyping of glioblastoma tumors was performed by The Cancer Genome Atlas Consortium (TCGA), with the intention to gain a detailed picture of the molecular setup of glioblastoma tumors. The unsupervised transcriptome analysis of nearly 600 glioblastoma tumors revealed four glioblastoma subtypes, referred to as classical, mesenchymal, neural and proneural signatures (Phillips et al., 2006, Verhaak et al., 2010). The mesenchymal sub-class of a glioblastoma is characterized by strong cellular invasion and poor outcome (Phillips et al., 2006, Verhaak et al., 2010, Xie et al., 2014). These facts, the positive correlation of PDPN with tumor grade and its overexpression in invasive mesenchymal tumors have altogether led to the assumption that PDPN might drive the invasive and aggressive behavior of glioblastoma cells. This hypothesis was supported by publications that have shown decreased proliferation and migration of NCH421k and LN308 glioblastoma cells upon an RNAi-mediated knock down of PDPN (Ernst et al., 2009, Peterziel et al., 2012) or increased migration in response to *PDPN* overexpression in U373MG, U87MG cell lines (Grau et al., 2015). These results were in line with overexpression studies performed in cancer cell lines of other entities where PDPN was accordingly described as a migration-promoting protein (Martin-Villar et al., 2005, Wicki et al., 2006). These *in vitro* studies have further supported the idea of exploiting PDPN as therapeutic target. However, *in vivo* studies required to validate these *in vitro* findings as well as insight into the underlying mechanism were still lacking. Thus, I investigated the functional role of PDPN in human glioblastoma including strongly needed *in vivo* experiments.

An initial point of this study was the validation of previous findings that correlated PDPN with malignancy in order to establish a model for detailed investigations of the underlying mechanism. To investigate whether glioma cells that express high levels of PDPN are enriched with tumor promoting properties, I determined the gene expression profile of six patient-derived

glioblastoma PDPN^{high} and PDPN^{low} subpopulations. In PDPN^{high} cells, the analysis showed a significant higher expression of genes functionally associated with malignant traits such as cell migration. Thus, it was assumed that high *PDPN* expression is part of the malignant gene signature in glioblastoma. In order to examine whether the association of PDPN and malignancy holds true *in vivo*, serial transplantations of patient-derived material were used as a model of malignant progression of the disease. Flow cytometry of the tumor cells at every transplantation step revealed a steady increase of PDPN levels paralleled by a shortened survival of the corresponding recipients. This result indicated a positive correlation of PDPN expression and aggressiveness. The hypothesis of a tumor driving effect of PDPN was further strengthened when PDPN^{low} sorted glioblastoma cells drastically increased the expression of PDPN after xenotransplantation. This regain of high PDPN expression was interpreted as another indication for the tumor-promoting effect of PDPN. The correlation of high PDPN expression and tumor progression appeared to be repeatedly confirmed by different approaches. To finally clarify the causal link between PDPN and malignancy, I performed intracranial injections of PDPN deleted primary human glioblastoma cells and established glioma cell lines. Contrary to expectations, I could not observe an effect of PDPN ablation on tumor development. The survival of PDPN^{KO} tumor bearing mice was not significantly different to control mice. Subsequently, a more detailed analysis of malignant features was conducted, including tumor vascularization, apoptosis and proliferation. Concordantly with the result of unaffected survival, the analysis of these malignant features did not reveal any alterations in PDPN^{KO} compared to control tumors. The glioblastoma characteristic that has been associated most frequently with PDPN overexpression is invasive growth of the tumor cells. To investigate the effect on glioblastoma cell invasion more precisely, not only tumor sections have been microscopically examined for infiltrative growth, but the invasive capacity of glioblastoma cells was also quantitatively assessed in the *ex vivo* invasion assay. The two approaches consistently showed no impaired invasion of PDPN^{KO} cells. Hence, this study has validated the positive correlation of PDPN expression and malignancy. Concurrently, however, detailed *in vitro*, *ex vivo* and *in vivo* studies have shown the dispensability of PDPN for tumor cell invasion and tumor progression. The following section will discuss the obtained results in the context of recent literature to critically assess the value of the study and its limitations.

5.1 Technical limitations of the study

5.1.1 A malignant function of podoplanin might be restricted to mesenchymal glioblastoma tumors

A recent optimized transcriptome analysis of glioblastoma single cells, tumorspheres and tumor biopsies obtained from the TCGA portal (Wang et al., 2017) has validated three of the previous four molecular sub-classifications: classical, proneural and mesenchymal. The previously included neuronal subtype has emerged as non-tumor specific, presumably caused by high non-neoplastic cell contaminations in the initially investigated tumor samples. Although data generated by this recent study have validated the correlation of PDPN overexpression and poor outcome in glioma patients (Figure 5.1 A), it has also been shown that this correlation is absent in the glioblastoma patient cohort (Figure 5.1 B). Interestingly, when analyzing the individual molecular subtypes of glioblastoma, a correlation of high PDPN expression and poor overall survival is evident for the mesenchymal but not for the other glioblastoma subtypes (Figure 5.1 C). Considering that this correlation is restricted to the mesenchymal subtype, a potential malignant function of PDPN could depend on the signature of the tumor. An RNA-seq analysis, exome sequencing and subsequent biocomputational comparison with the previously defined subtypes would determine whether the mesenchymal subclass was covered by the here applied samples GBMF2; GBMF3 and cell lines LN308 and LN319. Without this information it cannot be excluded that PDPN has a pro-tumorigenic function in only one specific subtype of glioblastoma, which was not represented by the samples used in this study.

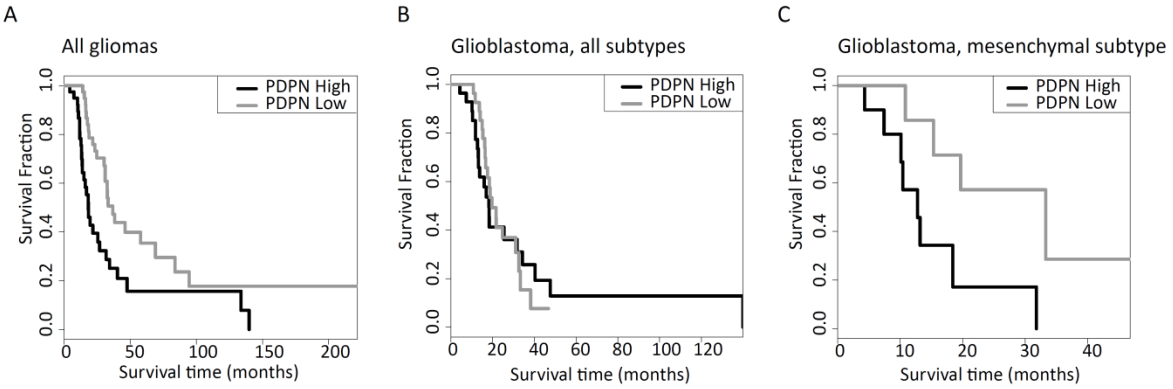

Figure 5.1 Correlations of PDPN expression and survival in different brain tumor subsets.
(A) PDPN expression in glioma patients significantly correlates with poor outcome, n = 39; p = 0.0034; whereas (B) survival of glioblastoma patients is not significantly correlated with PDPN expression, n = 28; p = 0.9046. (C) Patients with a mesenchymal subtype of glioblastoma show a significant correlation of high PDPN expression and poor survival, n = 9; p= 0.0136. Data obtained from Wang et al. (2017), accessed via http://recur.bioinfo.cnio.es/ on November 2017.

5.1.2 A potential malignant function of podoplanin could be compensated by other proteins

As noted, in this study the CRISPR/Cas9-based gene modification tool was used to induce the deletion of PDPN in glioblastoma cells, which has not revealed an impact on malignant features of the tumor cells. According to the here applied CRISPR/Cas9-edited knockout strategy, the cells may still translate an approximately 50 amino acid short truncated protein, as the applied guide RNA facilitates the double strand break within the second exon of the PDPN encoding gene. However, even if this peptide was transcribed and remained stable, it could not be positioned at the cell membrane, as it lacks, in addition to the cytoplasmic tail and large parts of the ectodomaine, the complete transmembrane domain, impeding the correct exposure and thus function of the protein on the cell surface. Thus, the presence of a truncated, yet functional, PDPN protein in the here generated $PDPN^{KO}$ cells was considered unlikely.

Previous studies that used an RNAi-mediated knock down of PDPN have in contrast attributed the protein with a pro-migratory and proliferative function (Ernst et al., 2009, Peterziel et al., 2012). The key difference between the two techniques is that the application of CRISPR/Cas9 results in true loss-of-function as the system interferes on the genetic level (Ran et al., 2013), whereas RNAi generally causes a reduced protein level (reviewed in Mohr et al., 2014). Divergent phenotypes in knockdown and knockout studies have frequently been reported and attributed, among other reasons, with changes in protein levels in the knockout cells that lead to the functional compensation of the deleted gene (Daude et al., 2012, Freudenberg et al., 2012, Rossi et al., 2015). Thus, the complete ablation of PDPN by the CRISPR/Cas9-induced knockout could have provoked compensatory reactions of the cell which might not take place in cells with a reduced PDPN protein level and thus resulted in different phenotypes. A potential compensation in response to the loss of PDPN could occur on a transcriptional or post-transcriptional level, whose identification would have required a microarray or a mass spectrometry and subsequent analysis of differentially expressed genes/translated proteins between $PDPN^{KO}$ and control cells. Due to the lack of known isofunctional PDPN paralogues, which represent the most likely compensation candidates, the search for a compensatory protein would have to focus on other proteins with comparable location and functions. Tetraspanins, integrins, ICAMs and CD44 may represent potential candidates as they are cell surface proteins and, similar to PDPN (Martin-Villar et al., 2006), have been reported to link the cell membrane with the cytoskeleton by members of the ezrin/radixin/moesin (ERM) protein family (Sala-Valdes et al., 2006, Tang et al., 2007, Yonemura et al., 1998). Similarly, the dispensability of PDPN in basal keratinocytes during skin development and wound healing has been proposed to result from the functional compensation by a yet undetermined ERM interaction partner (Baars et al., 2015).

The search for a PDPN-compensating protein, however, is a very laborious approach that would moreover not necessarily result in the identification of a potentially compensatory candidate as not only the transcriptional and post-transcriptional but also the spatial distribution of proteins affects their function (Perego et al., 2002). Finally, the identification of a compensating protein would still not provide insight into the mechanistic function of PDPN, as a potential compensation could depend on alternate pathways with different molecular mechanisms.

5.1.3 The usage of immunodeficient mice may mask a potential malignant function of PDPN

One technical limitation that could have masked a potential effect of PDPN on tumor progression is the usage of immunodeficient mice. In order to use tumor cells that have a genetic and epigenetic make up that resembles as closely as possible the situation in the patient (Lee et al., 2006), this study has used patient-derived primary glioblastoma cultures. However, orthotopic transplantations require in this case immunocompromised recipients to prevent the immune system-mediated rejection of the tumor cells (Morton and Houghton, 2007). Therefore, it cannot be excluded that PDPN attributes the tumor cells with immune suppressive functions that would, in an immunocompetent background, result in a growth advantage compared to PDPN deficient tumors. Although PDPN - at least on lymphatic endothelial cells - has been shown to interact with CLEC-2 on dendritic cells (Acton et al., 2012), there was no evidence that supported the idea of an immune suppressive function of PDPN. Thus, we decided for immunodeficient mice that enabled the usage of primary human glioblastoma cells in favor of the great resemblance to the patient.

5.2 Technical strengths of the study

5.2.1 The application of a novel gene editing tool with low off-target rates results in a complete PDPN knockout

The functional analysis of a protein requires either its overexpression or its ablation within the cell. Previous reports that associated PDPN with a pro-tumorigenic function in various cell lines were almost exclusively based on overexpression studies (Kunita et al., 2011, Martin-Villar et al., 2010, Martin-Villar et al., 2006, Martin-Villar et al., 2005, Wicki et al., 2006). Although this is a common tool in biomolecular research to assess the function of a protein, it has also been shown to involve disadvantages. One publication focusing on overexpression screens in *Saccharomyces*

cerevisiae has found single gene overexpression to cause variable negative effects on the cell, including decrased growth rates and toxicity (Tomala et al., 2014). These malfunctions were particularly pronounced when the overexpressed genes were transmembrane proteins (Osterberg et al., 2006, Tomala et al., 2014). The authors proposed two different mechanisms that could cause this effect. Firstly, the overexpression of the desired protein leads to an over-engagement of the translation and folding machinery which could result in metabolic stress of the cell. Furthermore, the overload of the cell with the transmembrane protein of interest could negatively affect the protein balance and thus function at the membrane. Secondly, the authors suggested that membrane proteins are, due to their transmembrane domains, prone to misfold and form aggregates, which tend to penetrate and damage cellular membranes (for review see Stefani, 2008). Thus, the overexpression of PDPN might not constitute the most appropriate approach to study its function. Instead, we decided to follow a loss-of function approach, which can be accomplished by numerous tools (Gaj et al., 2013). In this study, I used the novel RNA-guided CRISPR-Cas9 genome editing system, which provides many advantages. In contrast to the RNAi-mediated knockdown approach that causes a decreased protein level, the CRIPR/Cas9-based method interferes on the genetic level and results, dependent on the strategy, in a complete loss of the protein. This excludes the possibility that a potential effect is masked by the presence of residual protein that remains sufficient to maintain its cellular function. Furthermore, the RNAi-based knockdown approach has repeatedly been reported to induce off-target effects and variable on-target efficiencies (Jackson et al., 2003, Sigoillot et al., 2012). Conversely, a recent report has shown that the off-target effect of the CRISPR/Cas9 gene editing system is near the detection limit of targeted deep sequencing (Kim et al., 2015). Moreover, an experimental side-by-side comparison of RNAi- and CRISPR/Cas9-based screening methods recently demonstrated a higher variability and more off-target activity in the RNAi- compared to the CRISPR/Cas9-based approach (Evers et al., 2016). Thus, the discrepancy of this and previous studies regarding the effect of PDPN on tumor proliferation and invasion could be based on the different gene silencing tools. The application of RNAi-mediated knockdown of PDPN in previous studies (using identical hairpin sequences) could have resulted in pro-invasive and pro-proliferative off-target effects. In the present study, potential shRNA-mediated off-target effects were avoided by the usage of the CRISPR/Cas9 system.

5.2.2 The application of the three-dimensional *ex vivo* invasion assay enables the reliable assessment of tumor cell invasion

In the past decades tumor cell invasion has primarily been assessed by inexpensive and rapid two-dimensional assays. However, these cell culture models are very limited in their power to accurately predict the effect of proteins or small molecules on cell invasion *in vivo*, probably due to functional differences of proteins between two- and three-dimensional migration and the absence of environmental influences (Jensen et al., 2017, Pampaloni et al., 2007). Although animal models are thought to represent the most reliable method of investigating cell invasion, they involve not only high cost but also ethical and technical concerns. This has resulted in attempts to bridge the gap between over-simplified cell culture approaches and the more meaningful but laborious *in vivo* models with reproducible *ex vivo* techniques. The current state of the art to mimic the natural environment of glioma cells are organotypic brain slice cultures that can be cultivated *ex vivo* for several days to weeks without considerable loss of their cytoarchitecture (for reviews see Huang et al., 2012, Lossi et al., 2009). Retaining their physiological structure, brain slices provide an optimal three-dimensional matrix for *ex vivo* invasion assays. Mostly perinatal donors have been used for the preparation of organotypic brain slices due to their high mechanical and ischemic resistance (Cho et al., 2007). However, in rodents the ECM is substantially remodeled starting from 2 weeks after birth. This remodeled and thus significantly firmer ECM is subsequently maintained throughout adulthood (Zimmermann and Dours-Zimmermann, 2008). Similarly, myelination of nerve fibers occurs predominantly postnatally and can be extended to adulthood (Semple et al., 2013). Hence, absent or incomplete myelination and the immature and loose extracellular matrix represent profound differences between neonatal and mature adult brain tissue. In order to reflect the age-related disease of adult glioma, I decided to use adult brain slices that exhibit a mature myelination pattern and ECM composition.

While there are previous reports that used organotypic brain slices for tumor cell invasion assessment, we still lack a simple, standardized, and reproducible protocol that allows its application in basic and preclinical research. Various approaches for the co-cultivation of tumor cells and slices and the measurement of cell invasion have been published. For brain metastasis research, tumor cells have been seeded in a matrigel plug adjacent to the brain slice in order to investigate interactions between cancer and glial cells by fluorescence microscopy (Chuang et al., 2013). However, this model is unsatisfactory when used to examine the invasion of primary brain tumor cells, as they arise and migrate within the brain tissue and moreover do not encounter an environment comparable to matrigel. Other publications have developed this approach by seeding single cells on top of the slices (Chadwick et al., 2015). However, this technique comprises

disadvantages, as it is disturbed by the diffusion of single cells after seeding and requires life cell imaging, preferably by an upright confocal microscope, which is not universally available. Moreover, reduced invasion is observed when the tumor cells are seeded on top instead of within the tissue, as the cells migrate on the slice surface instead of efficiently penetrating the tissue. In contrast, I implanted tumor cells as spheroids within the tissue in order to position them at a specific location of the brain slice and to provide a comparable starting point for the assay. Indeed, other publications have reported this approach; however, they show a low grade of invasion that does not reflect the aggressive infiltration observed in patients (Aaberg-Jessen et al., 2013, Petterson et al., 2016, Xu et al., 2016). In contrast, the here established protocol resulted in strong invasion of a panel of human and murine glioma cell lines as well as primary cells. Moreover, imaging quality of implanted tumor cells could be improved by the usage of DiD, which drastically reduces autofluorescence compared to the commonly applied DiI or ectopic GFP expression. Thus, in the course of this work, the *ex vivo* invasion assay has been optimized in order to serve as a standardized protocol that allows for a variety of application options. The possibility of specifically manipulating either one or both compartments involved in tumor cell migration, the microenvironment and the tumor cells themselves, and to monitor the consequences of the manipulation on tumor cell invasion is a major advantage of this improved protocol. Besides the implantation of manipulated tumor cells, in this case $PDPN^{KO}$ and control cells, I demonstrated the flexibility of the protocol by manipulating the microenvironment with exogenous small molecule (jasplakinolide) treatment. Consequently, the *ex vivo* invasion assay is a powerful tool to identify critical factors in tumor cells and their putative interaction partners in the tumor microenvironment.

Thus, the potential involvement of PDPN in tumor cell invasion was most faithfully assessed using the optimized *ex vivo* invasion assay. The conducted experiments have shown that the transmembrane protein PDPN is dispensable for glioblastoma cell migration. Considering previous publications that reported on false-positive anti-invasive candidate compounds identified by conventional *in vitro* assays (Jensen et al., 2017) and discrepancies in protein function between two- and three-dimensional assays (Skau et al., 2016), conventional migration assays used in previous publications might have led to a false-positive result indicating a pro-invasive role for PDPN.

5.3 Podoplanin as a marker for glioblastoma cells

Although this study could validate previous findings on the correlation of PDPN expression and malignant progression of glioblastoma tumors, functional experiments have indicated that the progression of the disease is PDPN-independent. These results were moreover confirmed by a genetic engineered mouse model of glioblastoma generated by Dr. Barbara Costa in a collaboration of Prof. Dr. Peter Angel and Dr. Hai-Kun Liu's research groups, where *Pdpn* was deleted in combination with the tumor suppressors *Pten* and *Tp53* in neural stem cells. When compared to control mice carrying the double knockout of *Pten* and *Tp53*, no difference in tumor incidence, tumor growth or survival was examined.

The question remains why glioblastoma cells express *PDPN*, especially, if there is no selective advantage for PDPN positive tumor cells. In the course of this study, PDPN has been found to be part of a malignant signature. First, this has been interpreted as an indication for the malignant role of PDPN, however, due to the technical approach of using cells sorted for low or high PDPN levels and not $PDPN^{KO}$ and control cells, it cannot be concluded that the malignant nature of glioblastoma cells is caused by high *PDPN* expression. Instead, there is the opposite possibility that the malignant signature causes increased levels of PDPN. As noted in the introductory chapter, PDPN transcription has been shown to be powerfully regulated by AP-1 and STAT3 transcription factors (Durchdewald et al., 2008, Peterziel et al., 2012, Priester et al., 2013). The hyperactivation of the PI3K-AKT signaling pathway has been reported for the majority of glioblastoma tumors (Parsons et al., 2008). This signaling axis has been shown to induce AP-1-mediated PDPN expression in glioblastoma cells (Peterziel et al., 2012). Furthermore, TCGA sequencing data have revealed a transcriptional network regulated by STAT3 as a central malignant element in many glioblastoma tumors, and particularly in the mesenchymal subtype (Phillips et al., 2006, Verhaak et al., 2010). Thus, the constitutive activation of the PI3K/AKT and STAT3 signaling pathway in glioblastoma might be the cause for the broad overexpression of PDPN in glioblastoma. This, together with the results of the present study, indicates a great value of PDPN as a marker for aggressive glioblastoma cells but at the same time discourages the functional inactivation of PDPN as a novel therapeutic approach, due to the dispensability of PDPN for malignant behavior of glioblastoma cells.

5.4 Podoplanin expression – a common feature of tumor cells and reactive astrocytes

Although this study has unexpectedly not identified a malignant role for PDPN in glioblastoma, the question about the constitutive expression of PDPN by tumor cells despite its dispensability remains unsolved. One possible explanation is that PDPN expression lies downstream of PI3K-AKT and STAT3 signaling pathways, which have frequently been shown to be hyperactivated in glioblastoma. Thus, PDPN expression could be a side effect of hyperactivated upstream signaling pathways that drive malignancy in glioblastoma cells. Alternatively, the presence of PDPN in glioblastoma cells could be explained by their great transcriptional resemblance with astrocytes. The transcriptional activation of PDPN in response to STAT3 activity in tumor cells shows a parallel to reactive astrocytes. This overlap in gene expression is not surprising, as previous publications have shown a strong astrocytic signature in glioblastoma tumors (Phillips et al., 2006, Verhaak et al., 2010) and it has furthermore been reported that glioblastoma can arise from mature astrocytes (Endersby et al., 2011, Radke et al., 2013). In astrocytes, STAT3 activity has been reported as a master regulator of astrocyte activation (Ben Haim et al., 2015, Herrmann et al., 2008). Astrocytes have been shown to be activated in many CNS diseases, including stroke, injury and brain tumors (reviewed in Burda and Sofroniew, 2014, Pekny et al., 2016). A recent publication has shown that reactive astrocytes in the above mentioned settings do express PDPN (Kolar et al., 2015), presumably induced by pSTAT3. Although the function of PDPN *de novo* expression in reactive astrocytes has not been identified, it is conceivable that the protein is involved in the functions of reactive astrocytes including tissue regeneration and regulation of inflammatory responses – processes that could influence tumor growth and progression and could thus make *PDPN* expression by tumor cells dispensable. Hence, the physiological function of PDPN in reactive astrocytes and other cells of the glioma microenvironment remains an exciting open research topic, as well as the resulting question whether and how this affects tumor cells.

5.5 Conclusion and perspectives

Using correlative and descriptive approaches as well as the analysis of loss-of-function experiments, this study has concluded that PDPN is not rate-limiting for glioblastoma progression and invasion. This finding is important for further preclinical studies, as previous publications have indicated a tumor promoting role for PDPN and proposed the protein as a therapeutic target. However, this study suggests that the development and usage of compounds that functionally

inactivate PDPN would not result in the desired tumor suppressing effect. Instead, this study has validated PDPN as a valuable marker for clinical applications as PDPN has been found to be part of a malignant gene signature in glioblastoma, marking tumors with poor prognosis. Thus, if glioma research will continue to focus on PDPN as a therapeutic target, I suggest using PDPN as a gate entry to mediate the targeted delivery of cytotoxic or immunogenic compounds into very malignant glioma cells, for instance by antibodies that target cancer-specific PDPN (Kato and Kaneko, 2014).

6 REFERENCES

6 REFERENCES

AABERG-JESSEN, C., NORREGAARD, A., CHRISTENSEN, K., PEDERSEN, C. B., ANDERSEN, C. & KRISTENSEN, B. W. 2013. Invasion of primary glioma- and cell line-derived spheroids implanted into corticostriatal slice cultures. *International Journal of Clinical and Experimental Pathology,* 6**,** 546-560.

ACTON, S. E., ASTARITA, J. L., MALHOTRA, D., LUKACS-KORNEK, V., FRANZ, B., HESS, P. R., JAKUS, Z., KULIGOWSKI, M., FLETCHER, A. L., ELPEK, K. G., BELLEMARE-PELLETIER, A., SCEATS, L., REYNOSO, E. D., GONZALEZ, S. F., GRAHAM, D. B., CHANG, J., PETERS, A., WOODRUFF, M., KIM, Y. A., SWAT, W., MORITA, T., KUCHROO, V., CARROLL, M. C., KAHN, M. L., WUCHERPFENNIG, K. W. & TURLEY, S. J. 2012. Podoplanin-rich stromal networks induce dendritic cell motility via activation of the C-type lectin receptor CLEC-2. *Immunity,* 37**,** 276-89.

ALDAPE, K., ZADEH, G., MANSOURI, S., REIFENBERGER, G. & VON DEIMLING, A. 2015. Glioblastoma: pathology, molecular mechanisms and markers. *Acta Neuropathol,* 129**,** 829-48.

ASKOXYLAKIS, V., BADEAUX, M., ROBERGE, S., BATISTA, A., KIRKPATRICK, N., SNUDERL, M., AMOOZGAR, Z., SEANO, G., FERRARO, G. B., CHATTERJEE, S., XU, L., FUKUMURA, D., DUDA, D. G. & JAIN, R. K. 2017. A cerebellar window for intravital imaging of normal and disease states in mice. *Nat Protoc,* 12**,** 2251-2262.

ASTARITA, J. L., ACTON, S. E. & TURLEY, S. J. 2012. Podoplanin: emerging functions in development, the immune system, and cancer. *Front Immunol,* 3**,** 283.

ASTARITA, J. L., CREMASCO, V., FU, J., DARNELL, M. C., PECK, J. R., NIEVES-BONILLA, J. M., SONG, K., KONDO, Y., WOODRUFF, M. C., GOGINENI, A., ONDER, L., LUDEWIG, B., WEIMER, R. M., CARROLL, M. C., MOONEY, D. J., XIA, L. & TURLEY, S. J. 2015. The CLEC-2-podoplanin axis controls the contractility of fibroblastic reticular cells and lymph node microarchitecture. *Nat Immunol,* 16**,** 75-84.

AUSMAN, J. I., SHAPIRO, W. R. & RALL, D. P. 1970. Studies on the chemotherapy of experimental brain tumors: development of an experimental model. *Cancer Res,* 30**,** 2394-400.

BAARS, S., BAUER, C., SZABOWSKI, S., HARTENSTEIN, B. & ANGEL, P. 2015. Epithelial deletion of podoplanin is dispensable for re-epithelialization of skin wounds. *Experimental Dermatology,* 24**,** 785-787.

BAO, S., WU, Q., LI, Z., SATHORNSUMETEE, S., WANG, H., MCLENDON, R. E., HJELMELAND, A. B. & RICH, J. N. 2008. Targeting cancer stem cells through L1CAM suppresses glioma growth. *Cancer Res,* 68**,** 6043-8.

BARROS, C. S., FRANCO, S. J. & MULLER, U. 2011. Extracellular matrix: functions in the nervous system. *Cold Spring Harb Perspect Biol,* 3**,** a005108.

BEN HAIM, L., CEYZERIAT, K., CARRILLO-DE SAUVAGE, M. A., AUBRY, F., AUREGAN, G., GUILLERMIER, M., RUIZ, M., PETIT, F., HOUITTE, D., FAIVRE, E., VANDESQUILLE, M., ARON-BADIN, R., DHENAIN, M., DEGLON, N., HANTRAYE, P., BROUILLET, E., BONVENTO, G. & ESCARTIN, C. 2015. The JAK/STAT3 Pathway Is a Common Inducer of Astrocyte Reactivity in Alzheimer's and Huntington's Diseases. *Journal of Neuroscience,* 35**,** 2817-2829.

BENDA, P., LIGHTBODY, J., SATO, G., LEVINE, L. & SWEET, W. 1968. Differentiated rat glial cell strain in tissue culture. *Science,* 161**,** 370-1.

BERTOZZI, C. C., SCHMAIER, A. A., MERICKO, P., HESS, P. R., ZOU, Z., CHEN, M., CHEN, C. Y., XU, B., LU, M. M., ZHOU, D., SEBZDA, E., SANTORE, M. T., MERIANOS, D. J., STADTFELD, M., FLAKE, A. W., GRAF, T., SKODA, R., MALTZMAN, J. S., KORETZKY, G. A. & KAHN, M. L. 2010. Platelets regulate lymphatic vascular development through CLEC-2-SLP-76 signaling. *Blood,* 116**,** 661-70.

BRAT, D. J., CASTELLANO-SANCHEZ, A. A., HUNTER, S. B., PECOT, M., COHEN, C., HAMMOND, E. H., DEVI, S. N., KAUR, B. & VAN MEIR, E. G. 2004. Pseudopalisades in glioblastoma are

hypoxic, express extracellular matrix proteases, and are formed by an actively migrating cell population. *Cancer Res,* 64**,** 920-7.

BREITENEDER-GELEFF, S., MATSUI, K., SOLEIMAN, A., MERANER, P., POCZEWSKI, H., KALT, R., SCHAFFNER, G. & KERJASCHKI, D. 1997. Podoplanin, novel 43-kd membrane protein of glomerular epithelial cells, is down-regulated in puromycin nephrosis. *Am J Pathol,* 151**,** 1141-52.

BREITENEDER-GELEFF, S., SOLEIMAN, A., KOWALSKI, H., HORVAT, R., AMANN, G., KRIEHUBER, E., DIEM, K., WENINGER, W., TSCHACHLER, E., ALITALO, K. & KERJASCHKI, D. 1999. Angiosarcomas express mixed endothelial phenotypes of blood and lymphatic capillaries: podoplanin as a specific marker for lymphatic endothelium. *Am J Pathol,* 154**,** 385-94.

BURDA, J. E. & SOFRONIEW, M. V. 2014. Reactive gliosis and the multicellular response to CNS damage and disease. *Neuron,* 81**,** 229-48.

CANCER GENOME ATLAS RESEARCH, N. 2008. Comprehensive genomic characterization defines human glioblastoma genes and core pathways. *Nature,* 455**,** 1061-8.

CHADWICK, E. J., YANG, D. P., FILBIN, M. G., MAZZOLA, E., SUN, Y., BEHAR, O., PAZYRA-MURPHY, M. F., GOUMNEROVA, L., LIGON, K. L., STILES, C. D. & SEGAL, R. A. 2015. A Brain Tumor/Organotypic Slice Co-culture System for Studying Tumor Microenvironment and Targeted Drug Therapies. *J Vis Exp***,** e53304.

CHEN, W. S., CAO, Z., SUGAYA, S., LOPEZ, M. J., SENDRA, V. G., LAVER, N., LEFFLER, H., NILSSON, U. J., FU, J., SONG, J., XIA, L., HAMRAH, P. & PANJWANI, N. 2016. Pathological lymphangiogenesis is modulated by galectin-8-dependent crosstalk between podoplanin and integrin-associated VEGFR-3. *Nat Commun,* 7**,** 11302.

CHO, S., WOOD, A. & BOWBY, M. R. 2007. Brain slices as models for neurodegenerative disease and screening platforms to identify novel therapeutics. *Current Neuropharmacology,* 5**,** 19-33.

CHRISTENSEN, B. C., SMITH, A. A., ZHENG, S., KOESTLER, D. C., HOUSEMAN, E. A., MARSIT, C. J., WIEMELS, J. L., NELSON, H. H., KARAGAS, M. R., WRENSCH, M. R., KELSEY, K. T. & WIENCKE, J. K. 2011. DNA methylation, isocitrate dehydrogenase mutation, and survival in glioma. *J Natl Cancer Inst,* 103**,** 143-53.

CHUANG, H. N., LOHAUS, R., HANISCH, U. K., BINDER, C., DEHGHANI, F. & PUKROP, T. 2013. Coculture system with an organotypic brain slice and 3D spheroid of carcinoma cells. *J Vis Exp*.

CLAES, A., SCHUURING, J., BOOTS-SPRENGER, S., HENDRIKS-CORNELISSEN, S., DEKKERS, M., VAN DER KOGEL, A. J., LEENDERS, W. P., WESSELING, P. & JEUKEN, J. W. 2008. Phenotypic and genotypic characterization of orthotopic human glioma models and its relevance for the study of anti-glioma therapy. *Brain Pathol,* 18**,** 423-33.

CLARK, M. J., HOMER, N., O'CONNOR, B. D., CHEN, Z., ESKIN, A., LEE, H., MERRIMAN, B. & NELSON, S. F. 2010. U87MG decoded: the genomic sequence of a cytogenetically aberrant human cancer cell line. *PLoS Genet,* 6**,** e1000832.

COLONNA, M., SAMARIDIS, J. & ANGMAN, L. 2000. Molecular characterization of two novel C-type lectin-like receptors, one of which is selectively expressed in human dendritic cells. *Eur J Immunol,* 30**,** 697-704.

COSTA, B., EISEMANN, T., STRELAU, J., MÜLLER, J., SPAAN, I., KORSHUNOV, A., LIU, H., ANGEL, P. & PETERZIEL, H. Podoplanin expression in tumor cells triggers intratumoral platelet aggregation in a novel murine glioma model. *Manuscript in preparation*.

CUDDAPAH, V. A., ROBEL, S., WATKINS, S. & SONTHEIMER, H. 2014. A neurocentric perspective on glioma invasion. *Nat Rev Neurosci,* 15**,** 455-65.

CUENI, L. N. & DETMAR, M. 2009. Galectin-8 interacts with podoplanin and modulates lymphatic endothelial cell functions. *Exp Cell Res,* 315**,** 1715-23.

DANDY, W. E. 1928. Removal of right cerebral hemisphere for certain tumors with hemiplegia. Preliminary report. *Journal of the American Medical Association*.

DANG, L., WHITE, D. W., GROSS, S., BENNETT, B. D., BITTINGER, M. A., DRIGGERS, E. M., FANTIN, V. R., JANG, H. G., JIN, S., KEENAN, M. C., MARKS, K. M., PRINS, R. M., WARD, P. S., YEN, K. E., LIAU, L. M., RABINOWITZ, J. D., CANTLEY, L. C., THOMPSON, C. B., VANDER HEIDEN, M. G. & SU, S. M. 2009. Cancer-associated IDH1 mutations produce 2-hydroxyglutarate. *Nature,* 462**,** 739-44.

DAUDE, N., WOHLGEMUTH, S., BROWN, R., PITSTICK, R., GAPESHINA, H., YANG, J., CARLSON, G. A. & WESTAWAY, D. 2012. Knockout of the prion protein (PrP)-like Sprn gene does not produce embryonic lethality in combination with PrP(C)-deficiency. *Proc Natl Acad Sci U S A,* 109**,** 9035-40.

DOBBS, L. G., WILLIAMS, M. C. & GONZALEZ, R. 1988. Monoclonal-Antibodies Specific to Apical Surfaces of Rat Alveolar Type-I Cells Bind to Surfaces of Cultured, but Not Freshly Isolated, Type-Ii Cells. *Biochimica Et Biophysica Acta,* 970**,** 146-156.

DOUGLAS, Y. L., MAHTAB, E. A., JONGBLOED, M. R., UHRIN, P., ZAUJEC, J., BINDER, B. R., SCHALIJ, M. J., POELMANN, R. E., DERUITER, M. C. & GITTENBERGER-DE GROOT, A. C. 2009. Pulmonary vein, dorsal atrial wall and atrial septum abnormalities in podoplanin knockout mice with disturbed posterior heart field contribution. *Pediatr Res,* 65**,** 27-32.

DURCHDEWALD, M., GUINEA-VINIEGRA, J., HAAG, D., RIEHL, A., LICHTER, P., HAHN, M., WAGNER, E. F., ANGEL, P. & HESS, J. 2008. Podoplanin is a novel fos target gene in skin carcinogenesis. *Cancer Res,* 68**,** 6877-83.

EISEMANN, T., COSTA, B., STRELAU, J., MITTELBRONN, M., ANGEL, P. & PETERZIEL, H. 2017. An advanced glioma cell invasion assay based on organotypic brain slice cultures. *Manuscript in revision.*

ENDERSBY, R., ZHU, X., HAY, N., ELLISON, D. W. & BAKER, S. J. 2011. Nonredundant functions for Akt isoforms in astrocyte growth and gliomagenesis in an orthotopic transplantation model. *Cancer Res,* 71**,** 4106-16.

ENGLER, J. R., ROBINSON, A. E., SMIRNOV, I., HODGSON, J. G., BERGER, M. S., GUPTA, N., JAMES, C. D., MOLINARO, A. & PHILLIPS, J. J. 2012. Increased microglia/macrophage gene expression in a subset of adult and pediatric astrocytomas. *PLoS One,* 7**,** e43339.

ERNST, A., HOFMANN, S., AHMADI, R., BECKER, N., KORSHUNOV, A., ENGEL, F., HARTMANN, C., FELSBERG, J., SABEL, M., PETERZIEL, H., DURCHDEWALD, M., HESS, J., BARBUS, S., CAMPOS, B., STARZINSKI-POWITZ, A., UNTERBERG, A., REIFENBERGER, G., LICHTER, P., HEROLD-MENDE, C. & RADLWIMMER, B. 2009. Genomic and expression profiling of glioblastoma stem cell-like spheroid cultures identifies novel tumor-relevant genes associated with survival. *Clin Cancer Res,* 15**,** 6541-50.

EVERS, B., JASTRZEBSKI, K., HEIJMANS, J. P., GRERNRUM, W., BEIJERSBERGEN, R. L. & BERNARDS, R. 2016. CRISPR knockout screening outperforms shRNA and CRISPRi in identifying essential genes. *Nat Biotechnol,* 34**,** 631-3.

EYLER, C. E., WU, Q., YAN, K., MACSWORDS, J. M., CHANDLER-MILITELLO, D., MISURACA, K. L., LATHIA, J. D., FORRESTER, M. T., LEE, J., STAMLER, J. S., GOLDMAN, S. A., BREDEL, M., MCLENDON, R. E., SLOAN, A. E., HJELMELAND, A. B. & RICH, J. N. 2011. Glioma stem cell proliferation and tumor growth are promoted by nitric oxide synthase-2. *Cell,* 146**,** 53-66.

FARR, A., NELSON, A. & HOSIER, S. 1992. Characterization of an antigenic determinant preferentially expressed by type I epithelial cells in the murine thymus. *J Histochem Cytochem,* 40**,** 651-64.

FERLAY, J., SOERJOMATARAM, I., DIKSHIT, R., ESER, S., MATHERS, C., REBELO, M., PARKIN, D. M., FORMAN, D. & BRAY, F. 2015. Cancer incidence and mortality worldwide: sources, methods and major patterns in GLOBOCAN 2012. *Int J Cancer,* 136**,** E359-86.

FREUDENBERG, J. M., GHOSH, S., LACKFORD, B. L., YELLABOINA, S., ZHENG, X., LI, R., CUDDAPAH, S., WADE, P. A., HU, G. & JOTHI, R. 2012. Acute depletion of Tet1-dependent 5-hydroxymethylcytosine levels impairs LIF/Stat3 signaling and results in loss of embryonic stem cell identity. *Nucleic Acids Res,* 40**,** 3364-77.

FU, J., GERHARDT, H., MCDANIEL, J. M., XIA, B., LIU, X., IVANCIU, L., NY, A., HERMANS, K., SILASI-MANSAT, R., MCGEE, S., NYE, E., JU, T., RAMIREZ, M. I., CARMELIET, P., CUMMINGS, R. D., LUPU, F. & XIA, L. 2008. Endothelial cell O-glycan deficiency causes blood/lymphatic misconnections and consequent fatty liver disease in mice. *J Clin Invest,* 118**,** 3725-37.

GAJ, T., GERSBACH, C. A. & BARBAS, C. F., 3RD 2013. ZFN, TALEN, and CRISPR/Cas-based methods for genome engineering. *Trends Biotechnol,* 31**,** 397-405.

GANDARILLAS, A., SCHOLL, F. G., BENITO, N., GAMALLO, C. & QUINTANILLA, M. 1997. Induction of PA2.26, a cell-surface antigen expressed by active fibroblasts, in mouse epidermal keratinocytes during carcinogenesis. *Mol Carcinog,* 20**,** 10-8.

GIESE, A., LOO, M. A., TRAN, N., HASKETT, D., COONS, S. W. & BERENS, M. E. 1996. Dichotomy of astrocytoma migration and proliferation. *Int J Cancer,* 67**,** 275-82.

GITTENBERGER-DE GROOT, A. C., MAHTAB, E. A., HAHURIJ, N. D., WISSE, L. J., DERUITER, M. C., WIJFFELS, M. C. & POELMANN, R. E. 2007. Nkx2.5-negative myocardium of the posterior heart field and its correlation with podoplanin expression in cells from the developing cardiac pacemaking and conduction system. *Anat Rec (Hoboken),* 290**,** 115-22.

GRAU, S. J., TRILLSCH, F., TONN, J. C., GOLDBRUNNER, R. H., NOESSNER, E., NELSON, P. J. & VON LUETTICHAU, I. 2015. Podoplanin increases migration and angiogenesis in malignant glioma. *Int J Clin Exp Pathol,* 8**,** 8663-70.

GU, Y. M., MA, Y. H., ZHAO, W. G. & CHEN, J. 2011. Dickkopf3 overexpression inhibits pancreatic cancer cell growth in vitro. *World J Gastroenterol,* 17**,** 3810-7.

HAMBARDZUMYAN, D., PARADA, L. F., HOLLAND, E. C. & CHAREST, A. 2011. Genetic modeling of gliomas in mice: new tools to tackle old problems. *Glia,* 59**,** 1155-68.

HAMER, P. C. D. W., VAN TILBORG, A. A. G., EIJK, P. P., SMINIA, P., TROOST, D., VAN NOORDEN, C. J. F., YLSTRA, B. & LEENSTRA, S. 2008. The genomic profile of human malignant glioma is altered early in primary cell culture and preserved in spheroids. *Oncogene,* 27**,** 2091-2096.

HEGI, M. E., DISERENS, A. C., GORLIA, T., HAMOU, M. F., DE TRIBOLET, N., WELLER, M., KROS, J. M., HAINFELLNER, J. A., MASON, W., MARIANI, L., BROMBERG, J. E., HAU, P., MIRIMANOFF, R. O., CAIRNCROSS, J. G., JANZER, R. C. & STUPP, R. 2005. MGMT gene silencing and benefit from temozolomide in glioblastoma. *N Engl J Med,* 352**,** 997-1003.

HEISS, M., HELLSTROM, M., KALEN, M., MAY, T., WEBER, H., HECKER, M., AUGUSTIN, H. G. & KORFF, T. 2015. Endothelial cell spheroids as a versatile tool to study angiogenesis in vitro. *FASEB J,* 29**,** 3076-84.

HERRMANN, J. E., IMURA, T., SONG, B. B., QI, J. W., AO, Y., NGUYEN, T. K., KORSAK, R. A., TAKEDA, K., AKIRA, S. & SOFRONIEW, M. V. 2008. STAT3 is a critical regulator of astrogliosis and scar formation after spinal cord injury. *Journal of Neuroscience,* 28**,** 7231-7243.

HONG, Y. K., HARVEY, N., NOH, Y. H., SCHACHT, V., HIRAKAWA, S., DETMAR, M. & OLIVER, G. 2002. Prox1 is a master control gene in the program specifying lymphatic endothelial cell fate. *Dev Dyn,* 225**,** 351-7.

HONMA, M., MINAMI-HORI, M., TAKAHASHI, H. & IIZUKA, H. 2012. Podoplanin expression in wound and hyperproliferative psoriatic epidermis: regulation by TGF-beta and STAT-3 activating cytokines, IFN-gamma, IL-6, and IL-22. *J Dermatol Sci,* 65**,** 134-40.

HORING, E., HARTER, P. N., SEZNEC, J., SCHITTENHELM, J., BUHRING, H. J., BHATTACHARYYA, S., VON HATTINGEN, E., ZACHSKORN, C., MITTELBRONN, M. & NAUMANN, U. 2012. The "go or grow" potential of gliomas is linked to the neuropeptide processing enzyme carboxypeptidase E and mediated by metabolic stress. *Acta Neuropathologica,* 124**,** 83-97.

HOU, T. Z., BYSTROM, J., SHERLOCK, J. P., QURESHI, O., PARNELL, S. M., ANDERSON, G., GILROY, D. W. & BUCKLEY, C. D. 2010. A distinct subset of podoplanin (gp38) expressing F4/80+ macrophages mediate phagocytosis and are induced following zymosan peritonitis. *Febs Letters,* 584**,** 3955-3961.

HUANG, D. W., SHERMAN, B. T. & LEMPICKI, R. A. 2009. Systematic and integrative analysis of large gene lists using DAVID bioinformatics resources. *Nature Protocols,* 4**,** 44-57.

HUANG, Y., WILLIAMS, J. C. & JOHNSON, S. M. 2012. Brain slice on a chip: opportunities and challenges of applying microfluidic technology to intact tissues. *Lab Chip,* 12**,** 2103-17.

HUGHES, C. E., POLLITT, A. Y., MORI, J., EBLE, J. A., TOMLINSON, M. G., HARTWIG, J. H., O'CALLAGHAN, C. A., FUTTERER, K. & WATSON, S. P. 2010. CLEC-2 activates Syk through dimerization. *Blood,* 115**,** 2947-55.

HUMPEL, C. 2015. Organotypic brain slice cultures: A review. *Neuroscience,* 305**,** 86-98.

HUSE, J. T., PASHA, T. L. & ZHANG, P. J. 2007. D2-40 functions as an effective chondroid marker distinguishing true chondroid tumors from chordoma. *Acta Neuropathol,* 113**,** 87-94.

HUSZTHY, P. C., DAPHU, I., NICLOU, S. P., STIEBER, D., NIGRO, J. M., SAKARIASSEN, P. O., MILETIC, H., THORSEN, F. & BJERKVIG, R. 2012. In vivo models of primary brain tumors: pitfalls and perspectives. *Neuro Oncol,* 14**,** 979-93.

INOUE, H., MIYAZAKI, Y., KIKUCHI, K., YOSHIDA, N., IDE, F., OHMORI, Y., TOMOMURA, A., SAKASHITA, H. & KUSAMA, K. 2012. Podoplanin promotes cell migration via the EGF-Src-Cas pathway in oral squamous cell carcinoma cell lines. *J Oral Sci,* 54**,** 241-50.

IVKOVIC, S., BEADLE, C., NOTICEWALA, S., MASSEY, S. C., SWANSON, K. R., TORO, L. N., BRESNICK, A. R., CANOLL, P. & ROSENFELD, S. S. 2012. Direct inhibition of myosin II effectively blocks glioma invasion in the presence of multiple motogens. *Mol Biol Cell,* 23**,** 533-42.

JACKSON, A. L., BARTZ, S. R., SCHELTER, J., KOBAYASHI, S. V., BURCHARD, J., MAO, M., LI, B., CAVET, G. & LINSLEY, P. S. 2003. Expression profiling reveals off-target gene regulation by RNAi. *Nat Biotechnol,* 21**,** 635-7.

JENSEN, S. S., PETTERSON, S. A., HALLE, B., AABERG-JESSEN, C. & KRISTENSEN, B. W. 2017. Effects of the lysosomal destabilizing drug siramesine on glioblastoma in vitro and in vivo. *BMC Cancer,* 17**,** 178.

JIMENEZ, A. J., DOMINGUEZ-PINOS, M. D., GUERRA, M. M., FERNANDEZ-LLEBREZ, P. & PEREZ-FIGARES, J. M. 2014. Structure and function of the ependymal barrier and diseases associated with ependyma disruption. *Tissue Barriers,* 2**,** e28426.

JOYCE, J. A. & POLLARD, J. W. 2009. Microenvironmental regulation of metastasis. *Nat Rev Cancer,* 9**,** 239-52.

JUNG, S., KIM, H. W., LEE, J. H., KANG, S. S., RHU, H. H., JEONG, Y. I., YANG, S. Y., CHUNG, H. Y., BAE, C. S., CHOI, C., SHIN, B. A., KIM, K. K. & AHN, K. Y. 2002. Brain tumor invasion model system using organotypic brain-slice culture as an alternative to in vivo model. *J Cancer Res Clin Oncol,* 128**,** 469-76.

KANEKO, M. K., KATO, Y., KAMEYAMA, A., ITO, H., KUNO, A., HIRABAYASHI, J., KUBOTA, T., AMANO, K., CHIBA, Y., HASEGAWA, Y., SASAGAWA, I., MISHIMA, K. & NARIMATSU, H. 2007. Functional glycosylation of human podoplanin: glycan structure of platelet aggregation-inducing factor. *FEBS Lett,* 581**,** 331-6.

KATO, Y., FUJITA, N., KUNITA, A., SATO, S., KANEKO, M., OSAWA, M. & TSURUO, T. 2003. Molecular identification of Aggrus/T1alpha as a platelet aggregation-inducing factor expressed in colorectal tumors. *J Biol Chem,* 278**,** 51599-605.

KATO, Y., KANEKO, M., SATA, M., FUJITA, N., TSURUO, T. & OSAWA, M. 2005. Enhanced expression of Aggrus (T1alpha/podoplanin), a platelet-aggregation-inducing factor in lung squamous cell carcinoma. *Tumour Biol,* 26**,** 195-200.

KATO, Y. & KANEKO, M. K. 2014. A cancer-specific monoclonal antibody recognizes the aberrantly glycosylated podoplanin. *Sci Rep,* 4**,** 5924.

KAWASE, A., ISHII, G., NAGAI, K., ITO, T., NAGANO, T., MURATA, Y., HISHIDA, T., NISHIMURA, M., YOSHIDA, J., SUZUKI, K. & OCHIAI, A. 2008. Podoplanin expression by cancer associated fibroblasts predicts poor prognosis of lung adenocarcinoma. *Int J Cancer,* 123**,** 1053-9.

KERJASCHKI, D., REGELE, H. M., MOOSBERGER, I., NAGY-BOJARSKI, K., WATSCHINGER, B., SOLEIMAN, A., BIRNER, P., KRIEGER, S., HOVORKA, A., SILBERHUMER, G., LAAKKONEN, P., PETROVA, T., LANGER, B. & RAAB, I. 2004. Lymphatic neoangiogenesis in human kidney transplants is associated with immunologically active lymphocytic infiltrates. *J Am Soc Nephrol,* 15**,** 603-12.

KERRIGAN, A. M., NAVARRO-NUNEZ, L., PYZ, E., FINNEY, B. A., WILLMENT, J. A., WATSON, S. P. & BROWN, G. D. 2012. Podoplanin-expressing inflammatory macrophages activate murine platelets via CLEC-2. *J Thromb Haemost,* 10**,** 484-6.

KHATAU, S. B., BLOOM, R. J., BAJPAI, S., RAZAFSKY, D., ZANG, S., GIRI, A., WU, P. H., MARCHAND, J., CELEDON, A., HALE, C. M., SUN, S. X., HODZIC, D. & WIRTZ, D. 2012. The distinct roles of the nucleus and nucleus-cytoskeleton connections in three-dimensional cell migration. *Sci Rep,* 2**,** 488.

KIM, D., BAE, S., PARK, J., KIM, E., KIM, S., YU, H. R., HWANG, J., KIM, J. I. & KIM, J. S. 2015. Digenome-seq: genome-wide profiling of CRISPR-Cas9 off-target effects in human cells. *Nat Methods,* 12**,** 237-43, 1 p following 243.

KIMURA, N. & KIMURA, I. 2005. Podoplanin as a marker for mesothelioma. *Pathol Int,* 55**,** 83-6.

KITANO, H., KAGEYAMA, S., HEWITT, S. M., HAYASHI, R., DOKI, Y., OZAKI, Y., FUJINO, S., TAKIKITA, M., KUBO, H. & FUKUOKA, J. 2010. Podoplanin expression in cancerous stroma induces lymphangiogenesis and predicts lymphatic spread and patient survival. *Arch Pathol Lab Med,* 134**,** 1520-7.

KIZHATIL, K., RYAN, M., MARCHANT, J. K., HENRICH, S. & JOHN, S. W. 2014. Schlemm's canal is a unique vessel with a combination of blood vascular and lymphatic phenotypes that forms by a novel developmental process. *PLoS Biol,* 12**,** e1001912.

KOHSAKA, S., WANG, L., YACHI, K., MAHABIR, R., NARITA, T., ITOH, T., TANINO, M., KIMURA, T., NISHIHARA, H. & TANAKA, S. 2012. STAT3 inhibition overcomes temozolomide resistance in glioblastoma by downregulating MGMT expression. *Mol Cancer Ther,* 11**,** 1289-99.

KOLAR, K., FREITAS-ANDRADE, M., BECHBERGER, J. F., KRISHNAN, H., GOLDBERG, G. S., NAUS, C. C. & SIN, W. C. 2015. Podoplanin: a marker for reactive gliosis in gliomas and brain injury. *J Neuropathol Exp Neurol,* 74**,** 64-74.

KORFF, T. & AUGUSTIN, H. G. 1999. Tensional forces in fibrillar extracellular matrices control directional capillary sprouting. *J Cell Sci,* 112 (Pt 19)**,** 3249-58.

KOTANI, M., TAJIMA, Y., OSANAI, T., IRIE, A., IWATSUKI, K., KANAI-AZUMA, M., IMADA, M., KATO, H., SHITARA, H., KUBO, H. & SAKURABA, H. 2003. Complementary DNA cloning and characterization of RANDAM-2, a type I membrane molecule specifically expressed on glutamatergic neuronal cells in the mouse cerebrum. *J Neurosci Res,* 73**,** 603-13.

KRETH, S., HEYN, J., GRAU, S., KRETZSCHMAR, H. A., EGENSPERGER, R. & KRETH, F. W. 2010. Identification of valid endogenous control genes for determining gene expression in human glioma. *Neuro Oncol,* 12**,** 570-9.

KRISHNAN, H., OCHOA-ALVAREZ, J. A., SHEN, Y., NEVEL, E., LAKSHMINARAYANAN, M., WILLIAMS, M. C., RAMIREZ, M. I., MILLER, W. T. & GOLDBERG, G. S. 2013. Serines in the intracellular tail of podoplanin (PDPN) regulate cell motility. *J Biol Chem,* 288**,** 12215-21.

KRISHNAN, H., RETZBACH, E. P., RAMIREZ, M. I., LIU, T., LI, H., MILLER, W. T. & GOLDBERG, G. S. 2015. PKA and CDK5 can phosphorylate specific serines on the intracellular domain of podoplanin (PDPN) to inhibit cell motility. *Exp Cell Res,* 335**,** 115-22.

KUNITA, A., KASHIMA, T. G., OHAZAMA, A., GRIGORIADIS, A. E. & FUKAYAMA, M. 2011. Podoplanin is regulated by AP-1 and promotes platelet aggregation and cell migration in osteosarcoma. *Am J Pathol,* 179**,** 1041-9.

LEE, J., KOTLIAROVA, S., KOTLIAROV, Y., LI, A., SU, Q., DONIN, N. M., PASTORINO, S., PUROW, B. W., CHRISTOPHER, N., ZHANG, W., PARK, J. K. & FINE, H. A. 2006. Tumor stem cells derived from glioblastomas cultured in bFGF and EGF more closely mirror the phenotype and genotype of primary tumors than do serum-cultured cell lines. *Cancer Cell,* 9**,** 391-403.

LENTING, K., VERHAAK, R., TER LAAN, M., WESSELING, P. & LEENDERS, W. 2017. Glioma: experimental models and reality. *Acta Neuropathol,* 133**,** 263-282.

LI, A., WALLING, J., KOTLIAROV, Y., CENTER, A., STEED, M. E., AHN, S. J., ROSENBLUM, M., MIKKELSEN, T., ZENKLUSEN, J. C. & FINE, H. A. 2008. Genomic changes and gene

expression profiles reveal that established glioma cell lines are poorly representative of primary human gliomas. *Mol Cancer Res,* 6**,** 21-30.

LI, Y. Y., ZHOU, C. X. & GAO, Y. 2015. Podoplanin promotes the invasion of oral squamous cell carcinoma in coordination with MT1-MMP and Rho GTPases. *Am J Cancer Res,* 5**,** 514-29.

LOSSI, L., ALASIA, S., SALIO, C. & MERIGHI, A. 2009. Cell death and proliferation in acute slices and organotypic cultures of mammalian CNS. *Prog Neurobiol,* 88**,** 221-45.

LOUIS, D. N., PERRY, A., REIFENBERGER, G., VON DEIMLING, A., FIGARELLA-BRANGER, D., CAVENEE, W. K., OHGAKI, H., WIESTLER, O. D., KLEIHUES, P. & ELLISON, D. W. 2016. The 2016 World Health Organization Classification of Tumors of the Central Nervous System: a summary. *Acta Neuropathol,* 131**,** 803-20.

LOUVEAU, A., SMIRNOV, I., KEYES, T. J., ECCLES, J. D., ROUHANI, S. J., PESKE, J. D., DERECKI, N. C., CASTLE, D., MANDELL, J. W., LEE, K. S., HARRIS, T. H. & KIPNIS, J. 2015. Structural and functional features of central nervous system lymphatic vessels. *Nature,* 523**,** 337-41.

LOWE, K. L., FINNEY, B. A., DEPPERMANN, C., HAGERLING, R., GAZIT, S. L., FRAMPTON, J., BUCKLEY, C., CAMERER, E., NIESWANDT, B., KIEFER, F. & WATSON, S. P. 2015. Podoplanin and CLEC-2 drive cerebrovascular patterning and integrity during development. *Blood,* 125**,** 3769-77.

MADSEN, C. D., HOOPER, S., TOZLUOGLU, M., BRUCKBAUER, A., FLETCHER, G., ERLER, J. T., BATES, P. A., THOMPSON, B. & SAHAI, E. 2015. STRIPAK components determine mode of cancer cell migration and metastasis. *Nat Cell Biol,* 17**,** 68-80.

MAHESPARAN, R., READ, T. A., LUND-JOHANSEN, M., SKAFTNESMO, K. O., BJERKVIG, R. & ENGEBRAATEN, O. 2003. Expression of extracellular matrix components in a highly infiltrative in vivo glioma model. *Acta Neuropathol,* 105**,** 49-57.

MARIANI, L., BEAUDRY, C., MCDONOUGH, W. S., HOELZINGER, D. B., DEMUTH, T., ROSS, K. R., BERENS, T., COONS, S. W., WATTS, G., TRENT, J. M., WEI, J. S., GIESE, A. & BERENS, M. E. 2001. Glioma cell motility is associated with reduced transcription of proapoptotic and proliferation genes: a cDNA microarray analysis. *Journal of Neuro-Oncology,* 53**,** 161-176.

MARTIN-VILLAR, E., FERNANDEZ-MUNOZ, B., PARSONS, M., YURRITA, M. M., MEGIAS, D., PEREZ-GOMEZ, E., JONES, G. E. & QUINTANILLA, M. 2010. Podoplanin associates with CD44 to promote directional cell migration. *Mol Biol Cell,* 21**,** 4387-99.

MARTIN-VILLAR, E., MEGIAS, D., CASTEL, S., YURRITA, M. M., VILARO, S. & QUINTANILLA, M. 2006. Podoplanin binds ERM proteins to activate RhoA and promote epithelial-mesenchymal transition. *J Cell Sci,* 119**,** 4541-53.

MARTIN-VILLAR, E., SCHOLL, F. G., GAMALLO, C., YURRITA, M. M., MUNOZ-GUERRA, M., CRUCES, J. & QUINTANILLA, M. 2005. Characterization of human PA2.26 antigen (T1alpha-2, podoplanin), a small membrane mucin induced in oral squamous cell carcinomas. *Int J Cancer,* 113**,** 899-910.

MARTIN-VILLAR, E., YURRITA, M. M., FERNANDEZ-MUNOZ, B., QUINTANILLA, M. & RENART, J. 2009. Regulation of podoplanin/PA2.26 antigen expression in tumour cells. Involvement of calpain-mediated proteolysis. *Int J Biochem Cell Biol,* 41**,** 1421-9.

MATOUK, I. J., DEGROOT, N., MEZAN, S., AYESH, S., ABU-IAIL, R., HOCHBERG, A. & GALUN, E. 2007. The H19 Non-Coding RNA Is Essential for Human Tumor Growth. *Plos One,* 2.

MISHIMA, K., KATO, Y., KANEKO, M. K., NISHIKAWA, R., HIROSE, T. & MATSUTANI, M. 2006. Increased expression of podoplanin in malignant astrocytic tumors as a novel molecular marker of malignant progression. *Acta Neuropathol,* 111**,** 483-8.

MIYAI, M., TOMITA, H., SOEDA, A., YANO, H., IWAMA, T. & HARA, A. 2017. Current trends in mouse models of glioblastoma. *J Neurooncol*.

MOHR, S. E., SMITH, J. A., SHAMU, C. E., NEUMULLER, R. A. & PERRIMON, N. 2014. RNAi screening comes of age: improved techniques and complementary approaches. *Nat Rev Mol Cell Biol,* 15**,** 591-600.

MORTON, C. L. & HOUGHTON, P. J. 2007. Establishment of human tumor xenografts in immunodeficient mice. *Nat Protoc,* 2**,** 247-50.

NAKASHIMA, Y., YOSHINAGA, K., KITAO, H., ANDO, K., KIMURA, Y., SAEKI, H., OKI, E., MORITA, M., KAKEJI, Y., HIRAHASHI, M., ODA, Y. & MAEHARA, Y. 2013. Podoplanin is expressed at the invasive front of esophageal squamous cell carcinomas and is involved in collective cell invasion. *Cancer Sci,* 104**,** 1718-25.

NAKAZAWA, Y., SATO, S., NAITO, M., KATO, Y., MISHIMA, K., ARAI, H., TSURUO, T. & FUJITA, N. 2008. Tetraspanin family member CD9 inhibits Aggrus/podoplanin-induced platelet aggregation and suppresses pulmonary metastasis. *Blood,* 112**,** 1730-9.

NOUSHMEHR, H., WEISENBERGER, D. J., DIEFES, K., PHILLIPS, H. S., PUJARA, K., BERMAN, B. P., PAN, F., PELLOSKI, C. E., SULMAN, E. P., BHAT, K. P., VERHAAK, R. G. W., HOADLEY, K. A., HAYES, D. N., PEROU, C. M., SCHMIDT, H. K., DING, L., WILSON, R. K., VAN DEN BERG, D., SHEN, H., BENGTSSON, H., NEUVIAL, P., COPE, L. M., BUCKLEY, J., HERMAN, J. G., BAYLIN, S. B., LAIRD, P. W., ALDAPE, K. & NETWORK, C. G. A. R. 2010. Identification of a CpG Island Methylator Phenotype that Defines a Distinct Subgroup of Glioma. *Cancer Cell,* 17**,** 510-522.

OBEROI, R. K., PARRISH, K. E., SIO, T. T., MITTAPALLI, R. K., ELMQUIST, W. F. & SARKARIA, J. N. 2016. Strategies to improve delivery of anticancer drugs across the blood-brain barrier to treat glioblastoma. *Neuro Oncol,* 18**,** 27-36.

OHGAKI, H. & KLEIHUES, P. 2005. Epidemiology and etiology of gliomas. *Acta Neuropathol,* 109**,** 93-108.

ORDONEZ, N. G. 2005. D2-40 and podoplanin are highly specific and sensitive immunohistochemical markers of epithelioid malignant mesothelioma. *Hum Pathol,* 36**,** 372-80.

OSSWALD, M., JUNG, E., SAHM, F., SOLECKI, G., VENKATARAMANI, V., BLAES, J., WEIL, S., HORSTMANN, H., WIESTLER, B., SYED, M., HUANG, L., RATLIFF, M., KARIMIAN JAZI, K., KURZ, F. T., SCHMENGER, T., LEMKE, D., GOMMEL, M., PAULI, M., LIAO, Y., HARING, P., PUSCH, S., HERL, V., STEINHAUSER, C., KRUNIC, D., JARAHIAN, M., MILETIC, H., BERGHOFF, A. S., GRIESBECK, O., KALAMAKIS, G., GARASCHUK, O., PREUSSER, M., WEISS, S., LIU, H., HEILAND, S., PLATTEN, M., HUBER, P. E., KUNER, T., VON DEIMLING, A., WICK, W. & WINKLER, F. 2015. Brain tumour cells interconnect to a functional and resistant network. *Nature,* 528**,** 93-8.

OSTERBERG, M., KIM, H., WARRINGER, J., MELEN, K., BLOMBERG, A. & VON HEIJNE, G. 2006. Phenotypic effects of membrane protein overexpression in Saccharomyces cerevisiae. *Proc Natl Acad Sci U S A,* 103**,** 11148-53.

OSTROM, Q. T., GITTLEMAN, H., FARAH, P., ONDRACEK, A., CHEN, Y., WOLINSKY, Y., STROUP, N. E., KRUCHKO, C. & BARNHOLTZ-SLOAN, J. S. 2013. CBTRUS statistical report: Primary brain and central nervous system tumors diagnosed in the United States in 2006-2010. *Neuro Oncol,* 15 Suppl 2**,** ii1-56.

PAMPALONI, F., REYNAUD, E. G. & STELZER, E. H. 2007. The third dimension bridges the gap between cell culture and live tissue. *Nat Rev Mol Cell Biol,* 8**,** 839-45.

PAN, Y., YAGO, T., FU, J., HERZOG, B., MCDANIEL, J. M., MEHTA-D'SOUZA, P., CAI, X., RUAN, C., MCEVER, R. P., WEST, C., DAI, K., CHEN, H. & XIA, L. 2014. Podoplanin requires sialylated O-glycans for stable expression on lymphatic endothelial cells and for interaction with platelets. *Blood,* 124**,** 3656-65.

PARSONS, D. W., JONES, S., ZHANG, X., LIN, J. C., LEARY, R. J., ANGENENDT, P., MANKOO, P., CARTER, H., SIU, I. M., GALLIA, G. L., OLIVI, A., MCLENDON, R., RASHEED, B. A., KEIR, S., NIKOLSKAYA, T., NIKOLSKY, Y., BUSAM, D. A., TEKLEAB, H., DIAZ, L. A., JR., HARTIGAN, J., SMITH, D. R., STRAUSBERG, R. L., MARIE, S. K., SHINJO, S. M., YAN, H., RIGGINS, G. J., BIGNER, D. D., KARCHIN, R., PAPADOPOULOS, N., PARMIGIANI, G., VOGELSTEIN, B., VELCULESCU, V. E. & KINZLER, K. W. 2008. An integrated genomic analysis of human glioblastoma multiforme. *Science,* 321**,** 1807-12.

PATEL, A. P., TIROSH, I., TROMBETTA, J. J., SHALEK, A. K., GILLESPIE, S. M., WAKIMOTO, H., CAHILL, D. P., NAHED, B. V., CURRY, W. T., MARTUZA, R. L., LOUIS, D. N., ROZENBLATT-ROSEN, O.,

SUVA, M. L., REGEV, A. & BERNSTEIN, B. E. 2014. Single-cell RNA-seq highlights intratumoral heterogeneity in primary glioblastoma. *Science,* 344**,** 1396-401.

PEKNY, M., PEKNA, M., MESSING, A., STEINHAUSER, C., LEE, J. M., PARPURA, V., HOL, E. M., SOFRONIEW, M. V. & VERKHRATSKY, A. 2016. Astrocytes: a central element in neurological diseases. *Acta Neuropathol,* 131**,** 323-45.

PEREGO, C., VANONI, C., MASSARI, S., RAIMONDI, A., POLA, S., CATTANEO, M. G., FRANCOLINI, M., VICENTINI, L. M. & PIETRINI, G. 2002. Invasive behaviour of glioblastoma cell lines is associated with altered organisation of the cadherin-catenin adhesion system. *J Cell Sci,* 115**,** 3331-40.

PETERS, A., PITCHER, L. A., SULLIVAN, J. M., MITSDOERFFER, M., ACTON, S. E., FRANZ, B., WUCHERPFENNIG, K., TURLEY, S., CARROLL, M. C., SOBEL, R. A., BETTELLI, E. & KUCHROO, V. K. 2011. Th17 Cells Induce Ectopic Lymphoid Follicles in Central Nervous System Tissue Inflammation. *Immunity,* 35**,** 986-996.

PETERZIEL, H., MULLER, J., DANNER, A., BARBUS, S., LIU, H. K., RADLWIMMER, B., PIETSCH, T., LICHTER, P., SCHUTZ, G., HESS, J. & ANGEL, P. 2012. Expression of podoplanin in human astrocytic brain tumors is controlled by the PI3K-AKT-AP-1 signaling pathway and promoter methylation. *Neuro Oncol,* 14**,** 426-39.

PETTERSON, S. A., JAKOBSEN, I. P., JENSEN, S. S., AABERG-JESSEN, C., NIELSEN, M., JOHANSEN, J. & KRISTENSEN, B. W. 2016. Implantation of glioblastoma spheroids into organotypic brain slice cultures as a model for investigating effects of irradiation: a proof of concept. *International Journal of Clinical and Experimental Pathology,* 9**,** 4816-4823.

PFAFFL, M. W. 2001. A new mathematical model for relative quantification in real-time RT-PCR. *Nucleic Acids Res,* 29**,** e45.

PHILLIPS, H. S., KHARBANDA, S., CHEN, R., FORREST, W. F., SORIANO, R. H., WU, T. D., MISRA, A., NIGRO, J. M., COLMAN, H., SOROCEANU, L., WILLIAMS, P. M., MODRUSAN, Z., FEUERSTEIN, B. G. & ALDAPE, K. 2006. Molecular subclasses of high-grade glioma predict prognosis, delineate a pattern of disease progression, and resemble stages in neurogenesis. *Cancer Cell,* 9**,** 157-73.

PONTI, A., MACHACEK, M., GUPTON, S. L., WATERMAN-STORER, C. M. & DANUSER, G. 2004. Two distinct actin networks drive the protrusion of migrating cells. *Science,* 305**,** 1782-6.

PRIESTER, M., COPANAKI, E., VAFAIZADEH, V., HENSEL, S., BERNREUTHER, C., GLATZEL, M., SEIFERT, V., GRONER, B., KOGEL, D. & WEISSENBERGER, J. 2013. STAT3 silencing inhibits glioma single cell infiltration and tumor growth. *Neuro Oncol,* 15**,** 840-52.

RADKE, J., BORTOLUSSI, G. & PAGENSTECHER, A. 2013. Akt and c-Myc induce stem-cell markers in mature primary p53(-)/(-) astrocytes and render these cells gliomagenic in the brain of immunocompetent mice. *PLoS One,* 8**,** e56691.

RAMIREZ, M. I., MILLIEN, G., HINDS, A., CAO, Y., SELDIN, D. C. & WILLIAMS, M. C. 2003. T1alpha, a lung type I cell differentiation gene, is required for normal lung cell proliferation and alveolus formation at birth. *Dev Biol,* 256**,** 61-72.

RAN, F. A., HSU, P. D., WRIGHT, J., AGARWALA, V., SCOTT, D. A. & ZHANG, F. 2013. Genome engineering using the CRISPR-Cas9 system. *Nature Protocols,* 8**,** 2281-2308.

READ, R. D. 2011. Drosophila melanogaster as a model system for human brain cancers. *Glia,* 59**,** 1364-76.

RENART, J., CARRASCO-RAMIREZ, P., FERNANDEZ-MUNOZ, B., MARTIN-VILLAR, E., MONTERO, L., YURRITA, M. M. & QUINTANILLA, M. 2015. New insights into the role of podoplanin in epithelial-mesenchymal transition. *Int Rev Cell Mol Biol,* 317**,** 185-239.

RISHI, A. K., JOYCE-BRADY, M., FISHER, J., DOBBS, L. G., FLOROS, J., VANDERSPEK, J., BRODY, J. S. & WILLIAMS, M. C. 1995. Cloning, characterization, and development expression of a rat lung alveolar type I cell gene in embryonic endodermal and neural derivatives. *Dev Biol,* 167**,** 294-306.

ROHLE, D., POPOVICI-MULLER, J., PALASKAS, N., TURCAN, S., GROMMES, C., CAMPOS, C., TSOI, J., CLARK, O., OLDRINI, B., KOMISOPOULOU, E., KUNII, K., PEDRAZA, A., SCHALM, S.,

SILVERMAN, L., MILLER, A., WANG, F., YANG, H., CHEN, Y., KERNYTSKY, A., ROSENBLUM, M. K., LIU, W., BILLER, S. A., SU, S. M., BRENNAN, C. W., CHAN, T. A., GRAEBER, T. G., YEN, K. E. & MELLINGHOFF, I. K. 2013. An inhibitor of mutant IDH1 delays growth and promotes differentiation of glioma cells. *Science,* 340**,** 626-30.

ROSSI, A., KONTARAKIS, Z., GERRI, C., NOLTE, H., HOLPER, S., KRUGER, M. & STAINIER, D. Y. 2015. Genetic compensation induced by deleterious mutations but not gene knockdowns. *Nature,* 524**,** 230-3.

RUSSELL, W. L., KELLY, E. M., HUNSICKER, P. R., BANGHAM, J. W., MADDUX, S. C. & PHIPPS, E. L. 1979. Specific-locus test shows ethylnitrosourea to be the most potent mutagen in the mouse. *Proc Natl Acad Sci U S A,* 76**,** 5818-9.

SALA-VALDES, M., URSA, A., CHARRIN, S., RUBINSTEIN, E., HEMLER, M. E., SANCHEZ-MADRID, F. & YANEZ-MO, M. 2006. EWI-2 and EWI-F link the tetraspanin web to the actin cytoskeleton through their direct association with ezrin-radixin-moesin proteins. *J Biol Chem,* 281**,** 19665-75.

SANSON, M., MARIE, Y., PARIS, S., IDBAIH, A., LAFFAIRE, J., DUCRAY, F., EL HALLANI, S., BOISSELIER, B., MOKHTARI, K., HOANG-XUAN, K. & DELATTRE, J. Y. 2009. Isocitrate Dehydrogenase 1 Codon 132 Mutation Is an Important Prognostic Biomarker in Gliomas. *Journal of Clinical Oncology,* 27**,** 4150-4154.

SCHACHT, V., DADRAS, S. S., JOHNSON, L. A., JACKSON, D. G., HONG, Y. K. & DETMAR, M. 2005. Up-regulation of the lymphatic marker podoplanin, a mucin-type transmembrane glycoprotein, in human squamous cell carcinomas and germ cell tumors. *Am J Pathol,* 166**,** 913-21.

SCHERER, H. J. 1938. Structural Development in Gliomas. *American Association for Cancer Research*.

SCHNEIDER, C. A., RASBAND, W. S. & ELICEIRI, K. W. 2012. NIH Image to ImageJ: 25 years of image analysis. *Nat Methods,* 9**,** 671-5.

SCHOLL, F. G., GAMALLO, C., VILARO, S. & QUINTANILLA, M. 1999. Identification of PA2.26 antigen as a novel cell-surface mucin-type glycoprotein that induces plasma membrane extensions and increased motility in keratinocytes. *Journal of Cell Science,* 112**,** 4601-4613.

SCHRADER, C. H., KOLB, M., ZAOUI, K., FLECHTENMACHER, C., GRABE, N., WEBER, K. J., HIELSCHER, T., PLINKERT, P. K. & HESS, J. 2015. Kallikrein-related peptidase 6 regulates epithelial-to-mesenchymal transition and serves as prognostic biomarker for head and neck squamous cell carcinoma patients. *Molecular Cancer,* 14.

SCHUMACHER, T., BUNSE, L., PUSCH, S., SAHM, F., WIESTLER, B., QUANDT, J., MENN, O., OSSWALD, M., OEZEN, I., OTT, M., KEIL, M., BALSS, J., RAUSCHENBACH, K., GRABOWSKA, A. K., VOGLER, I., DIEKMANN, J., TRAUTWEIN, N., EICHMULLER, S. B., OKUN, J., STEVANOVIC, S., RIEMER, A. B., SAHIN, U., FRIESE, M. A., BECKHOVE, P., VON DEIMLING, A., WICK, W. & PLATTEN, M. 2014. A vaccine targeting mutant IDH1 induces antitumour immunity. *Nature,* 512**,** 324-7.

SCOTT, R. W., HOOPER, S., CRIGHTON, D., LI, A., KONIG, I., MUNRO, J., TRIVIER, E., WICKMAN, G., MORIN, P., CROFT, D. R., DAWSON, J., MACHESKY, L., ANDERSON, K. I., SAHAI, E. A. & OLSON, M. F. 2010. LIM kinases are required for invasive path generation by tumor and tumor-associated stromal cells. *J Cell Biol,* 191**,** 169-85.

SEMPLE, B. D., BLOMGREN, K., GIMLIN, K., FERRIERO, D. M. & NOBLE-HAEUSSLEIN, L. J. 2013. Brain development in rodents and humans: Identifying benchmarks of maturation and vulnerability to injury across species. *Prog Neurobiol,* 106-107**,** 1-16.

SHEN, Y., CHEN, C. S., ICHIKAWA, H. & GOLDBERG, G. S. 2010. SRC induces podoplanin expression to promote cell migration. *J Biol Chem,* 285**,** 9649-56.

SHERRY, M. M., REEVES, A., WU, J. K. & COCHRAN, B. H. 2009. STAT3 is required for proliferation and maintenance of multipotency in glioblastoma stem cells. *Stem Cells,* 27**,** 2383-92.

SHIBAHARA, J., KASHIMA, T., KIKUCHI, Y., KUNITA, A. & FUKAYAMA, M. 2006. Podoplanin is expressed in subsets of tumors of the central nervous system. *Virchows Arch,* 448**,** 493-9.

SIGOILLOT, F. D., LYMAN, S., HUCKINS, J. F., ADAMSON, B., CHUNG, E., QUATTROCHI, B. & KING, R. W. 2012. A bioinformatics method identifies prominent off-targeted transcripts in RNAi screens. *Nat Methods,* 9**,** 363-6.

SKAU, C. T., FISCHER, R. S., GUREL, P., THIAM, H. R., TUBBS, A., BAIRD, M. A., DAVIDSON, M. W., PIEL, M., ALUSHIN, G. M., NUSSENZWEIG, A., STEEG, P. S. & WATERMAN, C. M. 2016. FMN2 Makes Perinuclear Actin to Protect Nuclei during Confined Migration and Promote Metastasis. *Cell,* 167**,** 1571-1585 e18.

SMITH, S. M. & MELROSE, J. 2011. Podoplanin is expressed by a sub-population of human foetal rib and knee joint rudiment chondrocytes. *Tissue Cell,* 43**,** 39-44.

SOBANOV, Y., BERNREITER, A., DERDAK, S., MECHTCHERIAKOVA, D., SCHWEIGHOFER, B., DUCHLER, M., KALTHOFF, F. & HOFER, E. 2001. A novel cluster of lectin-like receptor genes expressed in monocytic, dendritic and endothelial cells maps close to the NK receptor genes in the human NK gene complex. *Eur J Immunol,* 31**,** 3493-503.

STEFANI, M. 2008. Protein folding and misfolding on surfaces. *Int J Mol Sci,* 9**,** 2515-42.

STUMMER, W., REULEN, H. J., MEINEL, T., PICHLMEIER, U., SCHUMACHER, W., TONN, J. C., ROHDE, V., OPPEL, F., TUROWSKI, B., WOICIECHOWSKY, C., FRANZ, K., PIETSCH, T. & GROUP, A. L.-G. S. 2008. Extent of resection and survival in glioblastoma multiforme: identification of and adjustment for bias. *Neurosurgery,* 62**,** 564-76; discussion 564-76.

STUPP, R., HEGI, M. E., MASON, W. P., VAN DEN BENT, M. J., TAPHOORN, M. J., JANZER, R. C., LUDWIN, S. K., ALLGEIER, A., FISHER, B., BELANGER, K., HAU, P., BRANDES, A. A., GIJTENBEEK, J., MAROSI, C., VECHT, C. J., MOKHTARI, K., WESSELING, P., VILLA, S., EISENHAUER, E., GORLIA, T., WELLER, M., LACOMBE, D., CAIRNCROSS, J. G., MIRIMANOFF, R. O., EUROPEAN ORGANISATION FOR, R., TREATMENT OF CANCER BRAIN, T., RADIATION ONCOLOGY, G. & NATIONAL CANCER INSTITUTE OF CANADA CLINICAL TRIALS, G. 2009. Effects of radiotherapy with concomitant and adjuvant temozolomide versus radiotherapy alone on survival in glioblastoma in a randomised phase III study: 5-year analysis of the EORTC-NCIC trial. *Lancet Oncol,* 10**,** 459-66.

SUZUKI-INOUE, K., FULLER, G. L., GARCIA, A., EBLE, J. A., POHLMANN, S., INOUE, O., GARTNER, T. K., HUGHAN, S. C., PEARCE, A. C., LAING, G. D., THEAKSTON, R. D., SCHWEIGHOFFER, E., ZITZMANN, N., MORITA, T., TYBULEWICZ, V. L., OZAKI, Y. & WATSON, S. P. 2006. A novel Syk-dependent mechanism of platelet activation by the C-type lectin receptor CLEC-2. *Blood,* 107**,** 542-9.

SUZUKI-INOUE, K., KATO, Y., INOUE, O., KANEKO, M. K., MISHIMA, K., YATOMI, Y., YAMAZAKI, Y., NARIMATSU, H. & OZAKI, Y. 2007. Involvement of the snake toxin receptor CLEC-2, in podoplanin-mediated platelet activation, by cancer cells. *J Biol Chem,* 282**,** 25993-6001.

SUZUKI, H., KATO, Y., KANEKO, M. K., OKITA, Y., NARIMATSU, H. & KATO, M. 2008. Induction of podoplanin by transforming growth factor-beta in human fibrosarcoma. *FEBS Lett,* 582**,** 341-5.

SZULZEWSKY, F., PELZ, A., FENG, X., SYNOWITZ, M., MARKOVIC, D., LANGMANN, T., HOLTMAN, I. R., WANG, X., EGGEN, B. J., BODDEKE, H. W., HAMBARDZUMYAN, D., WOLF, S. A. & KETTENMANN, H. 2015. Glioma-associated microglia/macrophages display an expression profile different from M1 and M2 polarization and highly express Gpnmb and Spp1. *PLoS One,* 10**,** e0116644.

TANG, P., CAO, C., XU, M. & ZHANG, L. 2007. Cytoskeletal protein radixin activates integrin alpha(M)beta(2) by binding to its cytoplasmic tail. *FEBS Lett,* 581**,** 1103-8.

THORNE, R. F., LEGG, J. W. & ISACKE, C. M. 2004. The role of the CD44 transmembrane and cytoplasmic domains in co-ordinating adhesive and signalling events. *J Cell Sci,* 117**,** 373-80.

TOMALA, K., POGODA, E., JAKUBOWSKA, A. & KORONA, R. 2014. Fitness costs of minimal sequence alterations causing protein instability and toxicity. *Mol Biol Evol,* 31**,** 703-7.

TOMOOKA, M., KAJI, C., KOJIMA, H. & SAWA, Y. 2013. Distribution of podoplanin-expressing cells in the mouse nervous systems. *Acta Histochem Cytochem,* 46**,** 171-7.

UHRIN, P., ZAUJEC, J., BREUSS, J. M., OLCAYDU, D., CHRENEK, P., STOCKINGER, H., FUERTBAUER, E., MOSER, M., HAIKO, P., FASSLER, R., ALITALO, K., BINDER, B. R. & KERJASCHKI, D. 2010. Novel function for blood platelets and podoplanin in developmental separation of blood and lymphatic circulation. *Blood,* 115**,** 3997-4005.

VALENTE, V., TEIXEIRA, S. A., NEDER, L., OKAMOTO, O. K., OBA-SHINJO, S. M., MARIE, S. K., SCRIDELI, C. A., PACO-LARSON, M. L. & CARLOTTI, C. G., JR. 2009. Selection of suitable housekeeping genes for expression analysis in glioblastoma using quantitative RT-PCR. *BMC Mol Biol,* 10**,** 17.

VERHAAK, R. G., HOADLEY, K. A., PURDOM, E., WANG, V., QI, Y., WILKERSON, M. D., MILLER, C. R., DING, L., GOLUB, T., MESIROV, J. P., ALEXE, G., LAWRENCE, M., O'KELLY, M., TAMAYO, P., WEIR, B. A., GABRIEL, S., WINCKLER, W., GUPTA, S., JAKKULA, L., FEILER, H. S., HODGSON, J. G., JAMES, C. D., SARKARIA, J. N., BRENNAN, C., KAHN, A., SPELLMAN, P. T., WILSON, R. K., SPEED, T. P., GRAY, J. W., MEYERSON, M., GETZ, G., PEROU, C. M., HAYES, D. N. & CANCER GENOME ATLAS RESEARCH, N. 2010. Integrated genomic analysis identifies clinically relevant subtypes of glioblastoma characterized by abnormalities in PDGFRA, IDH1, EGFR, and NF1. *Cancer Cell,* 17**,** 98-110.

VISSER, O., ARDANAZ, E., BOTTA, L., SANT, M., TAVILLA, A., MINICOZZI, P. & GROUP, E.-W. 2015. Survival of adults with primary malignant brain tumours in Europe; Results of the EUROCARE-5 study. *Eur J Cancer,* 51**,** 2231-2241.

VISVADER, J. E. & LINDEMAN, G. J. 2008. Cancer stem cells in solid tumours: accumulating evidence and unresolved questions. *Nat Rev Cancer,* 8**,** 755-68.

VITTORI, M., MOTALN, H. & TURNSEK, T. L. 2015. The study of glioma by xenotransplantation in zebrafish early life stages. *J Histochem Cytochem,* 63**,** 749-61.

WANG, Q., HU, B., HU, X., KIM, H., SQUATRITO, M., SCARPACE, L., DECARVALHO, A. C., LYU, S., LI, P., LI, Y., BARTHEL, F., CHO, H. J., LIN, Y. H., SATANI, N., MARTINEZ-LEDESMA, E., ZHENG, S., CHANG, E., SAUVE, C. G., OLAR, A., LAN, Z. D., FINOCCHIARO, G., PHILLIPS, J. J., BERGER, M. S., GABRUSIEWICZ, K. R., WANG, G., ESKILSSON, E., HU, J., MIKKELSEN, T., DEPINHO, R. A., MULLER, F., HEIMBERGER, A. B., SULMAN, E. P., NAM, D. H. & VERHAAK, R. G. W. 2017. Tumor Evolution of Glioma-Intrinsic Gene Expression Subtypes Associates with Immunological Changes in the Microenvironment. *Cancer Cell,* 32**,** 42-56 e6.

WATKINS, S., ROBEL, S., KIMBROUGH, I. F., ROBERT, S. M., ELLIS-DAVIES, G. & SONTHEIMER, H. 2014. Disruption of astrocyte-vascular coupling and the blood-brain barrier by invading glioma cells. *Nat Commun,* 5**,** 4196.

WEBER, H., CLAFFEY, J., HOGAN, M., PAMPILLON, C. & TACKE, M. 2008. Analyses of Titanocenes in the spheroid-based cellular angiogenesis assay. *Toxicol In Vitro,* 22**,** 531-4.

WETTERWALD, A., HOFFSTETTER, W., CECCHINI, M. G., LANSKE, B., WAGNER, C., FLEISCH, H. & ATKINSON, M. 1996. Characterization and cloning of the E11 antigen, a marker expressed by rat osteoblasts and osteocytes. *Bone,* 18**,** 125-32.

WICK, W., MEISNER, C., HENTSCHEL, B., PLATTEN, M., SCHILLING, A., WIESTLER, B., SABEL, M. C., KOEPPEN, S., KETTER, R., WEILER, M., TABATABAI, G., VON DEIMLING, A., GRAMATZKI, D., WESTPHAL, M., SCHACKERT, G., LOEFFLER, M., SIMON, M., REIFENBERGER, G. & WELLER, M. 2013. Prognostic or predictive value of MGMT promoter methylation in gliomas depends on IDH1 mutation. *Neurology,* 81**,** 1515-22.

WICKI, A., LEHEMBRE, F., WICK, N., HANTUSCH, B., KERJASCHKI, D. & CHRISTOFORI, G. 2006. Tumor invasion in the absence of epithelial-mesenchymal transition: podoplanin-mediated remodeling of the actin cytoskeleton. *Cancer Cell,* 9**,** 261-72.

WILLIAMS, M. C., CAO, Y., HINDS, A., RISHI, A. K. & WETTERWALD, A. 1996. T1 alpha protein is developmentally regulated and expressed by alveolar type I cells, choroid plexus, and ciliary epithelia of adult rats. *Am J Respir Cell Mol Biol,* 14**,** 577-85.

WINKLER, F., KIENAST, Y., FUHRMANN, M., VON BAUMGARTEN, L., BURGOLD, S., MITTEREGGER, G., KRETZSCHMAR, H. & HERMS, J. 2009. Imaging glioma cell invasion in vivo reveals mechanisms of dissemination and peritumoral angiogenesis. *Glia,* 57**,** 1306-15.

XIA, Y., LIU, L., XIONG, Y., BAI, Q., WANG, J., XI, W., QU, Y., XU, J. & GUO, J. 2016. Podoplanin associates with adverse postoperative prognosis of patients with clear cell renal cell carcinoma. *Cancer Sci,* 107**,** 1243-9.

XIAO, A., WU, H., PANDOLFI, P. P., LOUIS, D. N. & VAN DYKE, T. 2002. Astrocyte inactivation of the pRb pathway predisposes mice to malignant astrocytoma development that is accelerated by PTEN mutation. *Cancer Cell,* 1**,** 157-68.

XIE, Q., MITTAL, S. & BERENS, M. E. 2014. Targeting adaptive glioblastoma: an overview of proliferation and invasion. *Neuro Oncol,* 16**,** 1575-84.

XU, W. L., WANG, Y., WU, J. & LI, G. Y. 2016. Quantitative analysis of U251MG human glioma cells invasion in organotypic brain slice co-cultures. *European Review for Medical and Pharmacological Sciences,* 20**,** 2221-2229.

YAN, H., PARSONS, D. W., JIN, G., MCLENDON, R., RASHEED, B. A., YUAN, W., KOS, I., BATINIC-HABERLE, I., JONES, S., RIGGINS, G. J., FRIEDMAN, H., FRIEDMAN, A., REARDON, D., HERNDON, J., KINZLER, K. W., VELCULESCU, V. E., VOGELSTEIN, B. & BIGNER, D. D. 2009. IDH1 and IDH2 mutations in gliomas. *N Engl J Med,* 360**,** 765-73.

YANO, S., TAKEHARA, K., KISHIMOTO, H., TAZAWA, H., URATA, Y., KAGAWA, S., BOUVET, M., FUJIWARA, T. & HOFFMAN, R. M. 2016. In Vivo Selection of Intermediately- and Highly-Malignant Variants of Triple-negative Breast Cancer in Orthotopic Nude Mouse Models. *Anticancer Res,* 36**,** 6273-6277.

YONEMURA, S., HIRAO, M., DOI, Y., TAKAHASHI, N., KONDO, T., TSUKITA, S. & TSUKITA, S. 1998. Ezrin/radixin/moesin (ERM) proteins bind to a positively charged amino acid cluster in the juxta-membrane cytoplasmic domain of CD44, CD43, and ICAM-2. *J Cell Biol,* 140**,** 885-95.

YURRITA, M. M., FERNANDEZ-MUNOZ, B., DEL CASTILLO, G., MARTIN-VILLAR, E., RENART, J. & QUINTANILLA, M. 2014. Podoplanin is a substrate of presenilin-1/gamma-secretase. *Int J Biochem Cell Biol,* 46**,** 68-75.

ZIMMER, G., KLENK, H. D. & HERRLER, G. 1995. Identification of a 40-kDa cell surface sialoglycoprotein with the characteristics of a major influenza C virus receptor in a Madin-Darby canine kidney cell line. *J Biol Chem,* 270**,** 17815-22.

ZIMMER, G., LOTTSPEICH, F., MAISNER, A., KLENK, H. D. & HERRLER, G. 1997. Molecular characterization of gp40, a mucin-type glycoprotein from the apical plasma membrane of Madin-Darby canine kidney cells (type I). *Biochem J,* 326 (Pt 1)**,** 99-108.

ZIMMERMANN, D. R. & DOURS-ZIMMERMANN, M. T. 2008. Extracellular matrix of the central nervous system: from neglect to challenge. *Histochem Cell Biol,* 130**,** 635-53.

ZOLLER, M. 2009. Tetraspanins: push and pull in suppressing and promoting metastasis. *Nat Rev Cancer,* 9**,** 40-55.

7 SUPPLEMENT

7 SUPPLEMENT

7.1 Supplementary data

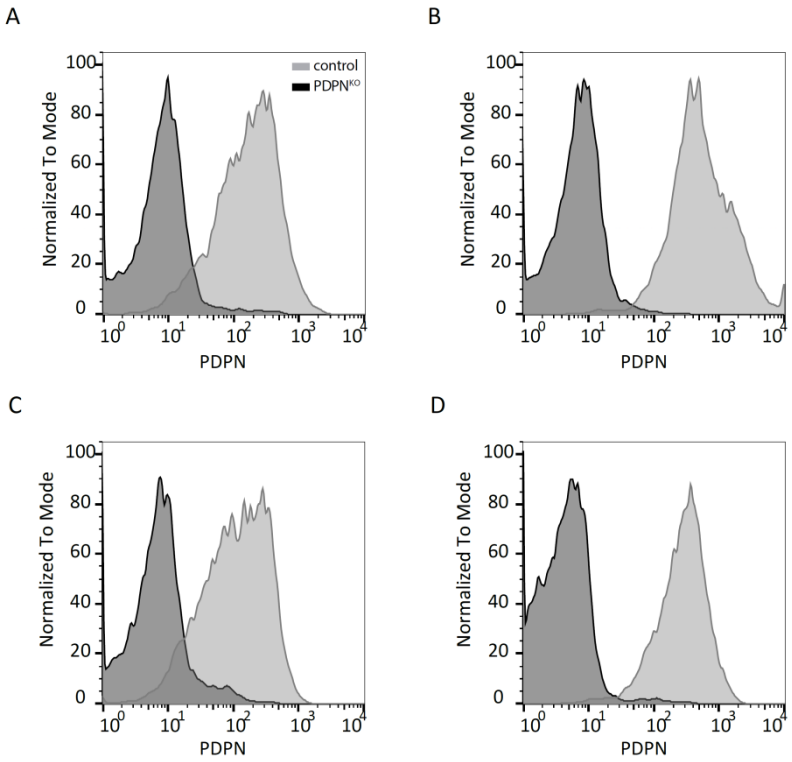

Figure 7.1 Flow cytometry plots of long-term glioblastoma cultures.
PDPN was successfully deleted in (A) T1132; (B) GBM41; (C) NMA59 and (D) NMA65; control cells in grey, $PDPN^{KO}$ cells in black.

Table 7.1 Overview of mouse numbers injected with long-term glioblastoma cultures.

Cells	Number of injected mice	Number of Tumor bearing mice	Termination
T1132 control	6	0	d285
T1132 $PDPN^{KO}$	6	0	d285
GBM41 control	6	0	d233
GBM41 $PDPN^{KO}$	6	0	d233
NMA59 control	6	0	d427
NMA59 $PDPN^{KO}$	6	0	d427
NMA65 control	6	2	d455
NMA65 $PDPN^{KO}$	6	0	d455

7.2 Declaration

I hereby declare that except where specific reference is made to the work of others, the contents of this dissertation are original and based on results of my own investigations. This dissertation has not been submitted for consideration for any other degree or qualification.

Heidelberg, December 2017

Tanja Eisemann

7.3 Acknowledgements

After the seemingly endless time of the PhD, it still feels unreal to finally finish it. But here I am, writing the last part of my thesis, the acknowledgements. It has been an incredible time full of ups and downs, frustrating setbacks, technical achievements and cheerful coffee breaks with the fantastic members of the Angel lab. For accompanying me through this exciting time, I want to thank many people. First of all, **Peter Angel**, for offering me a position in his lab, giving me the freedom to develop my own ideas and skills, and especially for his trust in me. I want to acknowledge **Heike Peterziel** for the numberless discussions, brain storming sessions and guidance. Thank you so much for supporting and inspiring me throughout the previous years, even after you have started a new position. In you I have not only found the most committed supervisor I could have wished for, but also a friend. Another big thank you goes to **Barbara Costa**; I appreciate your advice during the past years and your humorous manner, which has cheered up so many coffee breaks and working hours at the Podoplanini booth. In general, I want to thank the **Podoplanini**, present and past members, for the great team spirit and sharing excitement (and frustration) about our favorite protein. I also want to acknowledge the entire **A100 group**, for generating such a pleasant working atmosphere. **Doris**, **Barbara**, **Thomas**, **Kristin**, **Maria** thank you for answering all my technical and scientific questions I've had; **Sebastian**, **Aurora**, **Jule**, **Meli**, **Laura** and **Te** – my fellow sufferers ☺ – thank you for joining the "lamenting" club but also for sharing so many exciting and funny moments in the lab; **Tine**, **Betty**, **Sabrina**, **Melanie**, **Lena** and **Alina** thanks not only for your technical/administrative support but also for your contagious good mood.
I thank **Annette Kopp-Schneider** for her advice in statistical analysis, **Angelika Krischke** for technical support on histology samples, the center for preclinical research, in particular I want to thank the **animal care takers**; thanks to the **DKFZ core facilities** for light microscopy, gene expression profiling, and especially the flow cytometry team. I also want to acknowledge the **Preclinical Comprehensive Cancer Center (PCCC)** of the Helmholtz Alliance for generating an interactive platform for the exchange with scientists of all academic levels. Many thanks to **Ana Martín-Villalba** for being a member of my Thesis Advisory Committee and to her lab for sharing the stereotaxic device. I also want to acknowledge our collaboration partners **Patrick Harter** and **Michel Mittelbronn** in Frankfurt and Luxembourg. Michel, you have not only provided valuable patient material, but I could always address you with any kind of scientific or clinical question and I am really happy that the collaboration has developed into a friendship. Many thanks to **my family and friends** who endured me when I was frustrated and disappointed, but who also strengthened my motivation by showing true interest in what I have been working on. Finally, I want to thank **Tobi**, with your humorous and encouraging support you helped me through quite a few valleys of frustration and I'm happy to share all future adventures with you.